The Dissertation Committee for Debarshi Basu Certifies that this is the approved version of the following dissertation:

Charge Transport in Polymer Semiconductors

Committee:

Ananth Dodabalapur, Supervisor

Sanjay K. Banerjee

Leonard F. Register

Jack C. Lee

Yueh-lin Loo

Charge Transport in Polymer Semiconductors

by

Debarshi Basu, M.S.E; B. Tech.

Dissertation

Presented to the Faculty of the Graduate School of

The University of Texas at Austin

in Partial Fulfillment

of the Requirements

for the Degree of

Doctor of Philosophy

The University of Texas at Austin

August, 2007

Dedication

To the three sweetest person in my life Bony, Buani and Papai.

Acknowledgements

First of all, I would like to express my deep gratitude to my supervisor, Dr. Ananth Dodabalapur, for his support, encouragement, and guidance for my research work. His invaluable advice and ideas always inspired me to keep passionate about my work. I also would like to convey hearty thanks to my all committee members, Dr. Sanjay Banerjee, Dr. Jack Lee, Dr. Frank Register, and Dr. Yueh Lin Loo, for their helpful suggestions and advice on my dissertation.

I would like to thank all the past and present group members, Liang Wang, Tae Ho Jung, Daniel Fine, Byungwook Yoo, Suvid Nadkarni, Yeon Taek Jeong, Deepak Sharma, Lawrence Dunn, Chris Lombardo, Ashwin A. Madgavkar, Jae Won Shim, Shannon D. Lewis, Brian H. Cobb, Davianne A. Duarte, Dharmendar R. Palle, and Sebastian P. Schoefer for their support and help. It was a great pleasure to work and live with them. Financial support by the AFOSR, the NSF through a NIRT, and SPRING through CNM is also gratefully acknowledged.

Finally, my deepest gratitude goes to my wife, my sister and my parents. I really appreciate their continuous support and endless love throughout all my life. I would like to dedicate the dissertation to my wife, my sister and my aunt.

Charge Transport in Polymer Semiconductors

Publication No._____

Debarshi Basu, Ph.D.

The University of Texas at Austin, 2007

Supervisor: Ananth Dodabalapur.

This work is focused on the electrical characterization of polymer field effect transistors. Conventional method of characterizing organic polymeric semiconductors includes field-effect mobility measurement and optical time-of-flight measurement of drift mobility. In this dissertation we have introduced a new method that combines the advantages of both these methods. It involves the injection of carriers at the source of a transistor using a voltage pulse followed by their subsequent extraction at the drain. The delay between the two events is used to extract the velocity of carriers. The electronic time-of-flight method is a fast, simple and direct method to determine the charge transport properties of the semiconductor. In addition it also presents itself as a source of information for understanding injection into the semiconductor and determining the trap distribution.

Theoretical modeling of transport was performed. Simulation was also done to include effect of non-idealities that are forbiddingly difficult to be solved analytically. Time of flight measurements of drift mobility were performed in organic transistors with varying semiconductors and dielectrics. It was observed that the electronic time-of-flight

mobility lies in the range of the field-effect mobility. Variation in drift mobility was also observed with the applied pulse voltage. This was explained to be caused due to a combination of the increase in mobility with gate voltage and the increase in drift mobility at high lateral fields. Finally mobility measurements were done on transistors with varying channel length and it was concluded that the mobility increases proportional to the exponential square root of the electric field. Finally a derivation of the pulse voltage method is discussed that involves the use of a small signal electronic impulse instead of a large signal voltage pulse. It was shown that this method could not be used to calculate the drift velocity in a polymer transistor as it is valid only for low conductivity materials whose dielectric relaxation time is lower that the transit time of the carriers injected.

Table of Contents

List of Tables

List of Figures

1 INTRODUCTION

1.1 History

The invention of the semiconductor transistor by Bardeen, Brittain and Shockley in 1947[1] ushered in the era of solid state electronics. Silicon soon replaced germanium, the initial semiconductor, as the material of choice for fabrication. The discovery of integrated circuit in 1960[2] set off the semiconductor revolution. It was possible for the first time to perform complex calculations instantly at the touch of a button. Since the inception of microprocessors, the numbers of transistors have doubled every 18 months[3], and their sizes shrunk into the resolution of a couple of atoms. Cell phones, pagers, laptops, PDA's and other marvels of silicon fabrication, have revolutionized the way we communicate with each other.

Plastics on the other hand have been used as insulators since the last century for packaging and manufacture of household items. They are flexible lightweight materials that can be molded easily at low-temperatures making them ideal candidates for low cost manufacturing. The first use of organic materials as active materials for electronic applications was in 1960s when it was used in xerographic applications as photoconductors[4]. However it was the discovery of conducting polymers in 1977 that demonstrated the ability of organic polymers to conduct electricity. Shirakawa, McDiarmid and Heeger, the inventors won the Nobel Prize for chemistry in 2000 for their role in "Development of conducting polymers"[5].

The discovery of conducting polymers prompted research on conjugated organic molecules as it held the promise of producing cheap lightweight electronics and displays using organic field effect transistors (OFET) and organic light emitting diodes (OLED). The development of "e-paper" by Lucent Technologies (formerly Bell Labs) and E-ink Corp. bolstered the promise by demonstrating world's first flexible, plastic electronic display entirely made with a process similar to ink-on-paper printing[6].

The main advantage of using organic semiconductors for electronics is their ability to be processed from solution at room temperature onto any curved substrate. This makes them ideally suitable for large area, low cost, large volume manufacturing processes such as printing[7]. Therefore the cost of electronics is reduced as compared to those manufactured using standard silicon fabrication processes.

Furthermore the properties of organic semiconductor can be tailored and augmented by tools offered by organic chemistry via modification of molecular or monomeric units. The ability to tune molecular properties not only opens up new possibilities for inexpensive device manufacturing but also novel devices with new applications. This property has been utilized to develop sensors that can detect various analyte molecules[8]. Sensitivities of 1ppb have been achieved with an organic material, lead phthalocyanine, for the detection of harmful nitrogen dioxide gas[9].

Lastly, with fossil fuels becoming increasingly scarce the world is facing an energy crisis. As renewable and environmentally friendly sources of energy are being intensively researched, organic solar cells stands out as one of the leading contender with a promise to provide effective solution to the energy crisis[10].

All the above qualities present organic semiconductors as interesting if not important object of systematic research. Although they have existed for over more than four decades, understanding of charge transport processes within these materials is far

from complete. Therefore understanding of the charge transport mechanism in these materials is of vital importance for the improvement of these materials and devices, and the realizations of the promises they hold. In the following sections the most widely used theories of charge transport in organic semiconductors is presented. Emphasis is laid on mobility, which is the most important parameter that has been investigated for understanding charge transport in these materials. The scope of this thesis is in the description of charge transport in organic field effect transistors using a novel method to characterize the charge carrier mobility, which is the most important and most researched parameter of an organic semiconductor.

1.2 Charge Transport

1.2.1 INTRA-MOLECULAR PERSPECTIVE

Organic semiconductors are compounds composed mainly of carbon and hydrogen that show semiconducting properties. The carbon atoms in these compounds are sp^2 hybridized. Hybridization is an unusual property of the carbon atom in which the s, p_x and the p_y orbitals hybridize or fuse and reorient them selves along a plane separated from each other by 120 degrees as shown in Figure 1.1 a (from orgworld.de with permission from Dr K. Leo)[11]. The remaining p_z orbital extends perpendicularly above and below the plane. Two neighboring carbon atoms covalently bond with each other using an in-plane overlap of the hybridized orbital, also called a σ (sigma) bond, and another out of plane overlap of the p_z orbitals termed as pi bond.

When this structure is repeated over a large number of carbon atoms, the π (pi) electrons are delocalized above and below the plane which is termed as conjugation. Conjugation is marked by the presence of alternate single and double bonds as shown in a

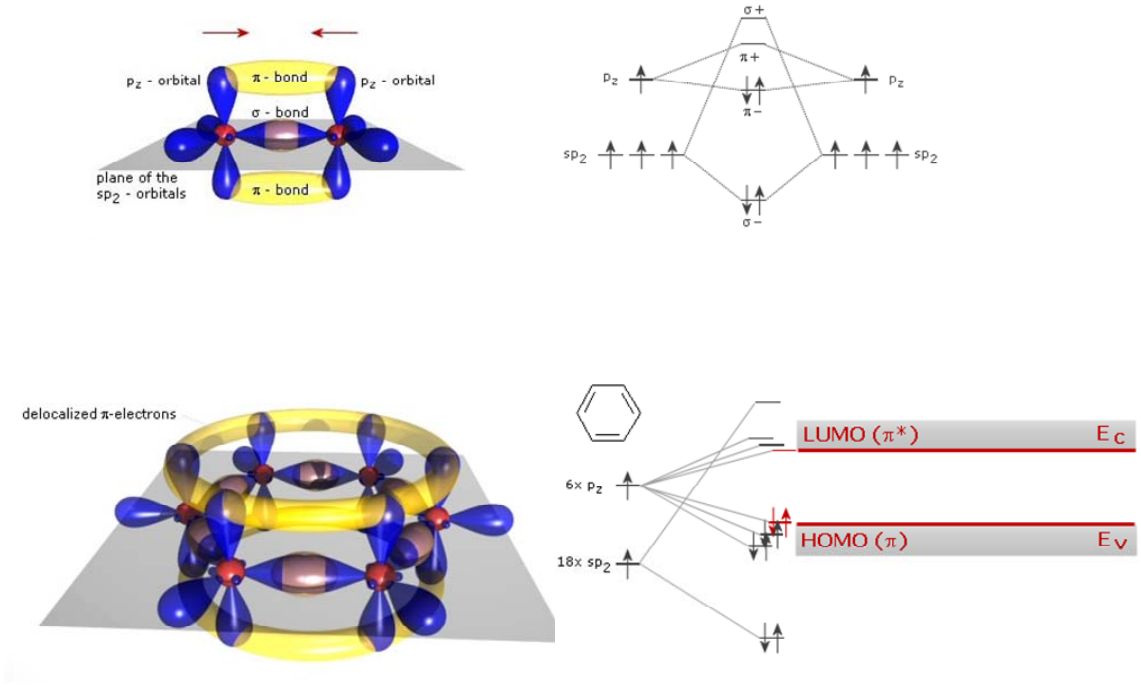

Figure 1.1 (a) Hybridization of carbon atoms help form sigma and pi bonds with neighboring atoms. (b) this leads to delocalization of the pi electron cloud over the entire molecule. (From 11 with permission from K. Leo)

benzene molecule in Figure 1.1 b. Equivalently the π bonding and antibonding orbitals can be visualized to form a continuum of energy states rather than a discreet one. The resultant continuum of antibonding and bonding orbitals are referred to as lowest unoccupied molecular orbital (LUMO) and highest occupied molecular orbital (HOMO) respectively (Figure 1.2). The HOMO and LUMO with an energy gap between them is analogous to the valence and conduction bands in any inorganic semiconductor.

Organic semiconductors mainly come in two varieties: Small molecules and polymers. Small molecules as the name suggests are relatively small molecular weight molecules with conjugated carbon atoms. These substances can be prepared as molecular single crystals. Due to the close coupling of the π-systems of the molecules in these

crystals, they show in a purified form remarkable transport properties with mobilities of 1-10 cm^2/Vs[12]. Most molecules can be easily evaporated to form polycrystalline layers.

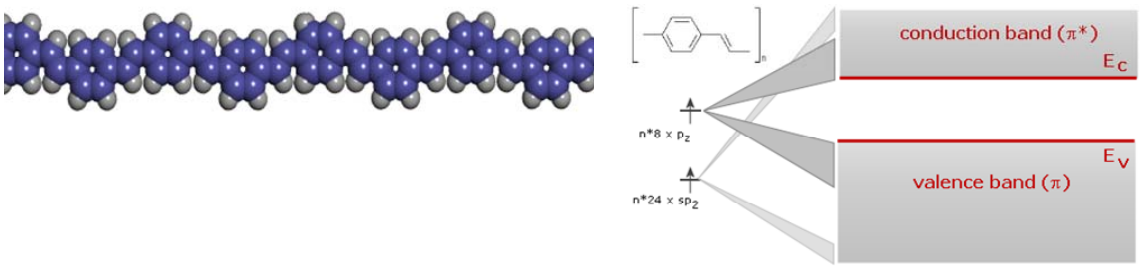

Figure 1.2 Formation of conduction and valence band due to conjugation of a considerable length over the molecule. (From 11 with permission from K. Leo)

Organic semiconducting polymers are long chain of conjugated carbon atoms composed of smaller repeating units called monomers. The advantage of polymers is that, when modified with suitable side chains, they can self organize when deposited from solution at room temperature yielding a fairly high mobility layer; hence they can be used to print circuits at a low manufacturing cost.

In addition there are also oligomers which are relatively smaller collection of monomers. Organic semiconductors are inherently neutral that is they do not possess any charges of their own. Carriers to be transported are injected into these materials through metal contacts.

1.2.2 INTER-MOLECULAR PERSPECTIVE

Organic molecules can be either deposited in vacuum or from solution. Their properties depend significantly on the conditions during deposition like temperature, rate of deposition/rate of evaporation of solvent and surface of deposition. These conditions

affect the morphology to a great extent. Molecules tend to arrange themselves spontaneously into herring bone structure as shown in Figure 1.3 . This effectively results in anisotropy in the ability to conduct electricity. Charges are conducted through the pi electron cloud; the greater coupling between the electron clouds of neighboring molecule

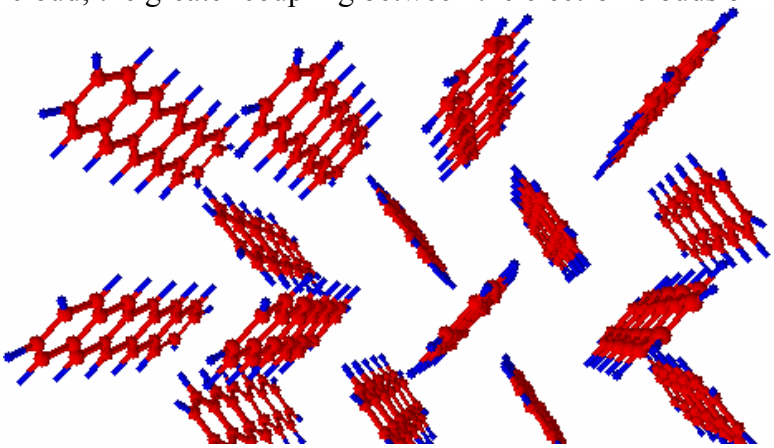

Figure 1.3 Herring bone structure of Pentacene.

the easier it is for the charge carriers to move[13]. The molecules are held together by weak usually van der Waals interactions with energies smaller than 10 kcal mol^{-1}. Unlike inorganic semiconductor with strong, covalently bonded atoms,(bond energy of Si is 76 kcal mol^{-1}) the vibrational energy of the molecule at or above room temperature reaches a magnitude close to that of the intermolecular bond energies[14]. This fact in solid state physics is referred to as having a high electron phonon coupling constant. A high electron-phonon coupling constant is responsible for limiting the mobility between 1-10 cm^2/Vs. the actual mechanism limiting the mobility of carriers is scattering of carriers by lattice vibrations. Band transport is inapplicable to disordered organic semiconductors in which the carrier transport takes place by hopping between localized states and carriers are scattered at every step. Hopping is assisted by phonons and mobility increases with temperature. Highly ordered semiconductors have a high mobility at room temperatures, however most semiconducting films are polycrystalline. Polymers when dispersed from

solution assemble parallel to each other forming small crystalline domains or lamellae that have short range order. These ordered regions are separated by disordered regions or grain boundaries (Figure 1.4). In the energy-momentum space the disordered region shows up as traps or energy state in the forbidden energy gap. One the other major reason for traps is polydispersity or variation of chain lengths. Since not all chains have the same length, they do not end at the same place thus terminating the ordered region formed by parallely placed chains. Moreover the ordered domains are not perfectly ordered either. Traps exist because of chain defects and impurities. Torsional strain within the chain makes it difficult for the chains to always stack up perfectly. It is accepted that for these polycrystalline materials there is a band tail of localized states within the grains and even more traps at grain boundaries[15]. The specific shape of the density of state is rarely investigated firstly because of the difficulty involved. Also the DOS is sensitive to chemical doping by dopant atoms and hence no unique DOS can be determined. The shape of the DOS is however important in understanding charge transport as carrier movement essentially takes place by hopping in this band tail. Carriers move from localized states to localized state between chains and even within a chain in order to move across the semiconductor films[16,17]. The morphology of the polymer chains critically affects the charge transport and semiconducting properties of the polymeric semiconductor. Therefore it is essential to understand structural and energetic disorder to comprehend transport in these materials.

1.2.3 HOPPING TRANSPORT

Motion of a charge carrier in an organic material can be described using hopping transport. Hopping is defined as a phonon assisted tunneling between two localized

electronic states centered at different locations[17,18]. It is usually observed in disordered

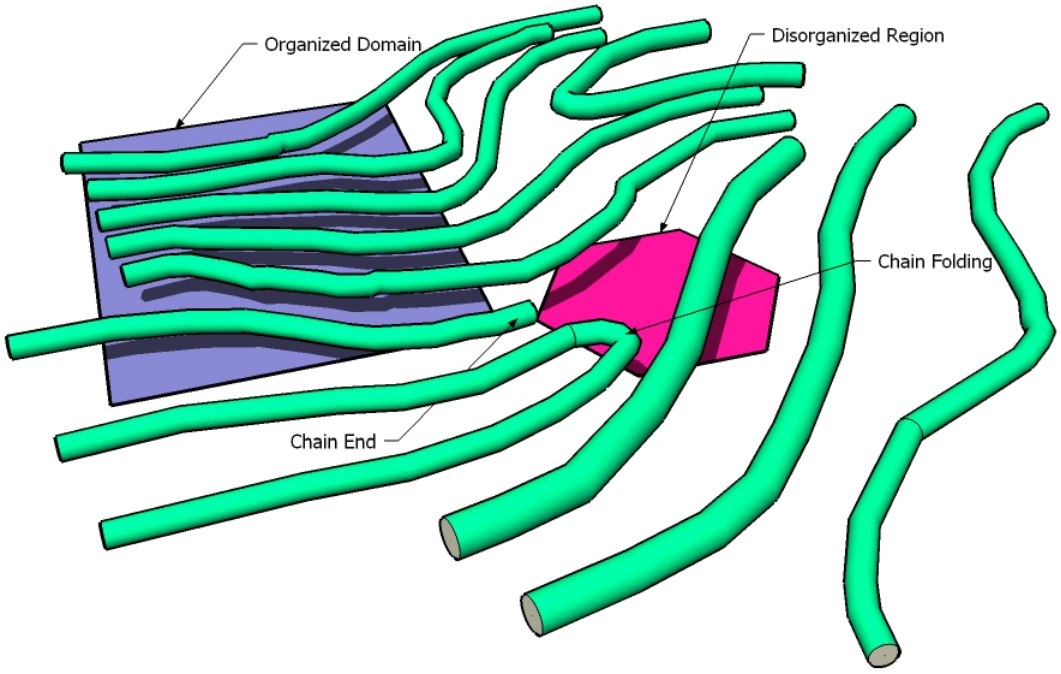

Figure 1.4 When dispersed from solutions polymers tend to self assemble parallel to each other forming organized domain. These organized domains are separated by disorganized regions formed due to irregularities in placement of polymer chains.

semiconductors due to localization of charges. This hopping transport takes place around the Fermi level. Many of the hopping models are based on the single phonon jump rate description as proposed by Miller and Abrams[19]. In the Miller Abrams hopping model the hopping rate between an occupied site *i* and an adjacent unoccupied site *j* , which are separated in energy by *E*i − *E*j and in distance by *R*ij, is described by

$$\nu_{i\to j} = \nu_0 \cdot \exp(-2\gamma R_{ij}) \begin{cases} \exp(-\dfrac{E_i - E_j}{k_B T}) & E_i > E_j \\ 1 & E_i > E_j \end{cases} \qquad (1.1)$$

where γ^{-1} quantifies the wavefunction overlap between the sites, ν^0 is a prefactor, and k_B is Boltzmanns constant. The Miller-Abrams model addresses hopping rates at low temperatures between shallow three-dimensional impurity states, assuming that the electron phonon coupling is weak. When the Miller-Abrahams model is applied to polymeric semiconductors, it is assumed that the conjugated segments of the polymers play the role of nearly isolated impurity states, and that Equation1.1 is still valid at high temperatures[19]. Depending on the structural and energetic disorder of the system it can be energetically favorable to hop over a longer distance with a low activation energy (energy difference between sites), than over a shorter distance with a higher activation energy. This extension to the Miller-Abrahams model, proposed by Mott is called variable range hopping[20]. Monroe proved that the hopping transport around the Fermi level in an exponential density of states is similar to a model in which charge carriers are thermally activated to a transport level[21]. A percolation model describing the temperature and gate voltage dependencies of organic field-effect transistors was proposed by Vissenberg and Matters[22] which was based on variable range hopping in an exponential density of states.

1.3 Mobility

Development of low-cost, large-volume manufacturing processes using organic semiconductors will enable production of electronic paper, cheap RFID tags and other next generation portable electronic display and circuits. However low speeds of operation and less than desirable cut-off frequencies in circuits have prevented anticipated progress in realization of products. This is a result of low field effect mobility of organic transistors .Mobility is the most important parameter of the semiconductor that determines the speed with which charge carriers can move along an applied electric field.

In technical terms, the average directional velocity v of carriers superimposed on random thermal motion by the action of an electric field E is a linear function of the field, the proportionality constant of which is defined as the mobility tensor μ .

$$\vec{v} = \underline{\underline{\mu}} \cdot \vec{E} \tag{1.2}$$

Hence the mobility is a determinant of the performance of transistors and circuits composed out of it. As discussed in section 1.2.2 the small charge carrier mobility is a consequence of weak intermolecular interactions and resulting localization of charge carriers or trapping by chemical impurities and other trap states formed by structural disorder. However, the improvement in processing of existing organic semiconductors, and the discovery of new ones have resulted in dramatic improvements in the performance of organic transistors has seen in the last decade (Figure 1.5). Pentacene, mobilities of 1.5 cm^2/Vs were reported by Lin *et. al.*[23] High performance pentacene devices have also been fabricated using polymer dielectrics with carrier mobilities of 3 cm^2/Vs[24]. Pentacene is one of the most commonly used small molecule p-type organic semiconductor that is commercially available and displays one of the highest mobilities. Some of the other commonly used p-type or hole conducting and n-type or electron conducting organic semiconductors are shown in Figure 1.6 (a),(b) respectively[25]. It should be noted that a particular semiconductor efficiently transports only one type of charge carrier, an electron or a hole and very rarely both.

Mobilities of polymers have also gone up over the years from $10^{-4} – 10^{-5}$ cm^2/Vs[26] to that of 0.14 cm^2/Vs for PQT-12 reported by Ong *et. al.*[27] and 0.2 – 0.7 cm^2/Vs for pBTTT reported by McCulloch et.al[28]. Recently a mobility of 3.5 cm^2/Vs have also been reported with pBTTT with an electrolyte dielectric which induces large carrier densities

in the channel[29]. Comparable mobilities have also been demonstrated with electron transporting compounds.

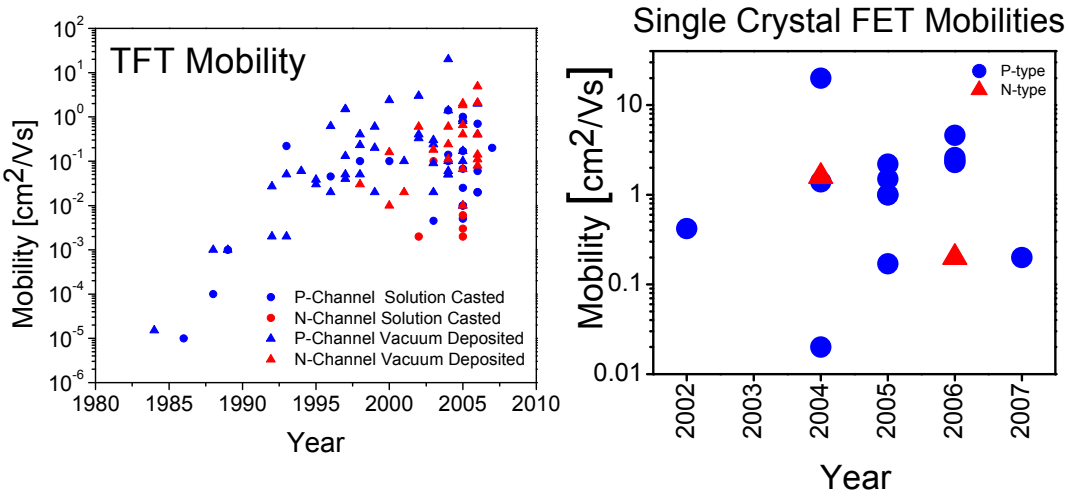

Figure 1.5 Record Mobilities of organic FETs (Single Crystal, Thin-film small molecule, and polymer)

1.3.1 CHARACTERIZATION METHODS

Mobility is the primary parameter that has been investigated to understand charge transport in organic materials. Mobility of an organic material is dependent on its Temperature, electric field applied, atmospheric conditions and molecular ordering hence it can rarely be theoretically calculated due to the complications involved. There are several ways of experimentally determining the mobility. The most prominent of these are the

1. Field effect mobility
2. Time of flight mobility.

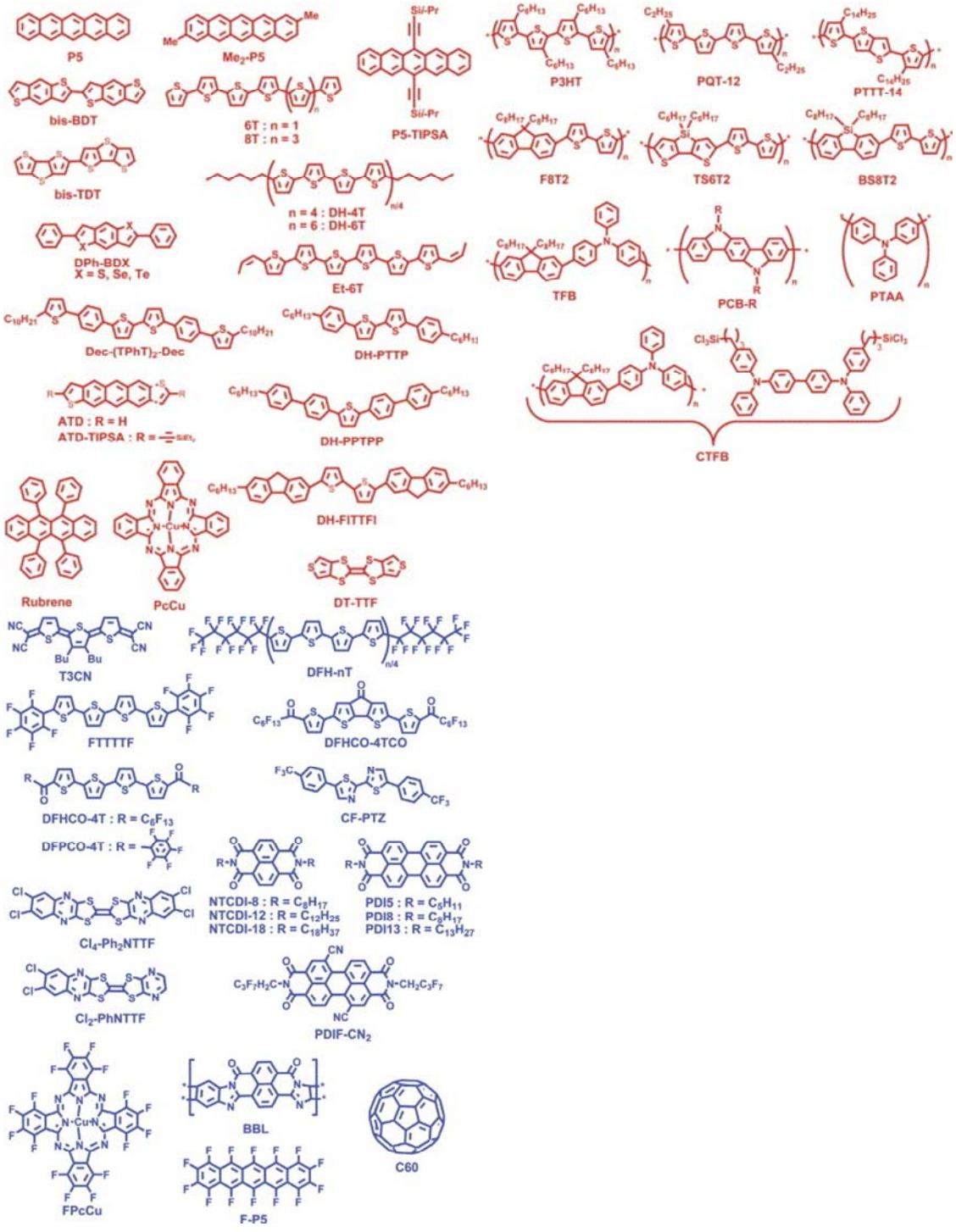

Figure 1.6 Commonly Used p-type (a) and n-type (b) organic semiconductors. (From 25 printed with permission from Elsevier)

1.3.1.1 Field Effect mobility

The mobility extracted from the transconductance curve of an organic field effect transistor operating in the linear or saturation region is termed as the field effect mobility or the field mobility. By placing the source/drain, gate and the dielectric layers in different orders while using the organic semiconductors as the active material, three different FET geometries can be constructed as shown in Figure 1.7. The top contact or bottom contact geometries differ from each other with respect to the placement of the gate and the source/drain metals, on different or same side of the semiconductor layer respectively. A bottom contact scheme has been used in this work.

The transistor action, irrespective of the design, can be explained using the energy band diagram picture of an organic MOS transistor Figure 1.8. It is important to mention here that these transistors operate in accumulation rather than in inversion regime. This is because of the low thermal generation of electron hole pairs and negligible diffusion of charge carriers along an organic molecule, which hinders the formation of an inversion layer. Another point to note (discussed in section 1.3) is that most organic thin films are able to transport only one charge carrier type, electron or hole and very rarely both. The transistor action is described here with an n-type semiconductor; the description for a p-type would be similar with corresponding changes in polarity of voltages and currents. Under normal conditions the conductivity between the source and drain is that of the bulk, in other words there is no channel available for conduction. The current that flow through the semiconductor is therefore quite low. Application of a positive bias, above a certain threshold 'V_{ON}', at the gate leads to the accumulation of negative charges at the semiconductor insulator interface, as a result of this the bands near the interface bend

down so that the Fermi level is continuous. The accumulation of charge carriers at the

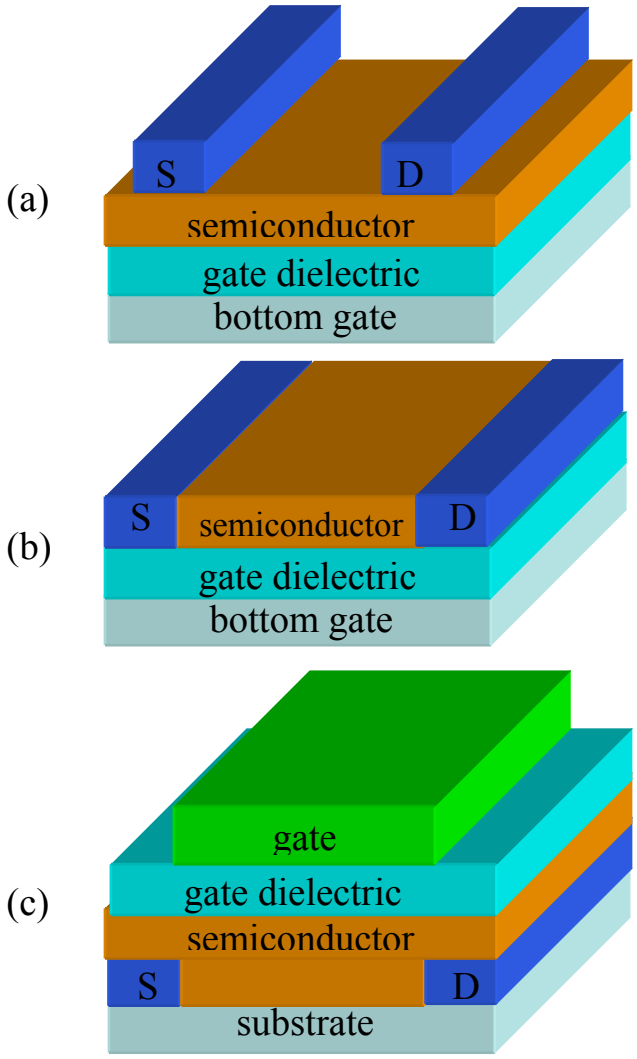

Figure 1.7 Schematic representation of OTFT structure; (a) top-contact configuration (b) bottom-contact configuration (c) top gate configuration.

semiconductor dielectric interface forms a low resistance pathway or a 'channel' for carriers to move. The concentration of carriers can be modulated using the voltage applied to the gate. Therefore a voltage differential between the source and the drain electrodes result in conduction of carriers through the channel. The current through the

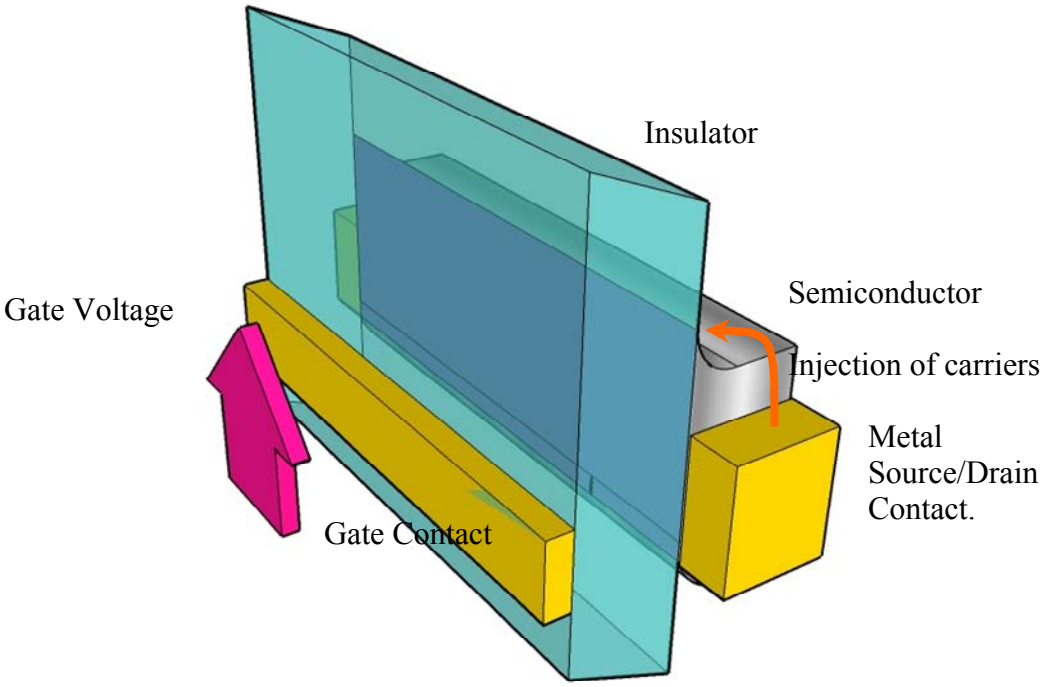

Figure 1.8 Band Diagram of a FET with a positive voltage applied to the gate which causes upward band bending. Carriers are injected from the source/drain contacts into the channel.

channel depend on the gate, source and drain biases, the mobility of the material, the geometry and a few other parameters like the injection at the metal semiconductor contacts, the morphology of the semiconductor etc. The exact equation to the current is extremely difficult, if not impossible to obtain due to the sheer complexity of the problem; however a simplistic approach leads to the equation 1.3, which is similar to the conventional MOSFET equation.

$$I_{Drain} = \begin{cases} 0 & V_{GS} < V_{ON} \\ \mu C_{INS} \dfrac{W}{L}(V_{GS} - V_{ON}) \cdot V_{DS} & V_{GS} > V_{ON};\ V_{GS} - V_{ON} > V_{DS} \\ \mu C_{INS} \dfrac{W}{2L}(V_{GS} - V_{ON})^2 & V_{GS} > V_{ON};\ V_{GS} - V_{ON} \le V_{DS} \end{cases} \qquad (1.3)$$

at higher drain voltages the current reaches a constant value and becomes almost independent of the drain voltage. This property can be used to calculate the mobility in this saturation region using equation 1.4.

$$\sqrt{I_{Drain}} = \underbrace{\sqrt{\mu C_{INS}\frac{W}{2L}}}_{SLOPE}(V_{GS} - V_{ON})$$

$$\mu = \frac{(SLOPE)^2}{C_{INS}\frac{W}{2L}} \tag{1.4}$$

Alternatively the mobility can also be extracted under the conditions, $V_{GS} - V_{ON} >> V_{DS}$. In this regime the current is linearly proportional to the applied drain bias. Hence the first differential of the current with respect to the gate voltage is proportional to the mobility (Equation 1.5).

$$\mu = \frac{1}{C_{INS}\frac{W}{L}}\frac{\partial I_{DRAIN}}{\partial V_{GS}}\bigg|_{V_{GS}>>V_{DS}} \tag{1.5}$$

This is called the linear region mobility. The saturation region mobility is usually higher than the linear region mobility for an organic transistor. This is a result of the non-ideal injection of charge carriers into the semiconductor through the metal contacts. Therefore to accurately measure the FET mobility it is necessary to have a good ohmic source and drain contact. A high mobility transistor is desirable as it implies a faster frequency of operation of circuits composed out of the semiconductor.

1.3.1.2 Time of flight mobility

The time of flight mobility is measured from the time a packet of photogenerated carriers take to cross the entire thickness of a semiconductor layer. This method is more

suited to organic LEDs in which the organic material is present between two parallely placed non-injecting electrodes at least one of which is transparent[30].

A schematic of the experiment is shown in Figure 1.9. In this method the sample is exposed to a short pulse of light. The pulse gets strongly absorbed in the semiconductor, through the transparent electrode, and generates positive and negative charge carrier pairs very close to the electrode. An electric field exists in the semiconductor due to the applied biases at the two electrodes. Depending on this preexisting electric field only one kind of carrier starts moving towards the other electrode which is nominally connected to ground through a resistor. The current through the resistor reflects the conduction and displacement currents flowing in the material due to the movement of the charges.

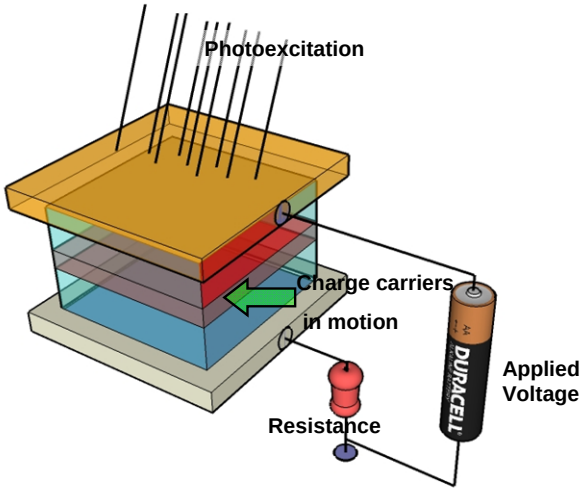

Figure 1.9 Schematic representation of optical time-of-flight experiment.

The measured current under these conditions can be expressed as the space averaged conduction current as shown in Equation 1.6.

$$I(t) = \frac{1}{L}\int_0^L j_{COND}(x,t)\cdot \partial x \tag{1.6}$$

The time for the carriers to travel the entire length of the organic material can be determined from the current profile which then yields the mobility. For the experiment to correctly determine the mobility of the material certain conditions need to hold true, firstly the RC time constant of the circuit should be much smaller than the time taken for carriers to cross the thickness of the material and this time must be small compared to the deep-trapping lifetime "τ_d", secondly the drift velocity needs to be uniform across the material, the spreading of the charge carriers due to coulombic repulsion needs to be small.

Figure 1.10 represents the plot of photocurrent with time in a *log-log* scale. For ideal trap free conditions equation 1.6 would result in a rectangular current profile that is constant from the time the light pulse is incident to the time when the carriers reach the ground electrode. However, as can be seen in Figure 1.10 the plot represents two distinct decreasing segments intersecting each other at t = τ. Where "τ" is the transit time of the carriers. This behavior is typical of disordered semiconductors with dispersive hopping transport and has been explained by Scher and Montrol[30] using a time dependent random walk. For a perfectly ordered semiconductor the time a carrier takes to hop can be expressed by Equation 1.7 which is cahacterized by a single hopping rate "W".

$$\psi(t) = W\cdot e^{-W\cdot t} \tag{1.7}$$

A single hopping rate leads to a Gaussian transport where the charge packet travels with a constant velocity, and the packet travels while maintaining its gaussian profile. However for a disordered semiconductor there is a distribution of hopping times rather than a distinct one. The distribution being given by Equation 1.8.

$$\psi(t) \sim (Const.)\cdot t^{-(1+\alpha)} \qquad 0<\alpha<1 \tag{1.8}$$

Where 'α' is a characteristics of the disorder in the semiconductor. The resultant expression for the photocurrent was shown to be asymptotically proportional to $t^{-1+\alpha}$ before $t < \tau$ and $t^{-1-\alpha}$ for $t > \tau$ .It was also seen that the average of the distribution takes a time equal to τ to cross the thickness of the material. The drift mobility is then calculated from τ using equation 1.9.

$$\mu_{Drift} = \frac{L^2}{V \cdot \tau} \tag{1.9}$$

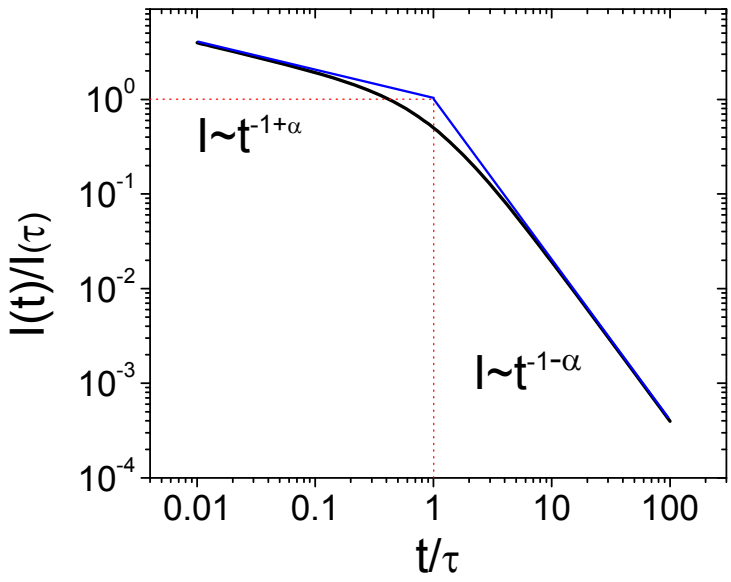

Figure 1.10 log-log plot of photocurrent versus time.

Both the FET and the drift mobility have their specific advantages, and either have been used to understand charge transport in organic semiconductors. However, the FET mobility for a particular semiconductor is different from the time-of-flight mobility. This is due to the different crystallographic direction in which the two transports take place. For a FET the charge carriers move along the channel while for an optical time-of-flight the carriers move perpendicular to the channel. Thus for an anisotropic

semiconductor these mobilities can differ substantially. In Chapter 3 we have introduced an electronic time-of-flight method that combines the advantages of the ease of the FET mobility measurement with the insightful time-of-flight mobility.

1.4 Conclusion

After this Introduction, the various charge transport theories are discussed in Chapter 2. In Chapter 3 a novel method of characterizing mobility is introduced and the theoretical aspect of the characterization discussed. Chapter 4 follows with a discussion of the experimental details of the method discussed in Chapter 3. Chapter 5 describes an alternate method for the extraction of mobility using a small signal impulse voltage rather than a large signal pulse. Finally this dissertation ends with a summarization in Chapter 6.

References:

[1] W. Shockley, Bell Syst. Techn. J. **28**, 435 (1949). U.S. Patent 2524035 — J. Bardeen et. al, U.S. Patent 2569347 — W. Shockley

[2] U.S. Patent 3138743 , U.S. Patent 3138747 , U.S. Patent 3261081, U.S. Patent 3434015 – J. Kilby.

[3] G.E. Moore, "Progress in Digital Integrated Electronics", *IEEE Int'l Electron Device Meeting Tech. Digest*, 11-13. (1975).

[4] U.S. Patent 4124287— Xerox Corp.

[5] http://nobelprize.org/nobel_prizes/chemistry/laureates/2000/presentation-speech.html.

[6] Rogers, J.A.; Bao, Z.; Baldwin, K.; Dodabalapur, A.; Crone, B.; Raju, V.R.; Katz, H.E.; Kuck, V.J.; Amundson, K.; Ewing, J.; Drzaic, P. *Proc. Nat. Acad. Sci.* **98**, 4835-4840 (2001).

[7] W. Clemens, W. Fix, J. Ficker, A. Knobloch, A. Ullmann, *J. Mater. Res.* **19**, 1963 (2004)

[8] B. Crone, A. Dodabalapur, A. Gelperin, L. Torsi, H. E. Katz, A. J. Lovinger, and Z. Bao. *Appl. Phys. Lett.* **78,** 2229-2231. (2001)

[9] B. R. Eggins, Chemical Sensors and Biosensors, J. Wiley & Sons. (2002).

[10] S. R. Forrest*, MRS Bulletin*, **30**, 28 - 32 (2005).

[11] http://www.orgworld.de/

[12] N. Karl, K.-H. Kraft, J. Marktanner, M. Münch, F. Schatz, R. Stehle, and H.-M. Uhde, *J. Vac. Sci. & Tech.* **17**, 2318-2328 (1999).

[13] J.L. Brédas, J.P. Calbert, D.A. da Silva Filho, J. Cornil, Organic semiconductors: a theoretical characterization of the basic parameters governing charge transport, *Proc. Nat. Acad. Science*. *USA* **99,** 5804-5809 (2002).

[14] C. Dimitrakopoulos and D. J. Mascaro, *IBM J. Res & Dev.* **45**, 1. (2001).

[15] A. Salleo, T. W. Chen, A. R. Völkel, Y. Wu, P. Liu, B. S. Ong, and R. A. Street, *Phys. Rev. B* **70**, 115311 (2004).

[16] M. Pope and C.E. Swenberg, *Electronic Processes in Organic Crystals and Polymers*, Oxford University Press (1999).

[17] H. Bässler, *Phys. Stat. Sol.* B **175**, 15 (1993).

[18] E.M. Conwell, *Phys. Rev.* **103**, 51 (1956).

[19] A. Miller and E. Abrahams, *Phys. Rev.* **120**, 745 (1960).

[20] N.F. Mott and E.A. Davies, *Electronic processes in non-crystalline materials*, 2*nd Edition*, Oxford University Press, London (1979).

[21] D. Monroe, *Phys. Rev. Lett*. **54**, 146 (1985).

[22] M.C.J.M. Vissenberg and M. Matters*, Phys. Rev. B* **57**, 12964 (1998).

[23] Y.-Y. Lin *et al.*, *IEEE Trans. Electron Dev. Lett.* **18** (1997), p. 606.

[24] H. Klauk *et al.*, *J. Appl. Phys.* **92** (2002), p. 5259.

[25] A. Facchetti, *Mater. Today,* **10**, 28 (2007)

[26] A. Assadi *et al.*, *Appl. Phys. Lett.* **53** (1988), p. 195.

[27] B.S. Ong *et al.*, *J. Am. Chem. Soc.* **126** (2004), p. 3378.

[28] I. McCulloch, M. Heeney, C. Bailey, K. Genevicius, I. MacDonald, M. Shkunov, D. Sparrowe, S. Tierney, R. Wagner, W. Zhang, M. L. Chabinyc, R. J. Kline, M. D. McGehee, and M. F. Toney, Nat. Mater. **5**, 328 _2006_.

[29] A. S. Dhoot, J. D. Yuen, M. Heeney, I. McCulloch, D. Moses, and A. J. Heeger, Proc. Natl. Acad. Sci. U.S.A. **103**, 11834 (2006).

[30] H. Scher. E. W. Montroll, *Phys. Rev. B.* **12**, 2455 (1975)

2 REVIEW OF CHARGE TRANSPORT THEORIES

2.1 Introduction

The transport properties of carriers through organic semiconductors are dominated by the presence and distribution of carrier trapping sites. The traps are mainly results of disorder in the organization of organic semiconducting molecules or polymer chains; however presence of chemical or physical impurities can also lead to trapping centers. The most important aspect of crystal defect is that they modify the available energy levels in their vicinity often leading to the presence of accessible vacant orbitals in the forbidden energy gap E_g, thereby making it possible for a carrier to become highly localized or trapped. Defects can also act as carrier scattering centers even if they do not trap carriers.

2.2 Defects

Method of crystal growth and its rate of formation determine the trap distribution in a particular organic semiconductor. The most common defects in an organic crystal is a schottky defect, which is a point defect formed by a vacancy; an empty site in the crystal structure. Any molecule which has its ionization energy lower or its electron affinity higher than that of the molecule of interest, behaves as a hole trap or an electron trap respectively. These unwanted molecules when present in small amount among the host molecules are termed as impurities. Chemical impurities, isolated or clustered, near vacancies or extended defects are the primary source of trap states in organic crystals[1]. The other major type of defects is a dislocation defects which can be reduced by

annealing at high temperatures[2]. It is therefore extremely important to use a purified semiconductor to reduce the point defects and trap distribution.

The traps are distributed spatially and energetically in a semiconducting layer. There are two important distribution functions that are used to characterize the dispersion in trap energies in the forbidden energy gap. One is the exponential distribution function proposed by Rose[3] and modified by Mark and Helfrich[4]. It is given by equation

$$H(E_t) = \frac{H_t}{kTl} \exp(-\frac{E_C - E_t}{kTl}) \tag{2.1}$$

Where *H(t)* is the density of trapping states at energy E_t and H_t is the total trap density, l is an empirical parameter[5], greater than unity, than defines how the trap density changes with trap energy. E_c is assumed to be above E_t.

The other is a Gaussian distribution proposed by Silinsh[6] is of the form

$$H(E_t) = \frac{H_t}{\sqrt{2\pi\sigma^2}} \exp(-\frac{(E_t - E_m)^2}{2\sigma^2}) \tag{2.2}$$

Where H_t is the total trap density, E_m is the center of the distribution and sigma is the dispersion of trap energies around E_m.

The exponential distribution is simpler to use and in many cases, will give results that are close to that obtained with the Gaussian distribution. Hence in most cases it is experimentally difficult to differentiate between the two trap distributions given by Equations 2.1 and 2.2.

In addition to the bulk traps described above there are also trap states at the surface due to impurities. When traps are present at the surface, a surface space charge layer is produced by the exchange of charges between the bulk and the surface. This redistribution of charges results in band bending at the surface. Unless most stringent

steps are taken to keep the surface clean, surface phenomenon caused primarily by the space charge layer, will play a major role in determining charge injection efficiencies in organic semiconductors.

2.3 Carriers processes and mechanisms

Mobile charge carriers introduced into a semiconducting layer through a contact or by radiative generation either

1. Gets trapped at a trap state and becomes mobile again by various detrapping mechanisms or
2. Recombines with a carriers of opposite polarity and undergo radiative or non-radiative decay or
3. Exit through contacts.

These mechanisms involving the charge carrier are described in the following sections.

2.3.1 CHARGE CARRIER INJECTION

Mobile carriers can be introduced into semiconducting organic materials by a variety of processes. If the charges enter through a contact at the boundary it is essentially referred to as charge injection[7]. The common feature between the charge injection mechanisms is the excess density of charge carriers at the contacts which energetically favors their introduction into the semiconductor. The different charge injection mechanisms are discussed below.

2.3.1.1 Thermal injection from metals.

At high temperatures the kinetic energy of a fraction of the available carriers in the metal contact becomes high enough so that they can cross over the potential barrier at the metal semiconductor junction and get injected into the semiconductor, this is known as thermionic emission. Thermionic emission follows Richardson's law (Equation 2.3)

$$J = A(1-\sigma)T^2 \exp\left(-\frac{\varphi_0}{kT}\right)$$
$$A = \frac{4\pi m k^2 e}{h^3} = 1.20173\times10^6\ A/m^2K^2 \tag{2.3}$$

Where J is the maximum current density that can be injected over an energy barrier φ_0 in the absence of high field effects. A is constant known as the Richardson's constant and σ is a reflection coefficient for carriers entering from metal to the semiconductor. The barrier for injection of electrons or holes depends on the relative values of the Fermi level of the metal and the HOMO or LUMO energies respectively.

In the presence of an electric field this barrier is reduced according to the field-enhanced thermionic emission theory proposed by Schottky.

$$J = A\left(1-\sigma\right)T^2 \exp\left(-\frac{E-\Delta E}{kT}\right)$$
$$\Delta E = \left(\frac{e^3 E_C}{4\pi\varepsilon_0}\right)^{1/2} \tag{2.4}$$

The metal and the semiconductor have different work functions i.e. when they are physically apart their Fermi levels are at different distances from the vacuum level. Therefore when they are brought into contact the bands within the semiconductor bend so that the Fermi level is constant. The vacuum level is assumed to bend accordingly. However recent studies[8] have shown that the vacuum level is not continuous due to the formation of an interfacial dipole layer. This effect of the dipole layer can be modified by

deliberately introducing a self-assembled monolayer[9] that aids injection of charge carriers into the semiconductor.

2.3.1.2 Optical excitation

When the material is optically excited, it results in the absorption of light that ultimately results in the formation of excitons. The exciton, if singlet in nature, either decays via the Förster transfer or form an electron hole pair. A triplet exciton on the other hand doesn't result in a carrier pair. The electron-hole pair once separated through the action of an external electric field can participate in conduction. The efficiency of formation of an electron hole pair depends on multiple things including the efficiency of the absorption of light, the creation and diffusion of the exciton, the impact of an exciton on the active surface, the dissociation of the exciton to produce a carrier pair and lastly the dissociation of the carrier pair under the action of an electric field.

2.3.1.3 Trapping of charge carriers.

A primary role in determining the mobility of carriers in an organic semiconductor is played by the trapping mechanisms in the solid. Trapped are created by the presence impurities and crystal defects, however even in the absence of these carriers can be trapped by interaction with phonons which is termed as self trapping. Self trapping is basically a result of local distortion caused by the polarization field associated with the moving carrier. Such carriers which are predominant in organic semiconductors are termed as polaron.

2.3.1.3.1 Polaron

A polaron[10] is a quasiparticle composed of an electron or a hole and its associated lattice distortion. It can be defined as a slow moving electron or a hole traveling in a dielectric medium, that interacts with the lattice ions through long range forces producing a polarization field around itself that travels with the electron or hole, shown in Figure 2 (a),(b). In other words it can be described as a cloud of phonon accompanying an electron/hole as it carries its lattice distortion while moving through the medium.

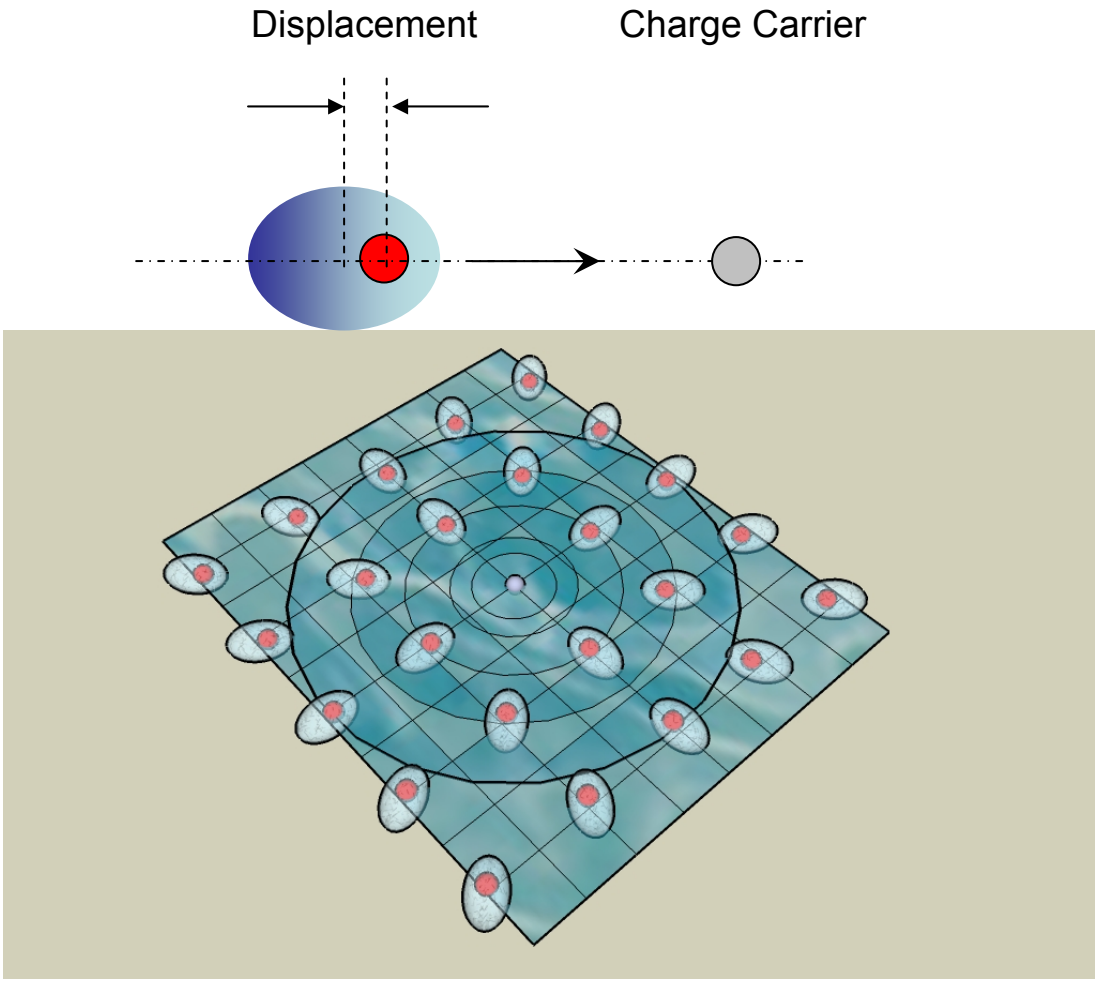

Figure 2.1 (a). Schematic description of a polaron the charge carrier (in the center) causes polarization of the molecule. (b) In a periodic lattice this results in a polarization field centered around the carrier that travels with the carrier.

In a pure crystal, an excess carrier state can display two rather distinct limiting types of behavior depending on the degree of spatial localization of the charge that arises from the phonon-carrier interaction. A delocalized charge is characterized by a mobility that is grater than 1 cm^2/Vs and a temperature coefficient varying as T^{-n}, where $n > 1$. A localized charge, on the other hand, has a mobility that is significantly less than 1 cm^2/Vs and has activation energy. It is possible in principle for both types of behavior to coexist, particularly if the solid is highly anisotropic[11]. In cases where the mobility is ≈ 1 cm^2/Vs, a situation obtains in which relatively small effects can combine to change a delocalized charge state into a localized state.

2.3.1.3.2 Small polaron – Holstein Model.

This is a simplified model of transport of polarons in organic systems. Simplifications were made so that the principal features of the problems are unchanged[12]. As shown in Figure 2.2, a one-dimensional molecular crystals consisting of diatomic molecular sites separated by distance ***a***, was considered. Each site possessed a single vibrational degree of freedom, that along the single dimension, represented by the deviation from its equilibrium internuclear separation, x_n. The 'local' energy of the molecule E at each site was assumed to be dependent on x_n (Equation 1.)thus introducing an electron-lattice interaction.

$$E(x_n) = -A \cdot x_n \tag{2.5}$$

Where A is the proportionality constant. A tight binding approach is used in the treatment for the motion of the electron, i.e. the electron wavefunction is represented as the superposition of the wave-functions of the individual molecules as in Equation 2.

$$\Psi(\vec{r},\, x_1,\, x_2, \ldots\, x_N) = \sum_n a_n(x_1,\, x_2, \ldots\, x_N)\ \phi(\,\vec{r}\ -\ n\vec{a},\, x_n\,) \tag{2.6}$$

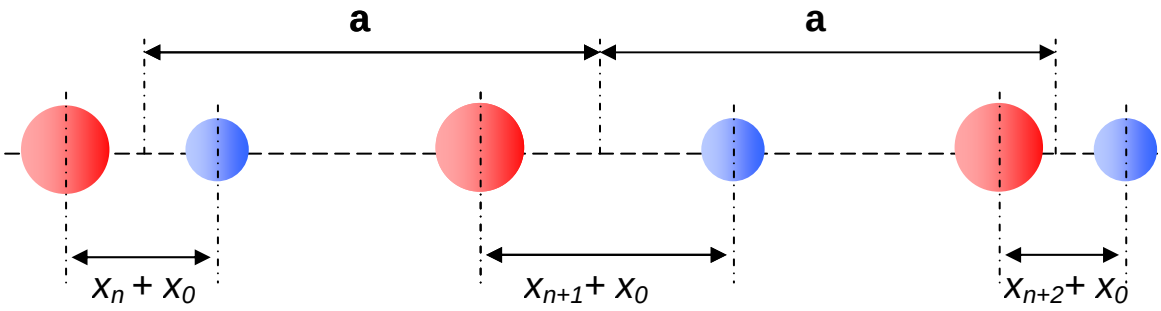

Figure 2.2. Schematic representation of the Holstein model that considers a one-dimensional molecular crystals consisting of diatomic molecular sites separated by distance '**a**'. Each site possessed a single vibrational degree of freedom, that along the single dimension, represented by the deviation from its equilibrium internuclear separation, 'x_n'.

The major advancement of this theory over conventional tight binding approximation was the lifting of the translational degeneracy by introduction of energy dependence on x_n.

The solution to the problem involved consideration of two cases depending on the linear dimension of the polaron L_P compared to the lattice spacing $\boldsymbol{a}$. In the case of large polaron or the dimension of the polaron being large compared to the lattice spacing an exact solution was obtained. It was shown that the linear dimension of a large polaron is of the order of

$$L_P \sim a\frac{4J}{\left(\frac{A^2}{2M\omega_0^2}\right)} \tag{2.7}$$

Where J is the wavefunction overlap between neighboring sites, which was assumed constant. M is the relative mass of the diatomic molecule. And ω_0 is the harmonic vibration frequency. It was therefore deduced that for the condition $L_P >> \boldsymbol{a}$, the electronic bandwidth $2J$ has to be large compared to $A^2/2M\omega_0^2$. It was also established that the polaron binding energy given by Equation 2.8

$$E_P = \frac{A^2}{2M\omega_0^2} - 2J \tag{2.8}$$

is maximum when the bandwidth is infinitely narrow and is given by $A^2/2M\omega_0^2$.

Therefore it was inferred that the ratio of the maximum binding energy to the electronic bandwidth determines the size of the polaron.

2.3.1.3.3 Self-trapping of charge carriers.

The charge carriers that conduct in organic semiconductors are polaronic in nature. When the linear dimension of the polaron becomes comparable to the lattice spacing and the lattice distortion essentially confined to the nearest neighbors, it is called a small polaron. The motion of a small polaron was analyzed by Holstein[13] using a similar framework, as described above. It was assumed that the electronic wave-function overlap is small compared to the total energy of the electron. In the Hamiltonian for the system these electronic overlap between neighboring sites ($n \rightarrow n \pm 1$) appeared as non-diagonal terms. The vibrational-mode of the system is represented by a quantum number N_k, which gives the degree of excitation of the electron. Thus the electronic overlap terms were interpreted as a small perturbation. In zeroth order: in the absence of these non-diagonal terms: the electron is localized at a given site n and is completely defined by the quantum number N_k. The presence of a non-vanishing electronic-overlap term gives rise to transitions in which the electron "jumps" to neighboring sites. At sufficiently low temperatures the diagonal transitions are dominant and they result in the formation of Bloch- type bands with bandwidths decreasing with temperature. The role of the non-diagonal elements in the Hamiltonian, in the low temperature regime, is essentially that of scattering. In the absence of other scattering mechanism such as impurity scattering they determine the electronic transport properties of the polaron including its mobility.

With rising temperature the probability of the off-diagonal goes up exponentially, this combined with the reduction in bandwidth results in an exponentially reducing mobility. The mobility continues to reduce until half of the Debye temperature is reached. The Debye temperature is the temperature of the maximum allowed phonon frequency. Under this condition the energy uncertainty associated with the finite lifetime of the states equals the electronic bandwidth and therefore the bands loose their individual characteristics. For temperatures higher than this the electron was considered to move by a process of diffusion. This process of diffusion constitutes of random jumps between neighboring sites which is termed as hopping.

The small polaron model was improved by Emin[14]. In the expanded model a carrier occupying a molecule can be coupled to multiple molecular vibration modes, or phonons, rather than just a single vibrational mode as envisioned in the original model. Therefore in the generalized model the activation energy for hopping is the sum of contributions associated with the activation energies of the coupled phonons.

Despite its simple framework, the predictions of the Holstein model were consistent with magnitudes and temperature dependence of mobilities calculated experimentally[15]. The exponential square-root dependence of mobility with electric field at high field strengths were also rationalized using the model.

2.3.1.4 Detrapping.

Carriers once trapped can become mobile by various detrapping mechanisms such as absorption of a phonon from the local surrounding or thermal detrapping. The probability for thermal detrapping follows standard Boltzman equations given by Equation 2.9

$$p\left(E_t\right)=\nu\cdot\exp\left(-\frac{E_C-E_t}{kT}\right) \tag{2.9}$$

Where attempt to escape frequency factor ν is given by Equation 2.10, v is the thermal velocity, σ is the capture cross-section of the trap and N_C is the effective density of states within kT of the conducting band edge.

$$\nu=\mathrm{v}\cdot\sigma\cdot N_C \tag{2.10}$$

In addition to thermal detrapping it is possible for optical and electric field detrapping to occur, through absorption of a photon or reduction in barrier height respectively.

2.3.1.5 Recombination of carriers.

Excess charge carriers of opposite polarity can annihilate each other by recombining through radiative and non-radiative processes. Recombination usually takes place through formation of a variety excited states such as singlet, triplet or charge-transfer excitons.

2.4 Carrier transport

Depending on the relative values of the nearest neighbor overlap, the electron-phonon coupling constant and the disorder energies, transport in organic semiconducting materials can be classified in to band transport or hopping transport.

2.4.1 BAND TRANSPORT

In an ordered crystal where the nearest neighbor overlap energy exceeds the disorder energy and the transport can be described using the conventional

Table 2.1. Temperature dependence of scattering processes (W is the bandwidth, $\hbar\omega$ is the optical phonon energy. From 16)

Scattering Processes	Mobility : Wide Band W>kT	Mobility : Narrow Band W≤ kT
Acoustic Phonon		
One-Phonon	$T^{-3/2}$	T^{-2}
Two-Phonon	--	T^{-3}
Coulombic	$T^{3/2}$	T^{-1}
Neutral Impurities	T^{0}	T^{-1}
Optical Phonon		
One-Phonon	$T^{1/2}[exp(\hbar\omega/kT) -1]$	$[exp(\hbar\omega/kT) -1]$
Two-Phonon	--	$[exp(\hbar\omega/kT) -1]^{2}$
Dislocation	$T^{-1/2}$	T^{-1}

Bloch band states represented by the crystal momentum $\hbar\mathbf{k}$, the spin quantum number *s* and a band index n. Carriers are delocalized and are transported in these bands until scattered from one Bloch state to another. In classical terms scattering is the process that causes carrier to loose their velocity. Scattering is possible by various processes including phonons, impurities or defect[16]. A list of scattering processes is listed in Table 2.1 along with its effect on the dependence of mobility with temperature.Therefore the mobilities are limited by scattering and it is usually inversely dependent on temperature[17]

(Figure 2.3.). In the Boltzman formalism applied to the band model the mobility μ is expresses in terms of the carrier velocity *v(**k**)* as

$$\mu = \frac{e}{kT} < \tau(\vec{k})v(\vec{k})v(\vec{k}) >_0 \tag{2.11}$$

Where *τ(**k**)* is the relaxation time, and the brackets denote the thermal average over the equilibrium distribution. The carrier velocity can be expressed in terms of the energy-momentum dispersion relation *E(**k**)* as given by Equation 2.12.

$$v(\vec{k}) = \hbar^{-1} \frac{\partial E(\vec{k})}{\partial \vec{k}} \approx \frac{Wa}{\hbar} \tag{2.12}$$

For an organic crystal the consistency of the band model requires that

$$\mu \geq \frac{ea^2}{\hbar} \frac{W}{kT} \tag{2.13}$$

This is about 1cm^2/Vs at 300 K. Thus the two regimes of transport are differentiated at room temperature by a border line mobility of 1 cm^2/Vs.

2.4.2 HOPPING TRANSPORT IN DISORDERED SOLIDS.

In a disordered material the lattice phonons are strongly coupled to the charge carrier. The wave momentum k that characterizes band states is not conserved. Therefore, the charge carrier motion, at each lattice site, is randomized by scattering, i.e., the strong phonon-electron coupling results in the formation of a localized polaron. This type of motion, namely a series of uncorrelated jumps is called hoping transport. The hopping mobility can be written as in Equation[18].

$$\mu = \frac{ea^2}{kT} P \tag{2.14}$$

Where *P* is the hopping probability per unit time. The expression of probability *P* differs between various hopping theories depending on approximations made. As shown in Figure 2.4 the transport model for hopping transport can vary depending on the density

of states[19]. The total number of hopping models that have been formulated and reported in the literature is large. A few prominent one are discussed here.

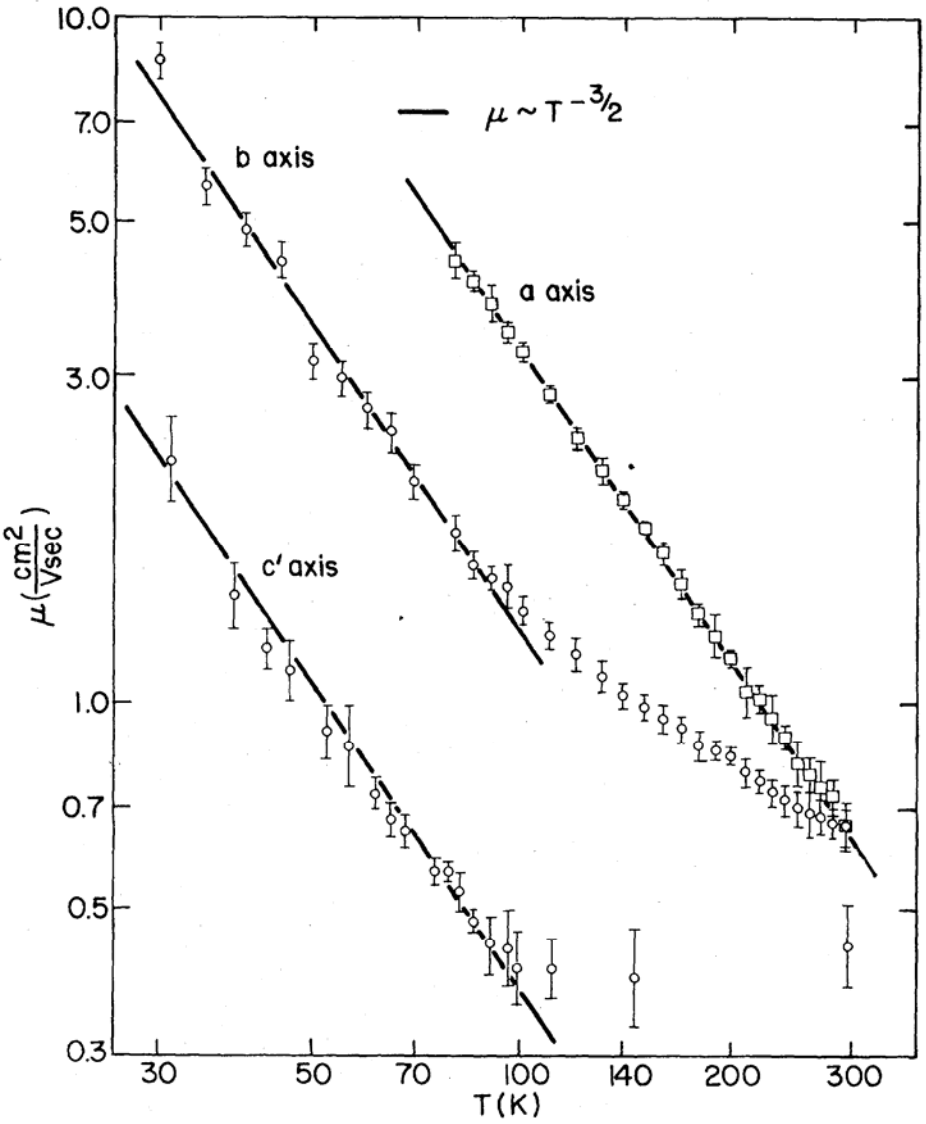

Figure 2.3 Measured electron drift mobilities along the a, b, c' directions in naphthalene as a function of temperature. The mobility is inversely proportional to a power of the temperature which indicates a band transport with scattering. From 17 printed with permission from APS.

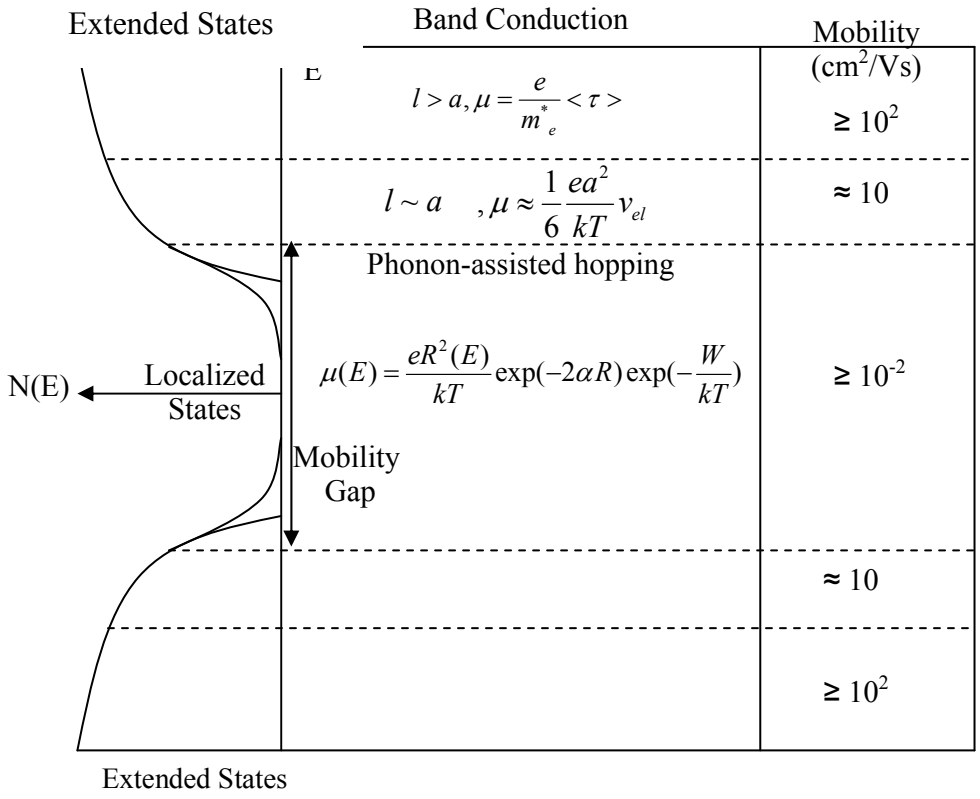

Figure 2.4 The types of transport model for hopping transport can vary depending on the density of states. W is the activation energy for hopping, ν_{ph} is the frequency of phonon, and ν_{el} is an electronic frequency of the order $\hbar/m_e a^2$. Adapted from 19.

2.4.2.1 Dispersive hopping.

The dispersive hopping transport is similar to the small polaron model discussed in section 2.2.2.2 in the sense that the probability of transition depends on the wavefunction overlap between the initial and the final states. The motion is thermal activated, activation being necessary to surmount the energy barrier. The transit time in the time-of-flight experiments depend according to equation

$$t_T \propto \left(\frac{L}{E}\right)^{\frac{1}{\alpha}} \quad 0 < \alpha < 1 \tag{2.15}$$

Where L is the length of transit, which is usually the thickness of the material, E is the electric field, and α is l^{-1} where l is the parameter defined for exponential distribution in Equation 2.1.

2.4.2.2 Trap controlled hopping.

In trap controlled hopping, a carrier is activated from its trapped state with an activation energy that is higher than the activation energy for small polaron hopping. This energy is used by the carrier to get detrapped and hop from one state to another until it encounters another trap state. As the name suggests the transit time for time-of-flight mobilities is controlled by the concentration of trap and therefore it follows an exponential dependence to the concentration of traps as given in Equation.

$$t_T \propto \exp\left(\frac{2\rho}{\rho_0}\right) \tag{2.16}$$

Where ρ denotes the concentration and ρ_0 is the spatial distribution of charge density outside a molecule, also known as its localization radius.

2.4.2.3 Multiple trapping.

The Multiple trap and release model is a derivation of the mobility-edge transport model used for hydrogenated amorphous silicon (a-Si:H)[20]. It was proposed by Horowitz et. al. as a step towards understanding charge transport in organic field effect transistors (OFETs)[21]. It differentiates the energy levels into localized and mobile states which are separated by a mobility edge that marks the boundary between the two. The model also assumes that a majority of the carriers injected into the semiconductor are trapped into states localized in the forbidden band. Carriers undergo thermal detrapping and get

excited into mobile states where they participate in conduction, until they come across a defect site and get localized into trapped state by releasing a phonon.

The conductivity sigma is therefore given by the concentration of free carriers n_f times a microscopic mobility μ_0, which is varies slowly with temperature.

$$\sigma = e \cdot n_f \cdot \mu_0 \tag{2.17}$$

where e represents the electronic charge. when θ, a parameter representing the fraction of free carriers, is introduced into the equation.

$$\theta = \frac{n_f}{n_{tot}}; n_{tot} = n_f + n_t \tag{2.18}$$

where n_{tot} is the total (free plus trapped) density of charges, equation 2.17 can be rewritten as

$$\sigma = e \cdot n_{tot} \cdot \theta \cdot \mu_0 \tag{2.19}$$

Equation 2.19 shows that a thermally-activated conductivity can be interpreted, either by a thermally activated charge density n_f that equals $\theta\, n_{tot}$ and a constant mobility μ_0, or a thermally activated mobility μ that equals $\theta\, \mu_0$ and a constant charge density n_{tot}. In this case, the field-effect mobility at low-gate biases equals the effective mobility μ, and is hence thermally activated, whereas it approaches the slowly varying microscopic mobility μ_0 at high V_G. The predicted high gate voltage regime is similar to the trap-filled regime described by Lampert[22], where all traps are filled and any additional injected charge can move freely with the microscopic mobility.

The success of the MTR model lies in its ability to explain temperature and gate voltage dependence of mobility. However it often yields unnaturally high values of trap density states. This is because the multiple trap and release model is valid only for a trap

distribution consisting of a shallow distinct energy level close to the main transport band (the conduction or valence band for classical n- and p-type semiconductors, respectively).

2.4.2.4 Percolation

Percolation, is the term used for movement of material through a random network of obstacles. The movement of charge carriers in disordered material is analogous to percolation in the sense that charge carriers move through high conductivity grains that are separated by low conductivity grain boundaries. There is a finite probability of the carrier making a transition over the grain boundaries. Percolation theory predicts that there is threshold of this transition probability below which transport is not possible. This is called the percolation threshold. If only nearest neighbor jumps are permitted , it has been shown that the dependence of the conductivity σ to the concentration of conducting sites C is given by

$$\sigma \propto (C - C_0)^{\gamma} \tag{2.20}$$

where γ is a constant. Percolation theory applied to the transport in PVK by Silver et. al[23] yielded a value of 1.8 for γ. Recently Vissenberg et. al.[24] has used percolation theory to understand gate voltage dependence of mobility in a polymer field effect transistor. The major achievement of this model was the successful explanation of simultaneous dependence of mobility on gate voltage and temperature as shown in Figure 2.5.

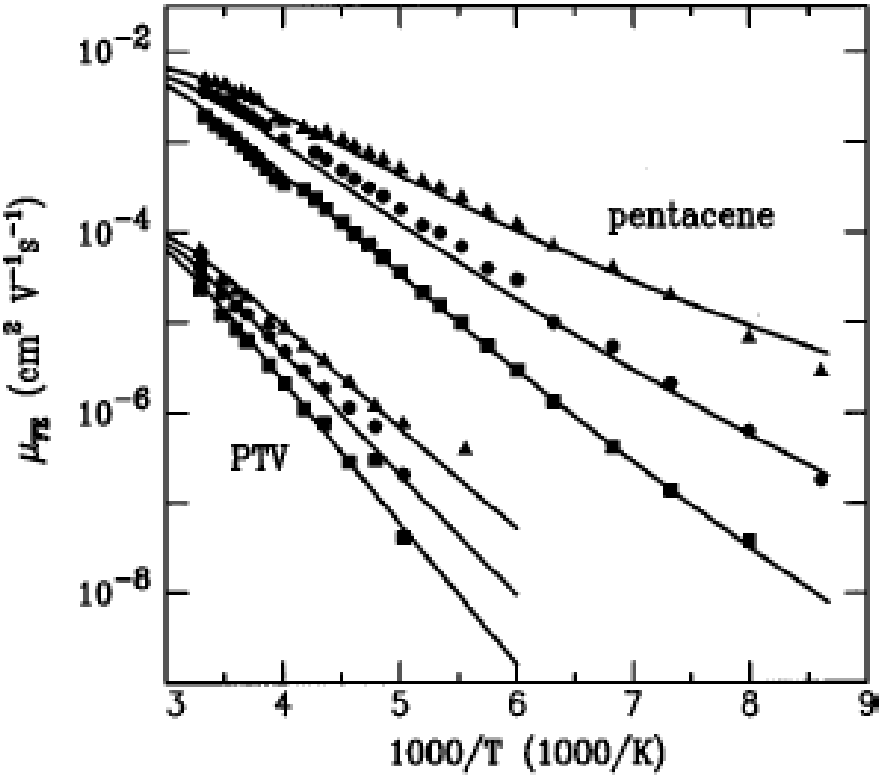

Figure 2.5. Solid dots represent field-effect mobility in a pentacene and poly(thienylene vinylene) OTFTs as a function of gate voltage and temperature. The lines are fit to the data using percolation theory based hopping model proposed by Vissenberg and Matters. .From 24 printed with permission from APS.

2.4.3 CARRIER TRANSPORT IN POLYMER AND MOLECULAR CRYSTALS

In the recent past there has been a lot of interest in polymeric semiconductors as active materials for organic thin-film transistors (OTFTs). This is primarily because of their ability to be processed from solution, which makes them ideal candidates for low cost large area applications such as wide screen displays and flexible circuits. Their commercial importance along with their unique charge transport properties necessitates the study of transport in this class of materials. There are several models that attempts to understand the charge transport properties, a few of which are discussed here.

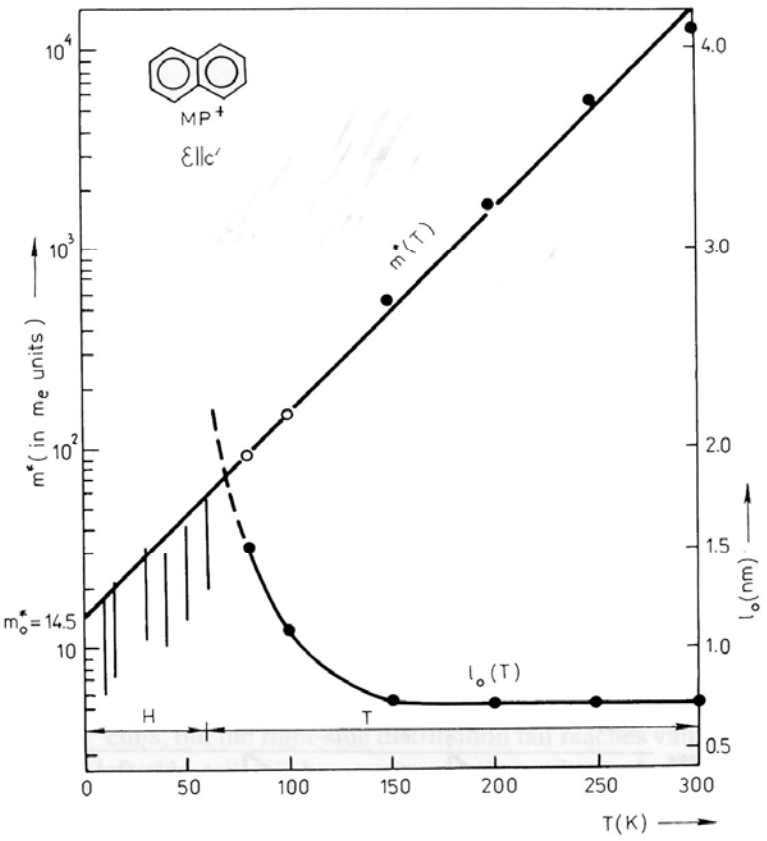

Figure 2.6 Plot of effective mass and mean free path with temperature as estimated by the Silinsh-Čápek model along the c' direction of naphthalene crystal. From 26 printed with permission from Elsevier.

2.4.3.1 Silinsh-Čápek Model.

The Silinsh-Čápek model is similar to the band transport theory for polarons with a temperature dependent effective mass to explain the temperature dependence of mobility.

$$m_{eff}(T) = m_{eff}(0)\exp(T/T_0) \tag{2.21}$$

Where $m_{eff}(0)$ is the effective mass at $T = 0\ K$, and T_0 is an constant[25]. However in the high temperature regime (T >100 K) the mobility in the conventional band transport

mobility reduces as an inverse power of the absolute temperature. In order to account for this, the theory introduces a temperature dependent mean-free path l_0 and the effective mass assumes a form given by equation 2.22.

$$m_{eff}(T) = \frac{3e^2 l_0^2}{\mu^2 kT} \tag{2.22}$$

The dependence of effective mass is shown in Figure 2.6[26].

2.4.3.2 Kenkre Formulation: Correlated disorder model.

The theoretical treatment of this model was done by Kenkre et. al[27] and the field dependence of charge carrier mobilities was worked out by Dunlap and Kenkre[28]

1. The following assumptions were made in order to solve the problem.
2. The mobility is thermally activated due to the carriers being polaronic in nature.
3. The diagonal disorder terms discussed in section 2.3.2.2 are small by non-zero.
4. The librational phonon plays a significant role in the transport along a particular direction although its different along different crystallographic directions.

The generalized master equation given by equation 2.23, which involves the transfer of charge from one site to another, is the primary tool in describing transport.

$$\frac{\partial P_m(t)}{\partial t} = \int_0^t ds \sum_i \left\{ W_{m,i}(t-s) P_i(s) - W_{i,m}(t-s) P_m(s) \right\} \tag{2.23}$$

$P_m(t)$ is the probability that a carrier is at site m at time t. A velocity auto-correlation function defined by Kenkre is used to calculate the mobility, which is given as

$$\mu_{ii} = \frac{2ea^2}{kT} \exp\left(-2g_i^2 \coth\left(\frac{\beta\hbar\omega_0}{2}\right)\right) \int_0^\infty dt \cdot M(t) \left|\frac{V_i}{\hbar}\right|^2 \qquad (2.24)$$

where g_i are the dimensionless electron-libration coupling constant, ω_0 is the libration frequency, V_i are the intersite interaction potential, and M(t) is a complex function composed of Bessel function. Figure 2.7. shows the excellent fits of this expression to the experimental data obtained for drift mobilities of naphthalene as a function of temperature.

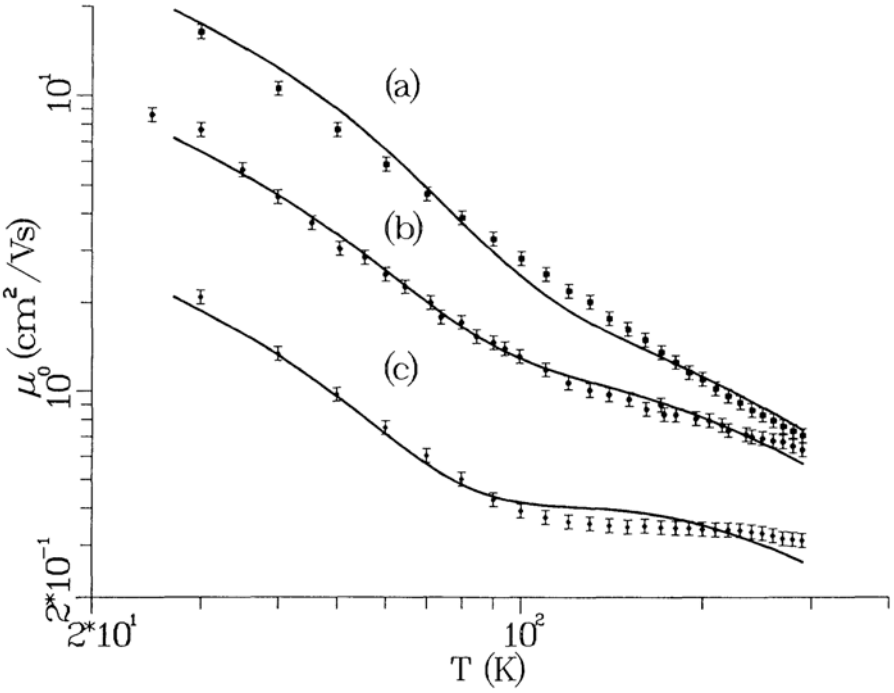

Figure 2.7 Fits to the drift mobility calculated along the 1, b, 3 axes of naphthalene to the Kenkre formalism (solid lines).Fit shows an excellent match to the experimental data. From 28 printed with permission from APS.

2.5 Conclusion

Theoretical characterization of charge transport in organic semiconductors, is difficult due to the presence of non-linearities created by defects and traps. It is understood that movement of carriers depend on density of states, which is determined by concentration and distribution of trapping centers. There have been multiple attempts to understand the density of states, most of which have involved either characterizing the field effect or the optical time-of-flight mobility. In the following chapter we have introduced a new method that combines the advantages of both these methods. It uses the time-of-flight of a charge packet injected by a voltage pulse to calculate the drift velocity and mobility of carriers. This technique can help to improve our understanding of charge transport by providing a new method to characterize the mobility.

References

[1] G. A. Cox, P. C. Knight, *J. Phys. Chem. Sol.* **34**, 1655, (1973).

[2] N. T. Corke, J. N. Sherwood, R. C. Jarnagin, *Crystal Growth* (1969).

[3] A. Rose, *Phys. Rev.* **97**, 1538, (1955).

[4] P. Mark, W. Helfrich, *J. App. Phys.*, **33**, 205, (1962).

[5] J. S. Bonham, D. H. Jarvis, *Aust. J. Chem.*, **30**, 705 (1977).

[6] E. A. Silinsh, *Organic Molecular Crystals: Their Electronic States* Springer-Verlag, (1980).

[7] N. F. Mott, R. W. Gurney, *Electronic processes in ionic crystals,* Oxford (1946).

[8] H. Ishii, K. Sugiyama, E. Ito and K. Seki, *Adv. Mater.* **11**, 605, (1999).

[9] Z. Bao *Adv. Mater.* **12**, 227 (2000)

[10] N. W. Ashcroft, N. D. Mermin, Solid State Physics, Saunders, 1976

[11] D. Emin, *Phys. Rev. Lett*., **28**, 604, (1972).

[12] T. Holstein, *Annals of Physics,* **281** 706-724 (2000).

[13] T. Holstein, *Annals of Physics,* **281** 725-773 (2000).

[14] D. Emin *Phys. Rev. B.* **43**, 11720 (1991)

[15] C. Wood, D. Emin *Phys. Rev. B*. **29**, 4582 (1985).

[16] L. B. Schein*, Phys. Rev. B*. **15**, 1024, (1977).

[17] J. D. Anderson, C. B. Duke, V. M. Kenkre, *Phys. Rev. Lett* **15**, 2202, (1983).

[18] J. Yamashita, T. Kurosawa, *J. Phys. Chem. Sol.* **5**, 34 (1958).

[19] W. E. Spear, Ann. Rept., Conf. Elect. Insul. Diel., Natl. Acad. Sci. Washington, DC., ISBN:0-309-02032-8 (1971).

[20] P. G. Le Comber and W. E. Spear, *Phys. Rev.Lett.* **25**, 509, (1970).

[21] G. Horowitz, P. Delannoy, *J. App. Phys.* **70**, 469, (1991).

[22] M. A. Lampert, *Phys. Rev.* **103**, 1648, (1956)

[23] M. Silver, K. Risko, H. Bässler, *Philos. Mag. B.* **40**, 247, (1979)

[24] M. Matters, M. C. J. M. Vissenberg, *Phys. Rev. B.*, **57**, 12964, (1998).

[25] E. A. Silinsh, V.Čápek, *Organic Molecular Crystals: Interaction, Localization, and Transport Phenomena* AIP-Press, New York, (1994).

[26] E. A. Silinsh, G.A. Shlihta, A. J. Jurgis, *Chem. Phys.*, **138**, 347, (1989).

[27] V. M. Kenkre, J. D. Andersen, D. H. Dunlap, C. B. Duke., *Phys. Rev. Lett.*, **62**, 1165, (1989).

[28] V. M. Kenkre, D. H. Dunlap, *Phil. Mag. B.*, **65**, 831, (1992).

3 ELECTRONIC TIME-OF-FLIGHT METHOD

3.1 Introduction

Organic and polymer transistor based circuits are being investigated for a number of low-cost, large-area applications, particularly those that are compatible with flexible plastic circuits[1, 2, 3]. The organic materials that have been used as active semiconductor materials include both sublimed and solution processed semiconductors such as pentacene[3], oligothiophenes[4], hexadecafluoro copper-phthalocyanine[5], polythiophene[6] etc. This choice of materials opens up several possibilities to develop integrated circuit technologies based on organic transistors for various large-area low-cost applications. However, the future of printed electronic displays and circuit applications utilizing organic transistors is dependent on the performance of solution processible semiconducting polymers. Therefore it is necessary to obtain a detailed understanding of charge transport in polymers such as poly(3-hexyl)thiophene.

Most studies of charge transport in polymers employ field-effect mobility measurements[7,8,9]. Temperature dependent measurement of the field effect transistor (FET) mobility has provided numerous insights on the characteristics of the charge carriers. Temperature dependent measurements of FET mobility have highlighted the role of disorder in transport. A percolation model for hopping applied to a slowly decaying exponential band-tail have been used with success to describe movement of carriers in solution processed amorphous polymers and small molecules[9]. However, in a non-crystalline semiconductor such as organic polymers, the FET mobility μ_{FET} is different the trap-free mobility μ as most of the carriers remain trapped in the band-tail

states[7,8,9]. Consequently the FET mobility doesn't necessarily reflect the drift velocity of the carriers.

In this chapter an alternate technique to characterize the drift velocity, drift mobility, and trap distribution in organic transistors have been discussed[10]. The electronic time-of-flight (TOF) technique discussed here directly measure the drift mobility in organic FETs. It involves the injection of carriers at the source of a p-type transistor followed by their subsequent extraction at the drain contact. The delay between the two events is used to extract the velocity of the carriers.

3.2 Mobility extraction by pulse voltage method.

The objective of the experiment is to study transport in p-type semiconductors by extracting the carrier velocity and hence the mobility of carriers in these materials. Carriers inside the semiconductor move in response to an electric field. The electric field is created by applying a voltage bias between two metal contacts, one kept nominally at ground. The contact at higher potential is the terminal where the carriers are injected. This contact therefore serves dual purpose. Firstly it helps establish the field and secondly it acts as an injection point. The other electrode is tied to the ground through a small resistor, so that the exiting carrier current produces a voltage that can be used to identify the time of their transit.

In a FET geometry the higher potential is applied to the source electrode and the drain electrode is connected to the resistor. The third gate electrode is kept at ground so that a low carrier concentration is maintained in the channel initially. An initial low carrier concentration is needed for reasons discussed in chapter 5. Another advantage of this method is that the electric-field can be varied to study its effect on the mobility.

3.3 Distinction between optical and electronic TOF.

Although the electronic time-of flight technique shares similarities with the optical time-of-flight it varies markedly in the conditions that govern transport. Firstly the direction of transport in electronic TOF is perpendicular to the direction of growth of crystal, whereas in an optical TOF experiment it is along the direction of crystal growth. For an organic semiconductor which is inherently anisotropic, these two directions can have markedly different mobilities. Secondly in an optical TOF the displacement component of the total current is equally important to the conduction current. However in an electronic TOF the displacement current is orders of magnitude smaller than the conduction current and hence can be neglected. Thirdly the carriers that transit in an optical TOF experiment are created by optical excitation; therefore the density of carriers in electronic states depends on the spectrum of the optical source used. The distribution of excess carriers does not follow the equilibrium statistics dictated by Fermi-Dirac distribution. On the other hand, injection of carriers in an electronic TOF flight is through a combination of field-aided thermionic emission, and tunneling through the energy barrier[11]. The injection process depends non-trivially on the distribution of band gap state, interface dipoles, phonon distribution[12]. The transit-times in an electronic TOF flight contain critical information about the injection process which cannot be obtained from the optical TOF data. Lastly an optical TOF experiment is extremely capital intensive and exceeds in its degree of complexity when compared to the simple electronic TOF experiment that requires electronic equipments like an oscilloscope and an pulse-voltage generator that are readily available in any electronic laboratory.

3.4 Mathematical description.

The problem deals with obtaining the time dependent carrier distribution $\rho(x,t)$ flowing through the channel in response to a voltage $V(x = 0, t)$ applied to the source ($x = 0$) of a transistor, the gate and drain ($x = L$) are connected to ground. The voltage waveform $V(x = 0, t)$ is assumed to be a step function $U(t)$ with the step occurring at the initial instant.

$$\begin{aligned} V(x=0,t) &= V \cdot U(t) \\ V(x=L,t) &= 0 \\ V_{GATE} &= 0 \end{aligned} \tag{3.1}$$

3.5 Analysis and solution.

The problem of pulse voltage technique can be approached in one of two equivalent ways. The first method involves the transmission line approach which considers the channel as an infinite resistance-capacitance ladder. The current flowing through the channel divides up into these two braches at every point, one that charge up the cannel and the other that flows towards the drain. The second method uses classical electrodynamics equations formulated by Maxwell with the assumption that the charge in the channel is controlled by the gate-substrate voltage difference. This helps in isolating this two-dimensional problem into a set of two independent linear differential equations along the two directions. Hence the name quasi-one dimensional approach.

3.5.1 TRANSMISSION LINE APPROACH.

This approach is useful for both the small as well as the large signal picture. As shown in Figure 3.1, the channel can be assumed to be composed of a series of resistor-

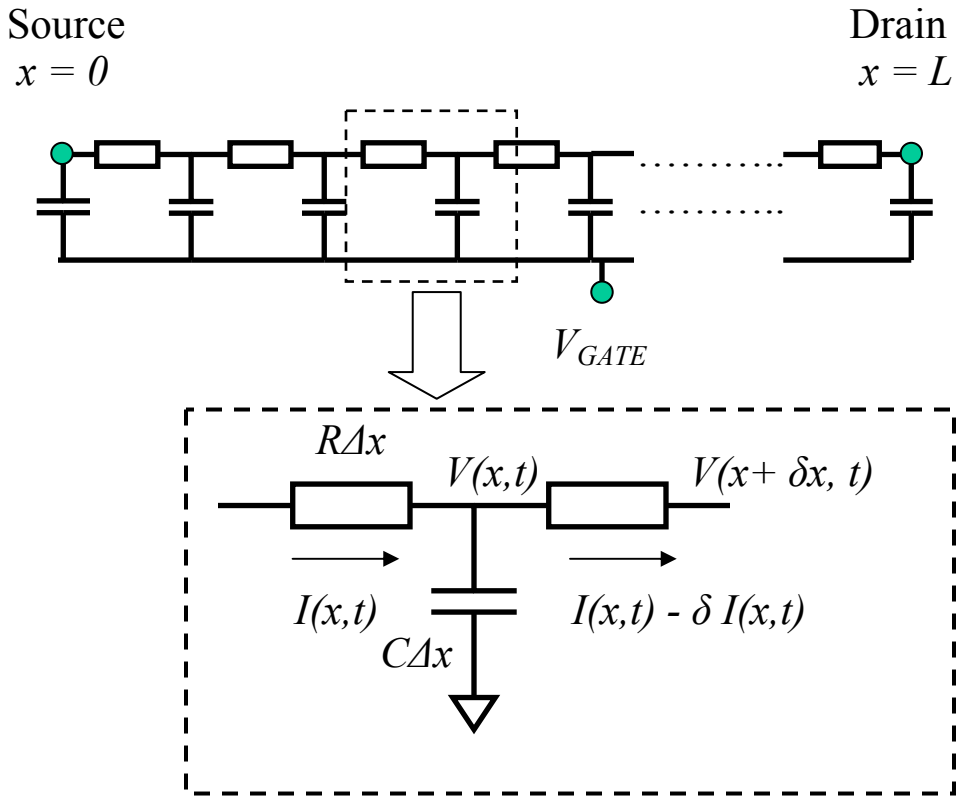

Figure 3.1 Schematic representation of RC transmission network approach to the pulse voltage problem.

capacitor network. An elemental portion of the channel is represented as a series resistor with and a parallel capacitor connecting to the gate electrode. The capacitance per unit length C is constant and is proportional to the insulator capacitance where as the resistance per unit length is a function of the charge induced by the gate-substrate voltage difference, hence it is a function of the channel voltage $V(x,t)$.

$$C = \frac{\varepsilon_0 \varepsilon_I}{T_I} W \tag{3.2}$$

where W is the channel width, ε_0 is the permittivity of free space, ε_I is the relative dielectric constant of the gate insulator and T_I is the insulator thickness.

$$G = R^{-1} = \mu \cdot C \cdot (V_G - V_{ON} - V(x,t)) \tag{3.3}$$

where μ is the hole mobility in the channel. G is the conductance per unit length which is inverse of the resistance R per unit length, and V_{ON} is the turn on voltage of the organic semiconductor channel defined in section 1.3.1.1. At a time t and a distance x from the source, the displacement current that flows through the capacitor results in reduction of $I(x,t)$ given by

$$-\frac{\partial I(x,t)}{\partial x} = C \cdot \frac{\partial (V(x,t) - V_{GATE})}{\partial t} \tag{3.4}$$

This helps in charging up the channel and reducing the resistance that causes more current to flow. The current flowing through the resistor reduces the voltage as given by.

$$\frac{\partial V(x,t)}{\partial x} = -I(x,t) \cdot R \tag{3.5}$$

This results in the voltage wavefront moving forward along the channel. The current $I(x,t)$ can there fore be written in terms of $V(x,t)$ as

$$I(x,t) = -\mu \cdot C \cdot \left(V_{GATE} - V_{ON} - V\left(x,t\right)\right) \cdot \frac{\partial V(x,t)}{\partial x} \tag{3.6}$$

Therefore Equation 3.6 and Equation 3.4 form a simultaneous differential equation pair that can be solved to obtain the equation for the voltage $V(x,t)$.

The equation pair can be simplified by the following substitution

$$V'(x,t) = V_{GATE} - V_{ON} - V(x,t) \tag{3.7}$$

Hence the simultaneous equation pair reduces to

$$\frac{\partial I(x,t)}{\partial x} = C\frac{\partial V'(x,t)}{\partial t}$$
$$I(x,t) = \mu \cdot C \cdot V'(x,t)\frac{\partial V'(x,t)}{\partial x} \tag{3.8}$$

By eliminating *I(x,t)* from the equation pair 3.8 we get

$$\mu\frac{\partial}{\partial x}\left(V'(x,t)\frac{\partial V'(x,t)}{\partial x}\right) = \frac{\partial V'(x,t)}{\partial t} \tag{3.9}$$

This equation must be solved for *V'(x,t)* subject to the boundary conditions.

$$\begin{aligned} V'(0,t) &= -V(0,t) = V_0 \cdot U(t) \\ V'(L,t) &= -V(L,t) = 0 \\ V'(x,0) &= -V(x,0) = 0 \end{aligned} \tag{3.10}$$

In deriving the boundary condition the gate voltage is taken a zero, and the turn on voltage which is usually small is neglected.

3.5.2 QUASI-ONE-DIMENSIONAL APPROACH.

Figure 3.2 shows the schematic representation of the problem. The two dimensional problem of transiting voltage wavefront is a complicated one without any additional simplifying assumptions. By introducing the condition that the charge in the channel is controlled only by the gate voltage we reduce the complex problem into a set of two independent differential equations. The assumption is justified by the fact that the transverse electric field due to gate, at any point in the channel, exceeds the longitudinal electric field due to the applied source drain bias. The charge concentration which depends on the electric field by gauss law is therefore dependent mainly on the gate voltage. It has been shown by Alam *et. al.* that the transport in an organic channel takes place in the first few monolayers from the semiconductor-insulator interface[13]. Hence we further assume that the channel is two dimensional rather than three. Hence the charge

density can be expressed as a sheet of charge that changes from point to point along the

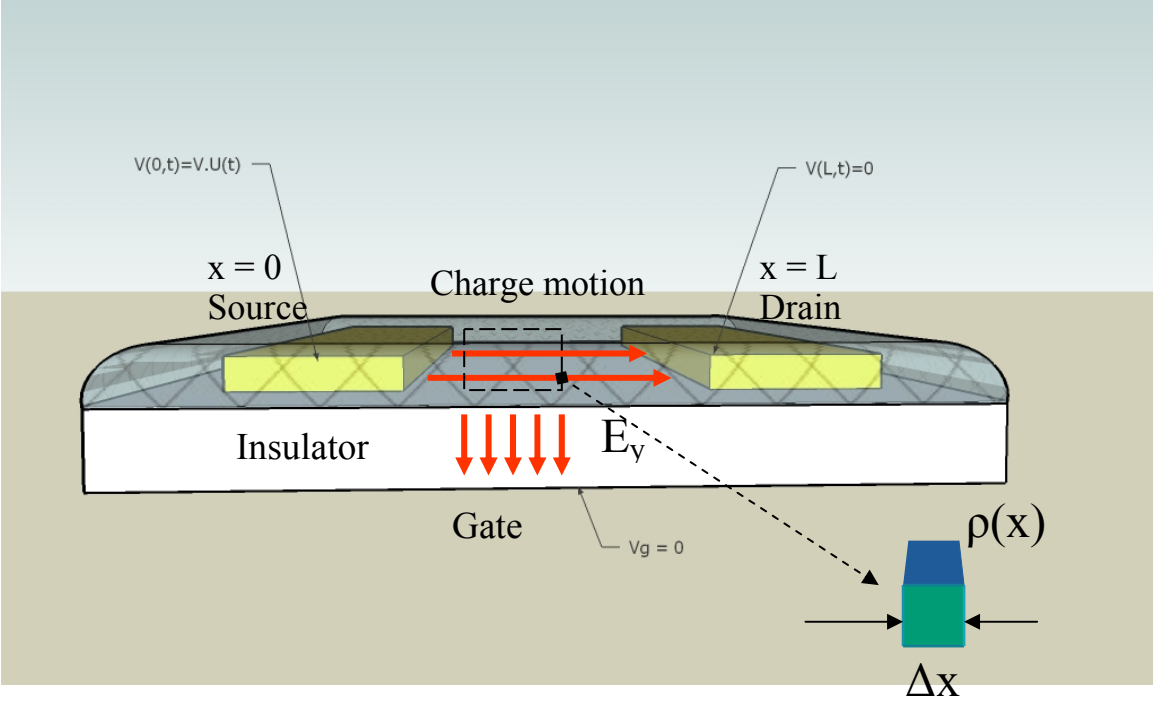

Figure 3.2. Schematic representation of the quasi-one-dimensional approach for solving the pulse voltage problem.

length of the channel while remaining uniform along the width of the channel. The continuity equation is there fore given by

$$\frac{\partial J}{\partial x}+\frac{\partial \rho}{\partial t}=0$$
$$\rho = ep(x,t) \tag{3.11}$$

By eliminating ρ from the above equation we get.

$$\frac{\partial J}{\partial x}=-\frac{e\partial p}{\partial t} \tag{3.12}$$

There current is conducted chiefly by holes as the mobility of electrons is much lower than that of holes in a p-type semiconductor. Also the drift component of the hole current is orders of magnitude large than it diffusion and displacement counterparts. These assumptions therefore lead to the current expression given in Equation 3.13

$$
\begin{aligned}
&J = J_N + J_P \\
&J_P >> J_N \;\; J \cong J_P \\
&J_P = -\mu ep\frac{\partial V}{\partial x} - eD_P\frac{\partial p}{\partial x} \\
&J_{P,Drift} >> J_{P,Diffusion} \\
&J = J_P = -\mu ep\frac{\partial V}{\partial x}
\end{aligned}
\tag{3.13}
$$

By elimination J from Equation 3.12 and 3.13, we get

$$
\frac{\partial}{\partial x}\left(\mu \cdot p \cdot \frac{\partial V}{\partial x}\right) = \frac{\partial p}{\partial t} \tag{3.14}
$$

The channel charge is given by Poisson's equation

$$
\begin{aligned}
&\nabla^2 V = \frac{\rho}{\varepsilon_0 \varepsilon_S} \;\; \rho = e(p-n) \\
&p >> n \\
&\frac{\partial^2 V}{\partial x^2} + \frac{\partial^2 V}{\partial y^2} = \frac{ep}{\varepsilon_0 \varepsilon_S}
\end{aligned}
\tag{3.15}
$$

Since the injected hole concentration is much higher than the electron concentration the resulting charge concentration can be assumed to be consisting entirely of hole. The Poisson's equation in integral form gives the gauss law

$$
\oint \varepsilon \vec{E} \bullet \partial A = Q_{enc} = \rho A \tag{3.16}
$$

For a long channel the x-component of the electric field can be neglected with respect to its y-component, this is also known as the long channel or the gradual channel approximation. Therefore Equation 3.16 yields.

$$
\begin{aligned}
&E_y >> E_x \;\; \vec{E} = E_y \hat{y} \\
&E_y = \frac{ep}{\varepsilon_{ox}}
\end{aligned}
\tag{3.17}
$$

The y-component of the electric field can be written in terms of the electric field as

$$E_y = \frac{V_{GATE} - V_{ON} - V(x,t)}{T_I} \tag{3.18}$$

Hence the charge concentration can be written in terms of the voltage as

$$\rho = e \cdot p(x,t) = e \cdot \varepsilon_0 \varepsilon_I \cdot \frac{V_{GATE} - V_{ON} - V(x,t)}{T_I} \tag{3.19}$$

p can be replaced in equation 3.14 to obtain the differential equation for the system.

$$\frac{\partial}{\partial x}\left(\mu \cdot (V_{GATE} - V_{ON} - V) \cdot \frac{\partial V}{\partial x} \right) = \frac{\partial (V_{GATE} - V_{ON} - V)}{\partial t} \tag{3.20}$$

3.5.3 EQUIVALENCE OF BOTH TECHNIQUES.

The introduction of the long channel approximation essentially reduces the differential equation for the quasi one dimension approach to the same differential equation. It can be seen that by applying the substitution in Equation 3.7 with the following conditions

V_{GATE} equals zero and the turn on voltage is small enough to be neglected, we arrive at the following differential equation

$$\frac{\partial}{\partial x}\left(\mu \cdot V' \cdot \frac{\partial V'}{\partial x} \right) = \frac{\partial V'}{\partial t} \tag{3.21}$$

Which is same as equation 3.9 for the RC transmission line approach. This can be further simplified into

$$\frac{\partial^2}{\partial x^2}(V')^2 = \frac{2}{\mu}\frac{\partial V'}{\partial t} \tag{3.22}$$

This is the equation of transport for the pulse voltage problem.

3.5.4 SOLUTION OF DIFFERENTIAL EQUATION.

To solve the equation we make the simplifying substitution result of which is to normalize the variables.

$$v = \frac{V'(x,t)}{V_o}$$
$$z = 1 - \frac{x}{L} \tag{3.23}$$
$$\tau = \frac{t}{T} \quad where \;\; T = \frac{L^2}{\mu V_0}$$

Equation 3.22 then reduces to

$$\frac{\partial v}{\partial \tau} = \frac{\partial}{\partial z}\left(v \frac{\partial v}{\partial z} \right) \tag{3.24}$$

With the following boundary condition

$$\begin{aligned} &v(1,\tau) = 1; \text{Gate to source voltage constant} = V_0 \\ &v(0,\tau) = 0; \text{Gate to drain voltage constant} = 0 \\ &v(z,0) = 0; \text{channel initially uncharged} \end{aligned} \tag{3.25}$$

From equation 3.24 it is apparent the rate of change of voltage is extremely slow at low voltages and identically zero at zero voltage. This characteristic is different from a linear resistor-capacitor circuit where the voltage is never identically zero at any finite distance or time. The solution can therefore be intuitively compared to a traveling wave and at a given time the voltage will be identically zero for distances greater than the wavefront.

The particular problem at hand belongs to a class of problems dealing with diffusion into a semi-infinite medium that have been discussed in depth by Wagner[14]. Following a similar approach the problem can be divided into two sections

1. For the duration of time before the wave front reaches the drain ($t < t_d$), the solution is similar to that of diffusion into semi-infinite medium.

During this period of time the boundary condition at the drain electrode is always satisfies because of the wave propagation behavior.

2. After the wavefront reaches the drain electrode. It stops progressing further and tries to settle down to its steady state value. $v = \sqrt{z}$.

The partial differential equation can be transformed into an ordinary differential equation by the substitution

$$y = \frac{1-z}{2\sqrt{\tau}} \tag{3.26}$$

which converts Equation 3.24 into

$$v\frac{\partial^2 v}{\partial y^2} + \left(\frac{\partial v}{\partial y}\right)^2 + 2y\frac{\partial v}{\partial y} = 0 \tag{3.27}$$

Equation 3.27 cannot be solved analytically hence the numerical solution is presented in Figure 3.3. As can be seen from Figure 3.3 the values of v greater than 0.81 are identically equal to zero. This implies for a particular point in the channel given by z_0, $v(z_0,\tau_0)$ is zero for a certain time in the beginning before the wave front reaches z_0. For the drain z_0 equals zero hence the time for the wave front to reach the drain is given by

$$\begin{aligned} z_0 = 0 &= 1 - 2\cdot 0.81\cdot\sqrt{\tau_0} \\ \tau_0 &= (1/1.62)^2 = 0.38 \end{aligned} \tag{3.28}$$

Hence the time for the carriers to reach the drain can be derived from Equation 3.28 to be

$$t_d = 0.38\frac{L^2}{\mu V_0} \tag{3.29}$$

For $t > t_d$ the voltage distribution tries to attain its equilibrium distribution given by

$$v = \sqrt{z} = \sqrt{1 - \frac{x}{L}} \tag{3.30}$$

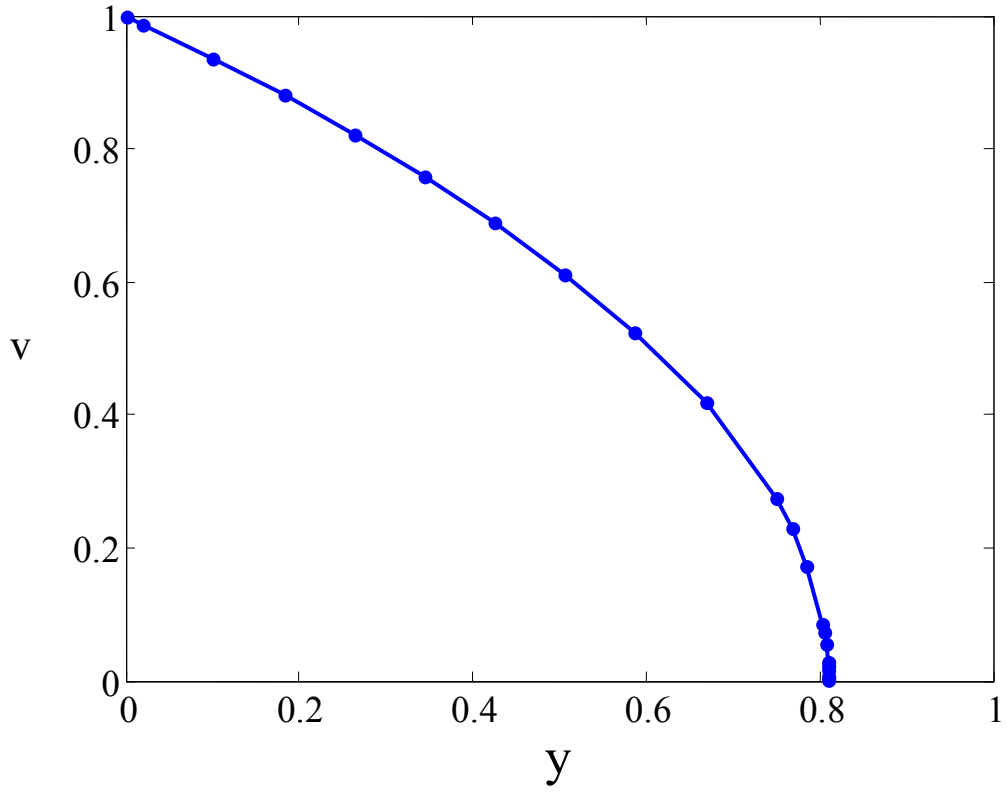

Figure 3.3. Numerical solution of Equation 3.27. It is evident that the variable v is identically equal to zero for values of y > 0.81.which implies that there is a finite amount of time for which there is no current at the drain.

Section 2 of this diffusion problem can be solved by making an approximation that the diffusion coefficient is a function of distance rather than voltage. This results in linearization of the partial differential equation 3.24 which then becomes.

$$\frac{\partial v}{\partial t} = \frac{\partial v}{\partial x} + x\frac{\partial^2 v}{\partial x^2} \tag{3.31}$$

In section 3.6 where we have simulated the transport it will be seen that the above approximation is justified due to the linear profile of the voltage distribution after it reaches the drain. It will also be seen in Figure 3.4 that the distribution doesn't change much after the wave front reaches the drain electrode; therefore it is reasonable to

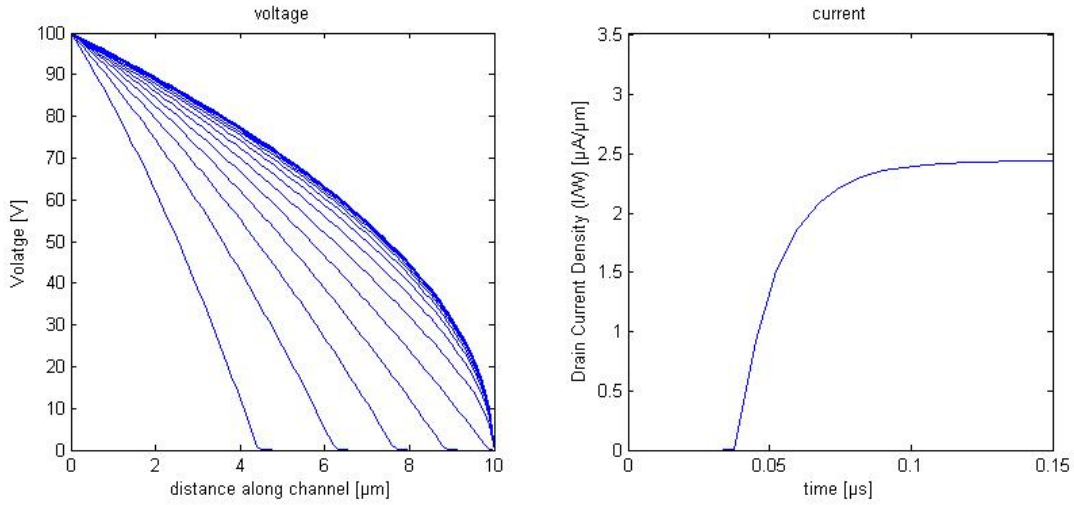

Figure 3.4. Simulation of transport of carriers along the channel of a transistor (L = 10 µm, µ = 0.1 cm2/Vs) in response to a step voltage (V0 = 100 V) applied at the source,(a) the voltage distribution along the channel at intervals of 10 nanoseconds.(b) the plot of drain current as a function of time.

approximate the solution as a sum of the steady state and an error term as in Equation 3.32

$$v(z,\tau) = \sqrt{z} + \frac{1}{2}\varepsilon(z\cdot\tau) \tag{3.32}$$

Substituting this into Equation 3.27 we obtain the following linear partial differential equation is obtained.

$$z^2\frac{\partial^2\varepsilon}{\partial z^2} + z\frac{\partial\varepsilon}{\partial z} - \frac{\varepsilon}{4z^{3/2}} = \frac{\partial\varepsilon}{\partial\tau} \tag{3.33}$$

This can be solved by standard separation of variables yielding a general solution of the form

$$\varepsilon(z,\tau-\tau_0)=\sum_{n=1}^{\infty}C_n J_{2/3}(\frac{4}{3}k_n\cdot Z^{3/4})\exp(-k_n^2\cdot(\tau-\tau_0)) \tag{3.34}$$

where k_n is the separation constant and $\tau > \tau_0$. J is a Bessel function of order 2/3 which ensures that the second boundary condition in Equation 3.25 is met since $J_{2/3}(0) = 0$.

the first boundary condition can be realized by choosing k_n appropriately so that

$$\begin{aligned} &J_{2/3}(\frac{4}{3}k_n)=0 \\ &\frac{4}{3}k_n=\alpha_n \end{aligned} \tag{3.35}$$

where α_n are the zeros of Bessel function $J_{2/3}$. Following the analysis of Burns[15] the constant factor C_n is chosen so that the best agreement between Equation 3.34 and the solution of Equation 3.31 is obtained. As shown in Figure 3.5 a weighing factor of 0.53 results in the best fit. Substituting equation 3.34 with appropriate values of constants into Equation 3.32 and using Equation 3.4, the defining relation of current, we obtain

$$\begin{aligned} &I_{Drain}(\tau)=0 \qquad\qquad \tau<0.38 \\ &I_{Drain}(\tau)=\frac{\mu C_I W}{L}V_0^{\,2}\left\{1-0.83\exp(-6.406(\tau-0.38))-0.17\exp(-2\cdot 6.406(\tau-0.38))\right\} \\ &\qquad\qquad\qquad\qquad \tau\geq 0.38 \\ &\tau=\frac{t}{L^2/\mu V_0} \end{aligned} \tag{3.36}$$

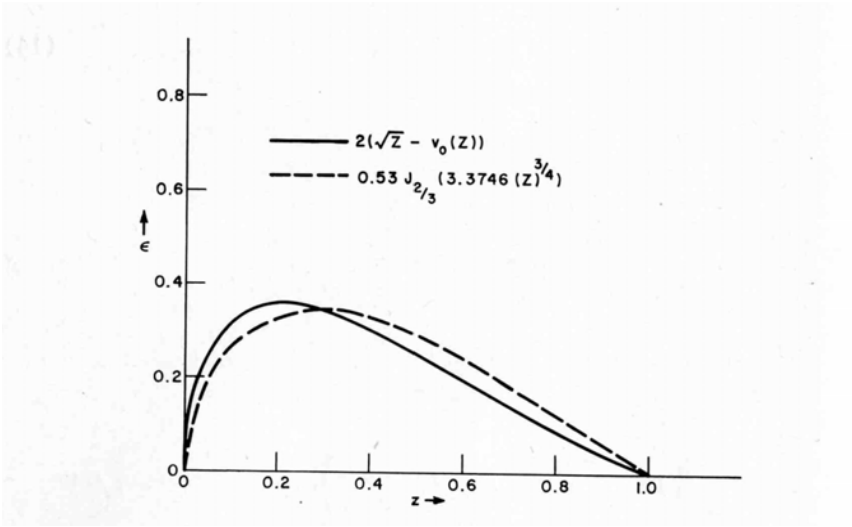

Figure 3.5. The solid curve represent the exact solution the pulse voltage problem obtained using numerically the dashes curve is an approximate solution to the problem given by equation 3.33. This solution is weighted by a factor of 0.53 to obtain the best match to the exact solution.(Reprinted from 15)

3.6 Simulation of transport.

Equation 3.36 provides an approximate solution to the problem of pulse voltage measurement of electronic TOF mobility. It is helpful in understanding the dynamics of the transport and extracting parameters of the semiconductor that affect transport of charge carriers. It is nevertheless essential to have an exact solution to the problem. Since it cannot be solved analytically we have to resort to numerical analysis.

We have simulated the movement of carriers in the channel in response to the application of a step voltage in MATLAB® (the program code for simulation of transport is given in Appendix I). The results of which are presented in Figure 3.4. There is finite amount of time when the drain current identically equal to zero, the time delay is inversely proportional to the mobility of the transistor. The inverse of the delay time gives the characteristic frequency of the transistor operating as an amplifier.

Determination of this parameter, therefore, specifies both the small-signal frequency and large-signal transient response of the device.

The simulation of Figure 3.4 is done assuming ideal step voltage, constant mobility, trapless semiconductor and ideal contacts. These ideal conditions do not exist in reality because, firstly there is always a finite amount of rise time for the pulse to go to its maximum, secondly the mobility of an organic semiconductor is dependent on a variety of conditions including the local field, the charge concentration etc. Thirdly traps in an organic semiconductor dominate transport, and finally non-ideal injection from contacts can adversely affect transport of charge carriers. In the following sub-sections we have tried to incorporate these effects into the simulation

3.6.1 RISE-TIME CORRECTION.

Assuming a linear rise from zero to maximum value V_0 of the voltage pulse we have simulated the transient response. Figure 3.6 shows the effect of finite rise time on the initial delay. As can be seen the curve shifts with increasing rise time, the shift being equal to half of the rise time. Therefore the expression for the initial from which the mobility is extracted needs to be modified as

$$t_{Delay}^{Ramped} = t_{Delay}^{unramped} + \frac{T_{ramp}}{2}$$
$$t_{Delay}^{unramped} = 0.38\frac{L^2}{\mu V_0} \tag{3.37}$$

In case of a non-linear rise, half of rise time (10% - 90%) can also be used as a approximate correction factor. Alternately the delay time can be measured from the time where the voltage is half of the maximum value. It will be seen later that for practical purposes it is always advisable to use a sharper pulse.

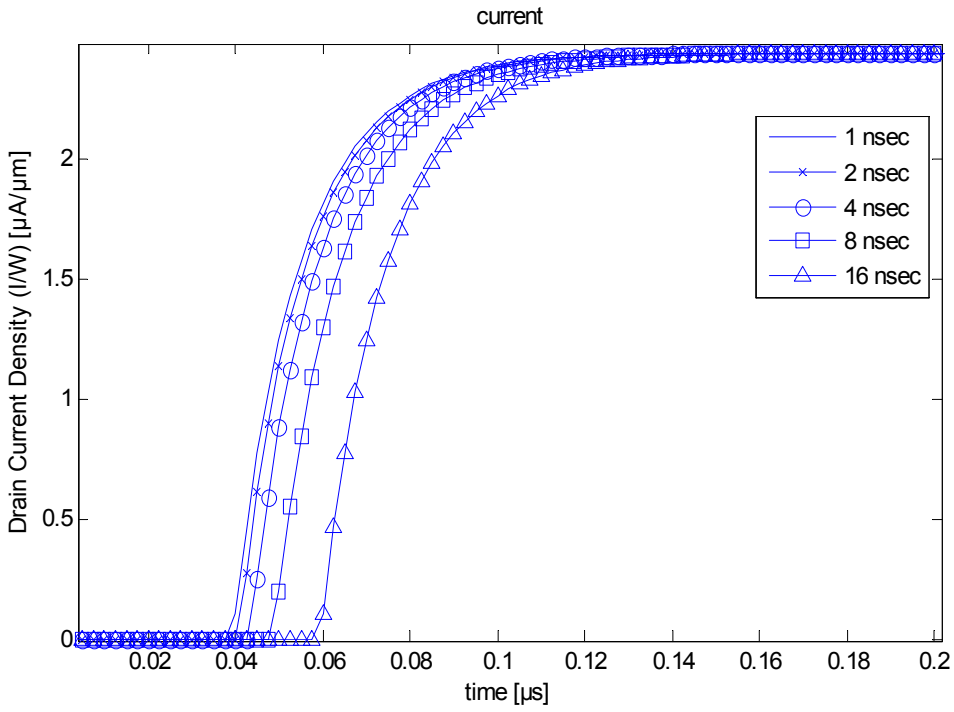

Figure 3.6 Effect of finite rise time on initial delay for the drain current to appear, Pulse applied to the source begins rise at t = 0. (L = 10 µm, V_0 = 100 V, µ = 0.1 cm^2/Vs)

3.6.2 EFFECT OF FIELD DEPENDENCE OF MOBILITY.

Investigation of *J-V* characteristics as a function of temperature has shown that the mobility of an organic semiconductor, under high fields, tends to follow a Poole-Frenkel behaviour[16] given as

$$\mu = \mu_i \exp\left(\frac{\beta\sqrt{E} - \Delta}{kT}\right) \tag{3.38}$$

Where where k is Boltzmann's constant, T is the temperature, E is the electrical field, Δ is zero field hopping barrier of the carriers, μ_i is intrinsic mobility without a hopping barrier, and β is the field-dependent coefficient. The expression of field dependence of mobility given in Equation 3.38 was originally proposed by Gill[17] and later modified by Poole and Frenkel[18]. The value of β is about 10^{-5}-10^{-4} eV/(V/cm)$^{1/2}$. on introducing the

field dependence of mobility (Equation 3.38.) in Equation 3.21 we get the field dependent transport equation

$$\frac{\partial}{\partial x}\left(\mu_0 \exp\left(\frac{\beta\left(\frac{\partial V'}{\partial x}\right)^{1/2}}{kT}\right)\cdot V'\cdot\frac{\partial V'}{\partial x}\right)=\frac{\partial V'}{\partial t} \tag{3.39}$$

Simulation were done for room temperature transient response with β varying between 10^{-6}-10^{-4} eV/(V/cm)$^{1/2}$ the results of which are shown in Figure 3.7. As is evident the initial delay isn't affected although the field dependence changes the final steady state value of the current. This is because of the simulation were done at room temperature where the effect is less prominent than at low temperatures. The electric field isn't also high enough to cause appreciable difference. Hence the delay time is given by the zero field mobility of the semiconductor.

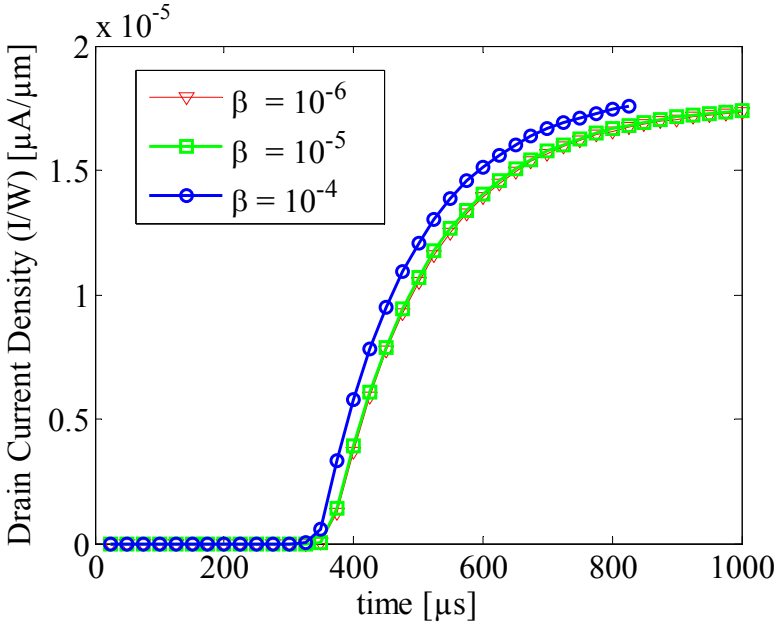

Figure 3.7. Simulation of electric field dependence of mobility at room temperature with L = 1 μm, V_0 = 1 V, μ_0 = 0.1 cm^2/Vs.

3.6.3 EFFECT OF A SINGLE TRAP LEVEL.

Defect and impurities, which lead to carrier localization, play a major role in transport of charge carriers in organic materials. As discussed in section 2.2 the density of states trail into the forbidden gap forming a band tail. The exact nature of the density of states in an organic semiconductor is not known precisely and it is a topic of intense investigation[7, 8, 9]. The effect of localized states is to slow down the carriers; therefore the response of the pulse voltage can also be expected to be slowed down by the presence of traps. Due to the uncertainty in the shape of the trap distribution and the computational complexity of simulating a distribution of trap states, we have used a simple model consisting of a single trap level characterized by a carrier lifetime τ. The current continuity equation can be rewritten as

$$\frac{1}{e}\frac{\partial J_p}{\partial x}+\frac{\partial \mathrm{p}}{\partial \mathrm{t}}=G_p-R_p$$
$$G_p=0; R_p=\frac{p-p_o}{\tau} \tag{3.40}$$

where p_0 is the intrinsic hole concentration in the semiconductor. The result of the simulation is shown in Figure 3.8. The blue curve represents transient response in the absence of trapping, while the life times of the green curves are marked beside them. It can be seen that for lifetimes larger than or equal to the delay time cause negligible change in the response. This is because the holes are transported across the channel before they can be trapped. The steady state current decreases as the lifetime is reduced because of the reduction in the number of carriers that participate in conduction by trapping. The result for multiple but finite number of trap levels would be similar with the lowest lifetime trap level dominating the transport. Studies of gate bias induced decay in current, also called bias-stress, indicate that the lifetime of carriers are in the order of a

fraction of a second[19]. Therefore the effect of a single trap level on the response would be negligible. However the distribution of states behaves much differently from a single or a collection of a finite number of trap states, which calls for a detailed study on its effect on the response.

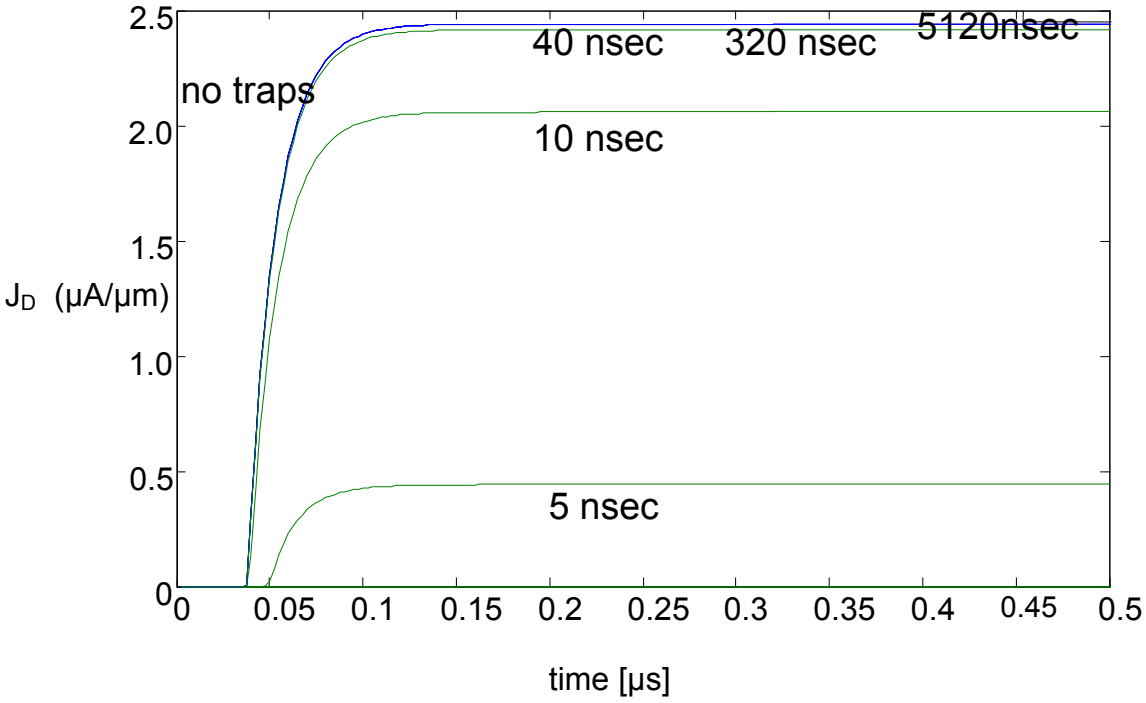

Figure 3.8. Simulation of the effect of a single trap level on the transient response at room temperature with L = 10 μm, V_0 = 100 V, μ = 0.1 cm^2/Vs. Blue curves represents trapless transport, and the lifetimes of carriers used for simulation are shown beside the green curves.

3.6.4 EFFECT OF INJECTION TIME.

For an ideal ohmic contact in an inorganic semiconductor the time for carriers to be injected from the metal to the semiconductor is much less than the dielectric relaxation time of the semiconductor[20], which is of the order of picoseconds. However, as discussed in section 3.3 the injection in organics is complicated and takes place through a

combination of field-aided thermionic emission and tunneling through the energy barrier. Baldo and Forrest[12] have recently proposed that injection is limited by charge hopping out of interfacial molecular sites whose energy distribution is broadened by disorder in the presence of the interfacial dipoles. The exact nature of trap distribution must be known to accurately determine the time it takes for carriers to be injected.

For the purpose of determining the delay in transient response at the drain of an organic transistor we have added a correction term t_{inj} in the expression for delay to account for the delays in injection and extraction at the contacts

$$t_d^{total} = t_{inj} + t_d^{channel} \tag{3.41}$$

3.7 Conclusion.

In this chapter we have discussed the theory behind an electronic method to directly obtain the drift mobility of carriers in an organic transistor. This technique is based on the application of a step voltage at the source of a transistor and measuring the consequent delay in the appearance of the injected carriers at the drain contact. The present techniques is a quick and easy way to determine the mobility, in addition it also present itself as a source of information for understanding injection into the semiconductor and determining the trap distribution. In the following chapters we will discuss the experimental detail and the characteristic of the mobility extracted using this method.

References

[1] Y-L. Loo, T. Someya, K. Baldwin, Z. Bao, P. Ho, A. Dodabalapur, H.E. Katz, J.A. Rogers, PNAS, 99, 10252 (2002).

[2] H. Klauk, M. Halik, U. Zschieschang, F. Eder, G. Schmid, C. Dehm, *Appl. Phys. Lett.* **82** 4175, (2003).

[3] C. D. Dimitrakopoulos, S. Purushothaman, J. Kymissis, A. Callegari, J. M. Shaw, *Science* **283**, 822 (1999)..

[4] G. Horowitz, D. Fichou, X. Peng F. Garnier, *Synth. Met.*, **45**, 163, (1991).

[5] B. Crone, A. Dodabalapur, Y. Lin, R. W. Filas, Z. Bao, A. LaDuca, R. Sarpeshkar, H. E. Katz, W. Li, (2000) Nature (London) 403, 521.

[6] Bao, Z., Dodabalapur, A. and Lovinger, A.J.(1996). Appl. Phys. Lett. 69, 4108-4110.

[7] Horowitz G., Hajlaoui R., Fichou D., El Kassmi A., J. App. Phy 85 (6) 1999.

[8] Street, R.A., Northrup, J.E., Salleo, A. Phy. Rev. B 71 16 (2005)

[9] Vissenberg M.C.J.M., Matters M., Phy. Rev. B 57 (20) 1998.

[10] L. Dunn, D. Basu, L. Wang, A. Dodabalapur, *Appl. Phys. Lett.*, **88** 063507, (2006).

[11] J. C. Scott, J. Vac. Sci. & Tech., 21, 521, (2003).

[12] M. A. Baldo, S. R. Forrest, Phys. Rev. B. 64, 085201, (2001)

[13] M. A. Alam, A. Dodabalapur, and M. Pinto, IEEE Trans. Elec.Dev. Spcl Issue, 44, 1332, (1997).

[14] C. Wagner, J. chem.. Phys. 18, 1227, (1950).

[15] J.R. Burns, RCA Review, 30, 15, (1969)

[16] L. Wang, D. Fine, D. Basu, A. Dodabalapur, J. App. Phys. 101, 054515, (2007).

[17] W. D. Gill, J. Appl. Phys. 43, 5033 (1972).

[18] J. Frenkel, Phys. Rev. 54, 647 (1938).

[19] H. Klauk, Organic Electronics: Materials, Manufacturing and Applications, Wiley-VCH, pp111 (2006)

[20] S. M. Sze Physics of Semiconductor Devices 2ed, John Wiley and Sons, pp 252, (1981)

4 MEASUREMENT OF DRIFT VELOCITY USING PULSE VOLTAGE METHOD.

4.1 Introduction

In Chapter 3 we discussed an electronic time-of-flight (TOF) method to directly and easily calculate the drift mobility and velocity of charge carriers in an organic thin film transistor[1]. The method is based on the application of a step voltage at the source which injects carriers and drives them towards the drain, the time taken for the carriers to traverse the channel is calculated for the time delay between the application of the source voltage pulse and the appearance of the resulting waveform at the drain. This method can be also used to explore trap states and achieve a more complete understanding of charge transport.

In this chapter the pulse voltage measurement is used to study the transport along various organic semiconductors. To study the effect of dielectric-semiconductor interface on the mobility we have compared the mobility of each of the semiconductors on multiple dielectrics. Finally we have characterized the dependence of mobility on both the channel length of the transistor and the voltage of the pulse waveform.

4.2 Materials used for fabrication.

A discussed before an organic transistor can be made in one of three possible ways. We have used the bottom contact bottom gate structure with the gate at the bottom, and source drain contact at the top. The fabrication of the structure is explained in detail

in section 4.3 after a short discussion of the organic semiconductor, insulators and self-assembled monolayers (SAMs) for surface treatment in that order.

4.2.1 ORGANIC SEMICONDUCTORS

The most important material required for fabricating an organic transistor is the organic semiconductor which forms the active layer for transporting carrier. It usually comes in two varieties, small molecules and polymers. Small molecules are usually deposited under vacuum by sublimation, whereas polymers are dispersed from solution. The crystallinity of the semiconductor is the principal factor in determining the mobility of the semiconductor, a high mobility enhances current density and increases switching speed and reducing voltages of operation to permit organic circuits to meet realistic specifications. For our experiment we have used a small molecule and another polymer semiconductor both of which have high mobility due to their relatively crystalline structure.

4.2.1.1 Pentacene.

Pentacene is a polycyclic aromatic hydrocarbon molecule consisting of five linearly-fused benzene rings (Figure 4.1 (a)) and has the appearance of a dark-blue powder. The chemical names with other details are listed in Table 4.1. Pentacene is one of the most commonly used organic semiconductors with the highest mobilities recorded till date. Pentacene, mobilities of 1.5 cm^2/Vs were reported by Lin *et. al.*[2] High performance pentacene devices have also been fabricated using polymer dielectrics with carrier mobilities of 3 cm^2/Vs[3]. However it is highly sensitive to light and oxygen and deteriorates in performance unless passivated. Most commercial samples of pentacene

appear dark purple due to ambient oxidization. Vacuum sublimation has been used to purify pentacene for fabricating our devices other methods for purification includes adsorption chromatography.

Pentacene is sublimed, at low pressures, onto the substrate, which is maintained at a relatively high temperature (75^{O} C), by heating pentacene above 350^{O} C. A smooth hydrophobic surface aids the formation of bigger grains and hence results in higher mobilities.

4.2.1.2 poly(2,5-bis(3-tetradecylthiophen-2yl)thieno[3,2-b]thiophene)-pBTTT

A polymer pBTTT which stands for poly(2,5-bis(3-tetradecylthiophen-2yl)thieno[3,2-b]thiophene) was also used for our experiments. It belongs to a class of polymers composed of regiosymmetric 2,5-bis(3-alkylthiophen-2yl)thieno[3,2-b]thiophene monomeric units. The chemical structure is shown in Figure 4.1 (b) and chemical names with other details are listed in Table 4.1. These polymers are marked by excellent self organization in ordered lamellar domain, and high pi orbital overlap resulting in high mobilities. The pBTTT polymer has been shown to achieve high charge-carrier field effect mobilities of up to 0.8 cm^2/Vs[4]. Its high mobility has been ascribed to its crystalline structure. Recently mobility of 3.5 cm^2/V s has also been obtained using an electrolyte dielectric which induces extremely large carrier densities in the channel[5].

A 5 mM solution was prepared by mixing pBTTT in 1, 2-dichlorobenzenethiol. Once dissolved the solution becomes gelatinous at room temperature. It was heated to convert it into its liquid form. The liquid was subsequently spin coated on the substrate in a nitrogen filled chamber. The substrate with the polymer film was then annealed by heating it into a liquid crystalline state and then cooled down to room temperature at 5^{O} C/min. Annealed pBTTT films exhibit unusually high degree of order[6].

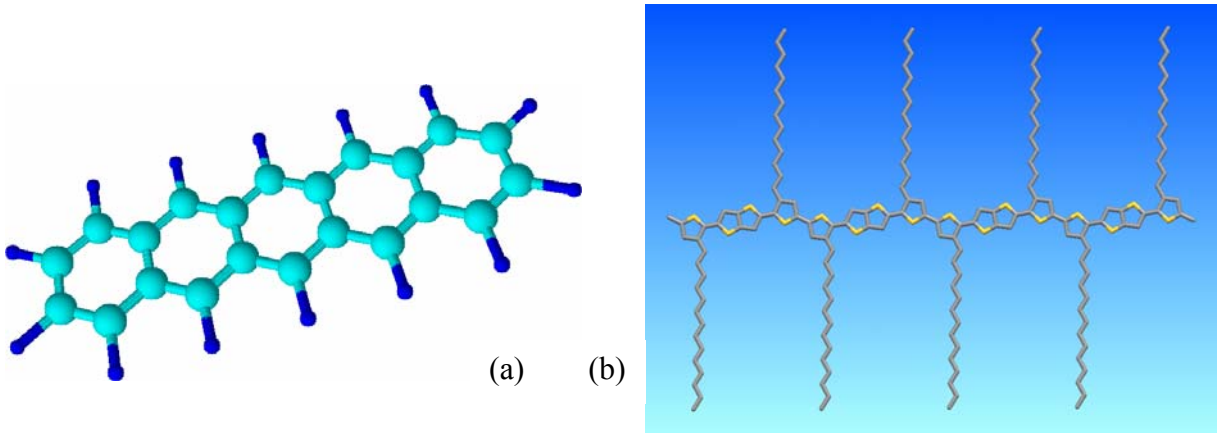

(a) (b)

Figure 4.1 (a) Pentacene molecule consisting of five fused benzene ring. Pentacene is one of the most common organic semiconductor with high mobilities. (b) structure of pBTTT, a high crystallinity polymer.

Table 4.1 Properties of pentacene and pBTTT.

Name	Pentacene	pBTTT
Structure	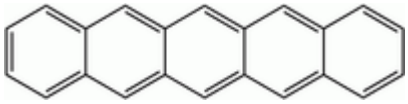	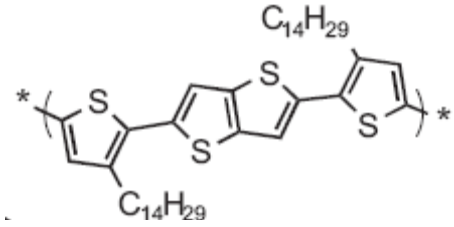
Chemical formula	$C_{22}H_{14}$	Poly(2,5-bis(3-alkylthiophen-2-yl)thieno[3,2- b]thiophene
Type of semiconductor	Small molecule	polymer
Highest recorded mobility cm^2/Vs	3	0.8 (3.5 with electrolyte dielectric)

4.2.2 DIELECTRIC.

The second most important material that affects the charge carrier mobility of a field effect transistor is the gate insulator. The surface roughness of the dielectric at the semiconductor insulator interface is a determining factor for the ordering of the semiconductor molecules or polymer strands. A higher roughness results in multiple nucleating sites which reduces the grain size of the semiconductor thus yielding low field-effect mobility[7]. This is also known that higher transverse gate field results in higher charge concentration leading to higher charge carrier mobilities. Smaller effective oxide thickness (EOT) of the insulator helps in producing a higher electric field. Reducing the physical thickness of the dielectric often leads to reliability issues due to higher leakage current through the dielectric. Therefore a lower EOT can be achieved using a high K dielectric; in addition use of high K dielectrics reduces voltages of operation to permit organic circuits to meet realistic specifications for transistor applications

4.2.2.1 Silicon dioxide.

Silicon dioxide is the most common insulator that has be been used in the semiconductor industry. It is one of the most well characterized insulators present. Hence it was an obvious choice when fabricating an organic transistor. Due to its low surface roughness, it presented itself as an excellent candidate for making high mobility transistors.

4.2.2.2 Tantalum oxide.

Tantalum oxide (Ta_2O_5) is a high refractive index, low absorption material useful for coatings in the near-UV to IR spectra regions; it decomposes only at temperatures >1470 °C. Ta_2O_5 is used to make capacitors in automotive electronics, cell phones, and pagers, electronic circuitry; thin-film components; and high-speed tools. In the 1990's, there was a very strong interest to do research on tantalum oxide as a high-k dielectric for DRAM capacitor applications. Subsequently in the 2000's, this strong interest has dropped very significantly. Due to its high index of refraction, Ta_2O_5 has been utilized in the fabrication of the glass of many photographic lenses.

Tantalum oxide is a high k dielectric that can be vacuum deposited. However due to problems of leakage through the insulator, tantalum metal was deposited instead of its oxidized form, followed by anodization of the tantalum thin film[8] at room temperature using a 0.01 M of citric solution as electrolyte, thereby obtaining 1,700 Å high-*k* Ta_2O_5 (ε_r: 25.0). The roughness of anodized Ta_2O_5 measured by AFM was around 22.9 Å, which was much larger than that of commonly-used thermally-grown SiO_2 2.6Å[9].

4.2.2.3 poly(vinyl phenol)-PVP.

PVP or poly(vinyl phenol) is a polymer dielectric. The advantage of using a polymer dielectric over an inorganic one is the ability to formulate a process which completely relies on solution processible materials. This process can potentially be used to print low cost circuits on plastic. However, the polymeric dielectrics like PVP differ from inorganic dielectrics with respect to its surface energy and reactivity to organic solvents. In addition, PVP can be easily patterned by etching in oxygen plasma, thus providing a method to fabricate multilayered integrated circuits using organic semiconductors such as pentacene[10].

The solution was formed by mixing PVP (30% by wt.) and a cross-linker methylated poly(melamine-co-formaldehyde) (70 % by wt.) in propylene glycol methyl ether acetate (PGMEA). The cross-linker is generally mixed in the solution to increase the chemical resistivity of the dielectric to organic solvents by connecting PVP molecules via covalent bonds. It also reduces the free volume of the dielectric as the dielectric shrinks after cross-linking. The solution is then spun on the substrate and the desired thickness is determined by the spin speed. In order to obtain a high gate control we have used the smallest possible thickness of the dielectric, approximately 1700 Å, by spinning at a speed of 3000 rpm. The thickness versus spin speed curve is shown in Figure 4.2.

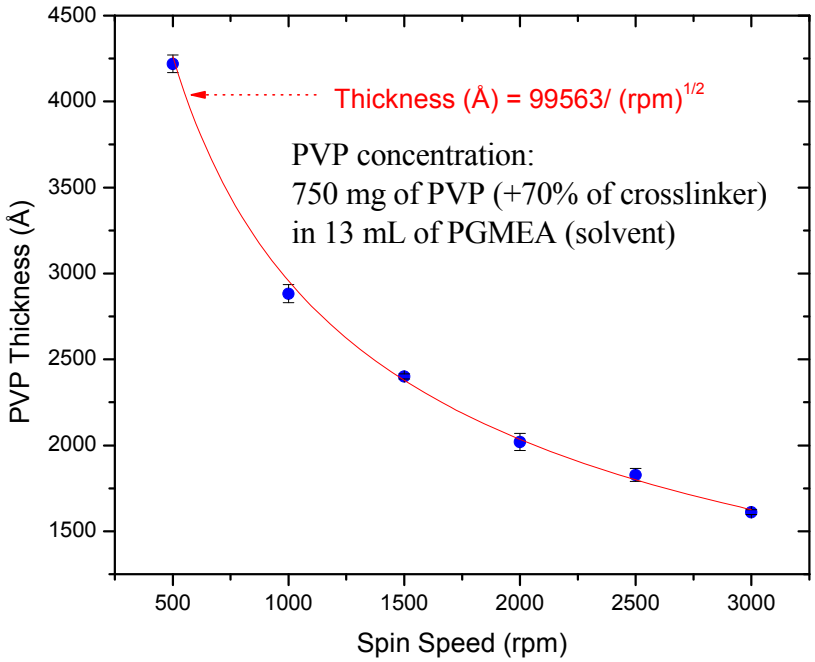

Figure 4.2 Thickness of PVP dielectric as a function of spin speed. The lowest possible thickness of 1700 Å is used for fabricating transistors.

4.2.2.4 Surface treatment of insulator.

The semiconductor insulator interface is the primary factor that determines the field effect mobility of charge carriers in an OFET. Vapor phase or solution based treatments with an alkyl silane or silazine group forms a self-assembled monolayer on the surface of the insulator. Such treatments prior to the deposition of the semiconductor reduces the surface energy which improves the mobility and hence the electrical performance of the transistor. Compounds that can be used for improving the surface for transistor fabrication include hexamethyldisilazine (HMDS), octyltrichlotosilane (OTS) and octadecyltrichlorosilane. Structure of OTS molecule is shown in Figure 4.3. OTS treatment has shown reduction in the surface nucleation density of bare oxide, resulting in micron-scale terraced pBTTT films with improved charge transport[7]. Figure 4.4 (b) shows the improved morphology of the OTS treated oxide surfaces as opposed to the surface of bare silicon dioxide Figure 4.4 (a). The strong dependence of morphology on the surface chemistry plays an important role in the large hole mobility of this polymer semiconductor.

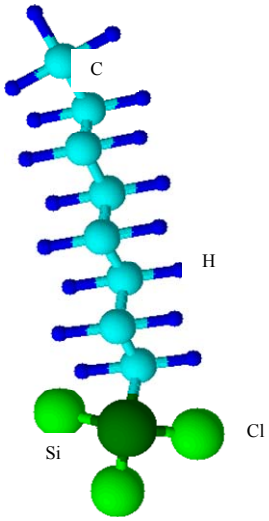

Figure 4.3 Structure of octyltrichlorosilane molecule. On treatment with OTS, it forms a self assembled monolayer on the surface of the oxide that aids the formation of crystalline domains.

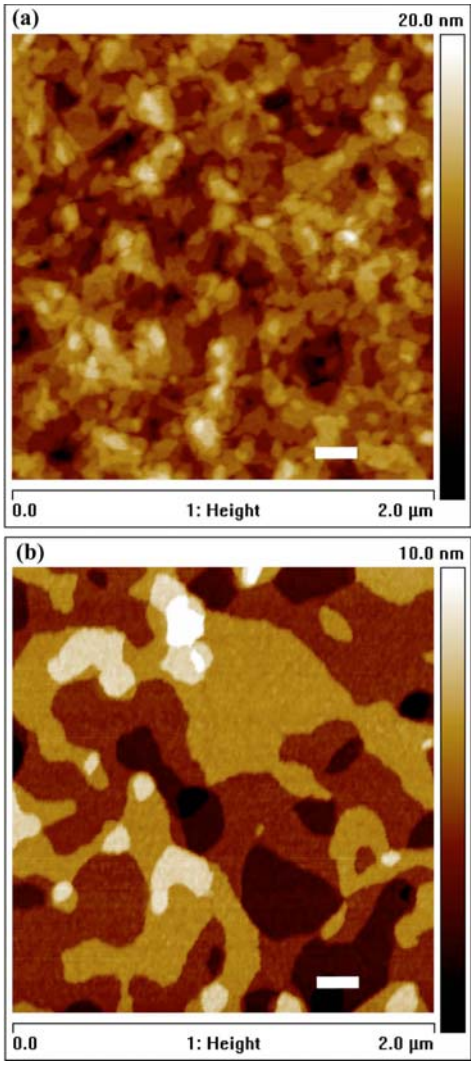

Figure 4.4. AFM images of Bare silicon surface(a) and surface of oxide treated with OTS (b) From 7, printed with permission from AIP.

4.2.2.5 Surface of contacts.

Non-ideal contacts can adversely affect the performance of OFETs by limiting the charge carrier injection, this results in superlinear behavior near the origin in transistor characteristics. This can be modeled as a high resistance in series to the transistor, the value of which depends on the applied voltage. The effect of this series resistance is a

reduction in the mobility of the transistor which ultimate affects its performance. Treatment with an organic thiol has been shown to improve injection at the contacts[11]. Such compounds include nitrobenzenethiol, octadecanethiol, 2, 4-dichlorobenzenethiol. The exact reason is not understood, however it has been proposed that formation of an organic layer over the gold electrode reduces its surface energy and help formation of ordered domains in the semiconductor, which improves the injection and transport of carriers[12]. Formation of a SAM has also been purported to reduce the energy barrier for injection thus increasing the efficiency and hence the mobility of the transistor[13].

4.3 Fabrication details.

We have used a bottom-contact geometry with a bottom gate structure for fabricating our field effect transistor. Using the various combinations of gate dielectric and metal contacts we have used three different structures as discussed below.

4.3.1 FABRICATION SCHEME A.

This is the simplest of the three structures. It consists of degenerately doped silicon acting as the gate contact. The gate dielectric consisted of 1000 Å of thermally grown silicon dioxide on top. The gold source and drain contacts were deposited photolithography by a process of image reversal using photoresist AZ 5214 E. Surface treatments were performed to increase the mobility of the semiconductor that was finally deposited on top of the structure. A schematic of the structure is shown in Figure 4.5 (a). The main disadvantage of this structure with respect to pulse voltage measurement was a high gate to source overlap which resulted in a high capacitive charging current in the beginning of the experiment that limits the ability to correctly extract the delay time.

4.3.2 FABRICATION SCHEME B

A schematic of the structure is shown in Figure 4.5 (b). This was prefabricated by Lucent Technologies (previously Bell Labs) by Crone. The channel width and length of the transistors were 2000 μm and 7.5 μm, respectively. The dielectric consisted of 2000 Å of Si_3N_4 under 1000 Å of SiO_2, with an estimated gate dielectric capacitance of 17 nF/cm^2. Aluminum was used as the interconnect metal and the source and drain metals used was gold.

4.3.3 FABRICATION SCHEME C

This scheme of fabrication improves upon the previous two by using a patterned gate and therefore reducing the overlap between the gate and the source. The channel lengths used are from 5, 10 and 20 μm. In order to connect t the bottom gate the dielectric was patterned. A schematic of the structure is shown in Figure 4.5 (c). The source and drain were composed of titanium and gold.

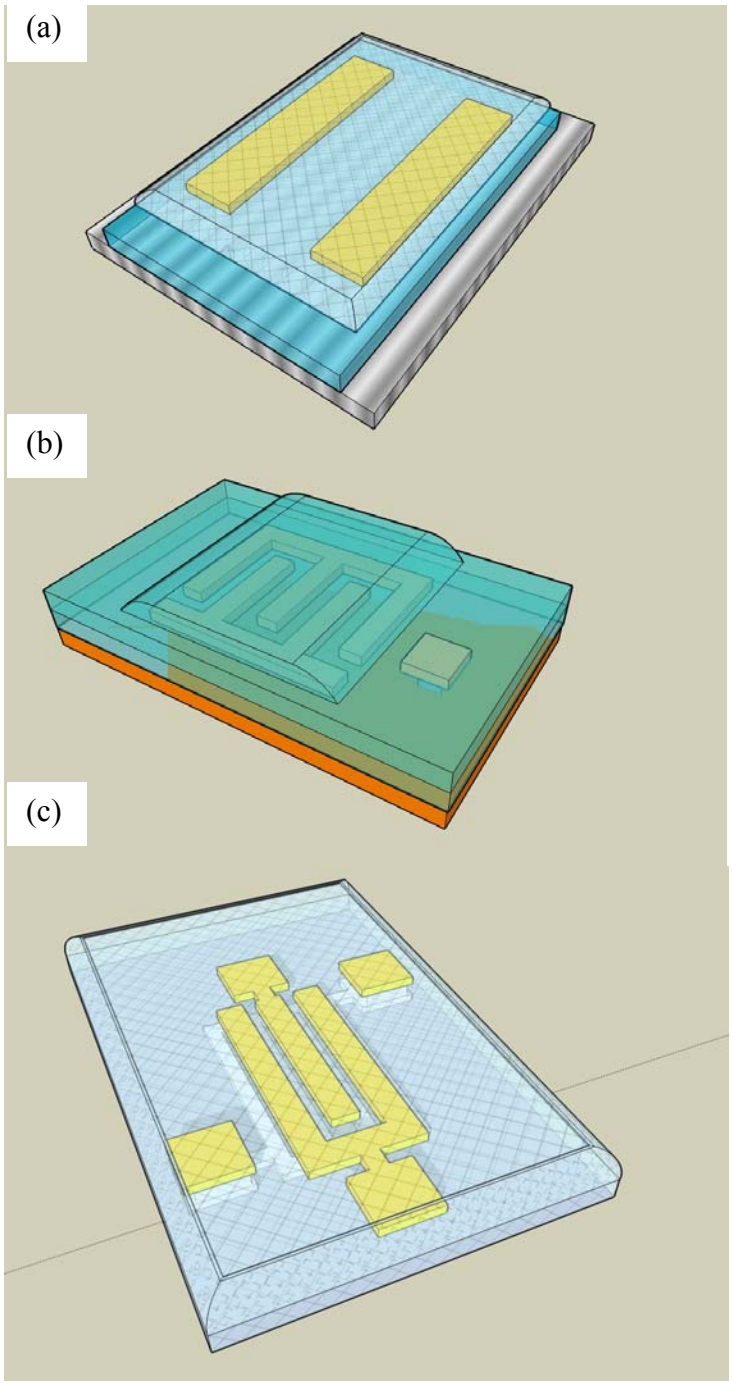

Figure 4.5 (a) Fabrication scheme A. being the simplest of the three it involves the least amount of processing. (b) Fabrication scheme B, the gate is patterned but exists below the source and drain contacts. (c) Fabrication Scheme C, gate is patterned and does not exist below the semiconductor

4.4 Experimental Set-up.

The circuit configuration used to measure the transient response of the device is shown in Figure 4.6. The assembly consists of a pulse voltage generator (HP/Agilent 214B), an oscilloscope (LeCroy 6030 Waverunner), and a resistor (750 Ω). The gate of the organic field effect transistor (OFET) was grounded, and a square wave from an HP/Agilent 214B voltage pulse generator was applied to the OFET source that switched between 0 V and a maximum positive voltage V_0. The duty cycle of the square wave voltage pulse was 0.1 with a pulse width of 300 μs. The rise time of the pulse was approximately 100 ns for all the voltage values. The input of the LeCroy 6030 oscilloscope was coupled to DC 1 MΩ. The resistor was connected to the drain contact of the OFET the other end of which was shorted to ground.

Due to the inherent instability of characteristics of OFET caused by bias stress effect, the response of the pulse is recorded at the first instant the pulse is applied. The resulting waveform is then analyzed using MATLAB® and fitted to the following expression

$$I = I_0 \left\{ 1 - \alpha \cdot \exp\left(-\frac{t - t_D}{\tau_1}\right) - \beta \cdot \exp\left(-\frac{t - t_D}{\tau_2}\right) \right\} \qquad (4.1)$$

where t_D is the delay in response and I_0, α, β, τ_1, τ_2, are fitting parameters. The code for extracting the delay time, by fitting to the expression is given in Appendix 1.

4.5 Results.

The results of the pulse voltage measurement on different semiconductor are discussed in this section. Every semiconductor has been used on more than one dielectric to observe the effect of insulators on the mobility of the semiconductor.

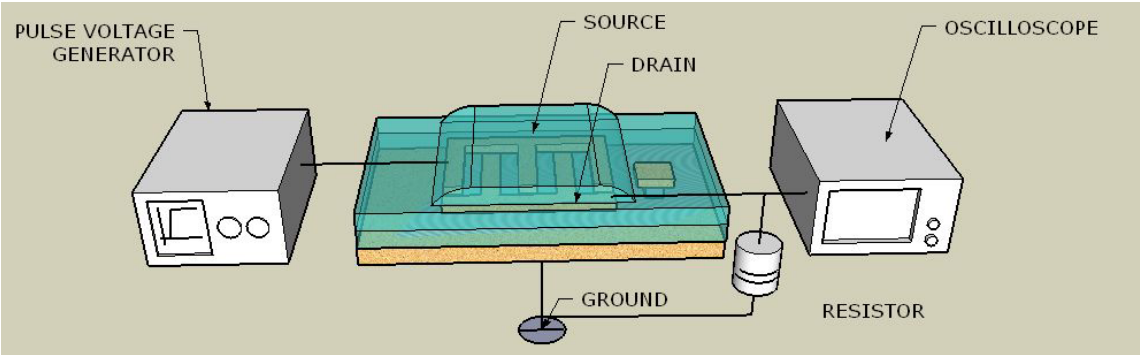

Figure 4.6. Experimental Setup consisting of an impulse voltage generator, an oscilloscope and a resistor.

4.5.1 TRANSIENT RESPONSE OF PENTACENE

Pentacene OFETS were characterized on silicon dioxide as well as tantalum oxide dielectric. The silicon dioxide sample was made using fabrication scheme A. Before depositing pentacene, it was purified via vacuum sublimation, the silicon dioxide surface was treated with a 10 mM solution of octadecyltrichlorosilane dissolved in Toluene for 50 minutes, and the gold contacts were treated with a 10 mM solution of nitrobenzenethiol dissolved in acetonitrile for 1 hour. A film of 400 Å of pentacene was thermally deposited at a base pressure < $4x10^{-7}$ torr at 0.3 Å/s for the first 50 Å, and then 1 Å/s for the remaining 350 Å. All measurements were carried out under a vacuum < $2x10^{-3}$ torr at room temperature. Figure 4.7 (a) shows the I_d-V_{ds} characteristics obtained from an HP/Agilent 4145B semiconductor parameter analyzer. The pulse voltage response of pentacene is shown in Figure 4.7 (b). The maximum voltage of the pulse, V_0, was varied from 20 V to 50 V in increments of 5 V. A finite delay between the application of the source pulse and the drain waveform is seen. The transient mobility was calculated and plotted against the field effect mobility in Figure 4.7 (c). Both the transient and the DC mobility increases with the voltage of the pulse from a value of 0.04 and 0.03 cm^2/Vs respectively at 20 V to a value of 0.07 and 0.06 cm^2/Vs respectively at

50 V. A possible explanation is given in section 4.6. The DC mobility appears to be a higher than the transient mobility however the difference is small enough to be caused by experimental error.

Transient experiments were also performed on pentacene OFETs with tantalum oxide as the dielectric. The channel length used was 50 μm, so that the effect of the initial displacement current can be eliminated. Fabrication scheme A was used in making the OFETs. The substrates were treated with vapors of hexamethyldisilazine (HMDS). The HMDS treatment resulted in decreased threshold voltage, and an increase in I_{on}/I_{off} ratio by more than an order of magnitude[9]. The steady state characteristics of the transistor are shown in Figure 4.8 (a). The saturation region mobility obtained from the FET curve is 0.2 cm^2/Vs. The maximum voltage of the pulse, V_0, was varied from 15 V to 35 V in increments of 2.5 V. The reduction in the range of operating voltage is due to an increase in the dielectric constant of the insulator that enables higher current densities at lower operating voltages. Figure 4.8 (b) shows the fitting of the transient response for 35 V to the expression in equation 4.1; the fit is in good agreement to the data. The plot of the drift mobility obtained from the transient time extracted by fitting to data for different pulse voltages is plotted in Figure 4.8 (c) along with the delay times. In the case of tantalum oxide dielectric the FET mobility lies within the range of the FET mobility. The drift mobility of pentacene almost doubles with applied voltage for the silicon dioxide dielectric; however the drift mobility for the sample with tantalum oxide dielectric doesn't show a clear trend with voltage. This may be because of its large channel length which results in reduced electric field. Field dependence of transient mobility is discussed in detail in section 4.6.

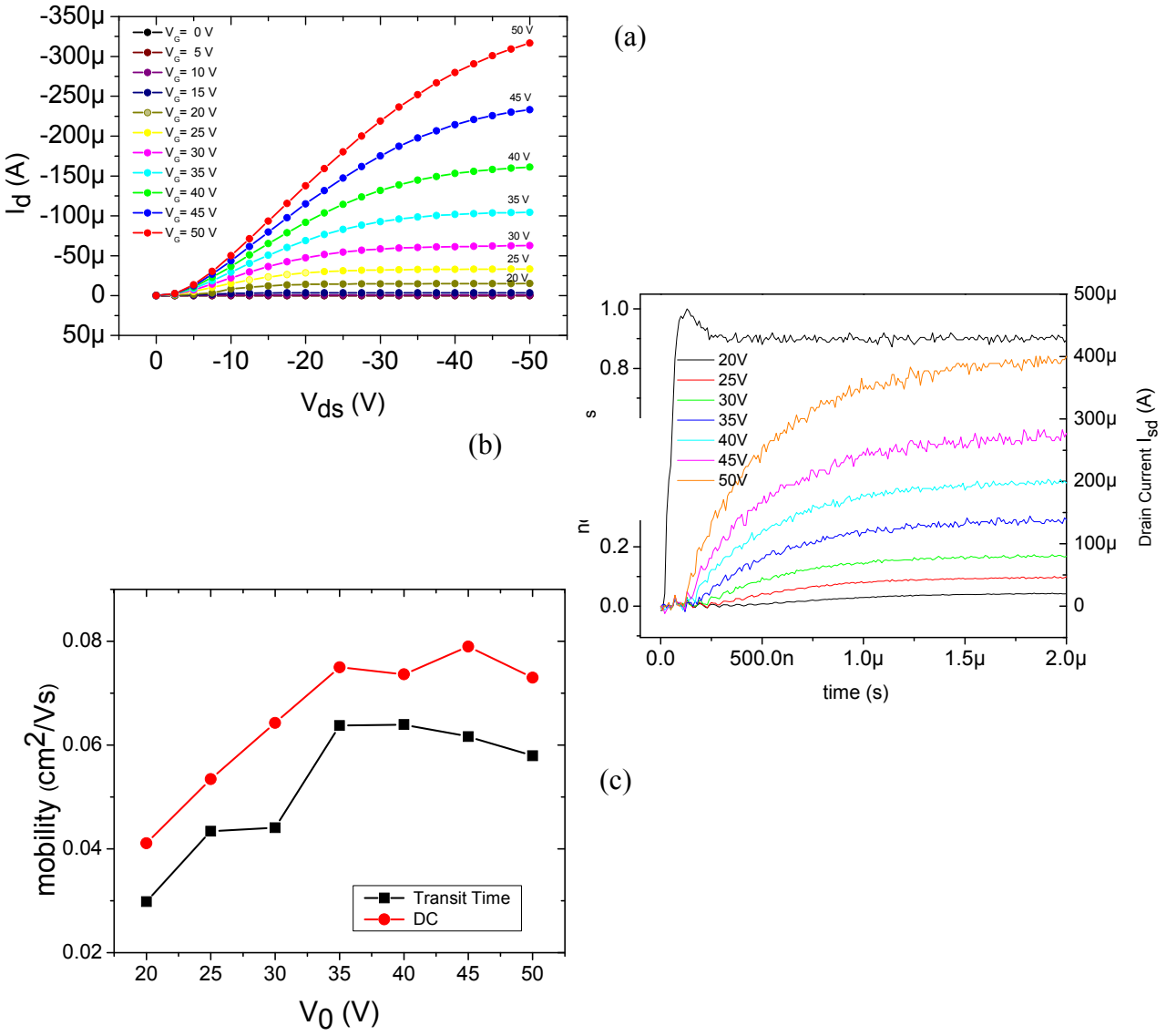

Figure 4.7 (a) Steady state characteristics of pentacene transistors on silicon dioxide dielectric. (b) Transient response of pentacene transistors on Silicon dioxide dielectric. (c) Pentacene drift and DC mobilities for fabrication scheme B.(L = 7.5 µm)

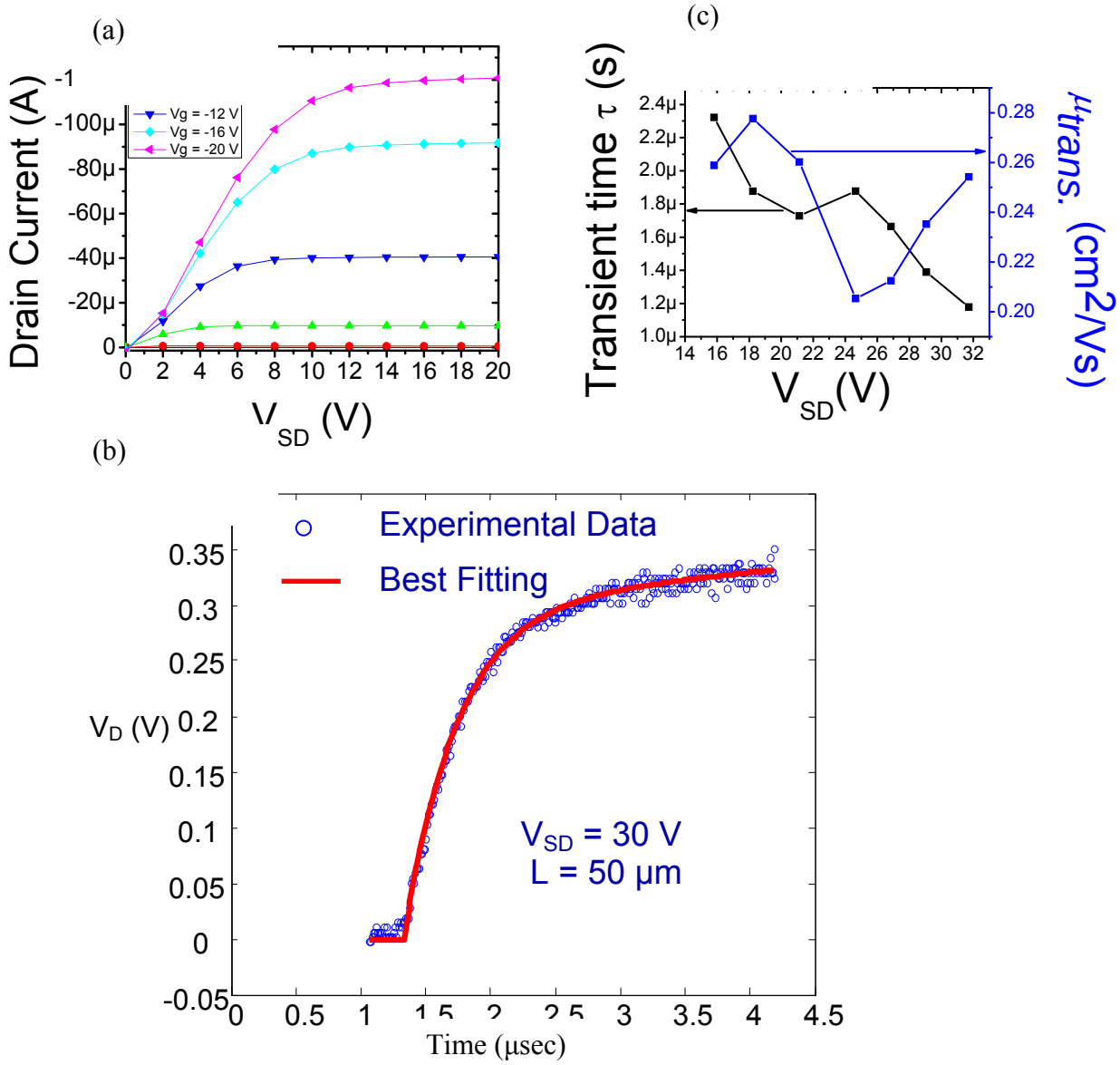

Figure 4.8 (a) Steady state characteristics of pentacene transistors on tantalum dioxide dielectric. (b) Transient response of pentacene transistors on tantalum dioxide dielectric. The dots represent experimental data while the red line is the fit to expression 4.1. the fit is in agreement with the data. (c) Figure 4.8 c Plot of transient TOF mobility and delay times for pentacene on tantalum oxide.(L = 50 µm, μ_{FET} = 0.2 cm^2/Vs at V_G = -20 V)

4.5.2 TRANSIENT RESPONSE OF PBTTT

Scheme B for fabrication of transistors was used for making pBTTT OFETs. The surface of silicon dioxide, the insulator, was clean with oxygen plasma (25 Watts, 5 minutes) followed by treatment with 0.1 M solution of octyltrichlorosilane in toluene to improve the ordering of the polymer chains. The pBTTT solution is then spin coated. The substrate is annealed from 120^{O} C to room temperature at a slow rate in nitrogen ambient. The transistor characteristics are shown in Figure 4.9 (a). The solid lines represent simulation using a two-dimensional device simulator called MEDICI® which simulated the device characteristics using a drift- diffusion model. The dots represent experimentally obtained data points. Simulation of the device characteristics is done assuming an ordered semiconductor with ideal contacts; however an OFET is far from an ideal device. This is the reason deviation is observed between the simulation and data. Pulse voltage measurements were also performed the maximum voltage of the pulse, V_0, ranging from 30 V to 100 V in increments of 10 V. The pulse voltage response of pBTTT is shown in Figure 4.10 (a), (b) along with the pulse voltage applied to the source (normalized by its maximum voltage V_0). The response is fitted to the expression given in Equation 4.1 to extract the delay time, the delay time was then used to calculate the transient mobility. The graph of transient TOF mobilities versus the pulse voltage is shown in Figure 4.10 (b) along with the extracted delay times. The DC mobility and the drain current for the condition

$$V_{Source-Gate} = V_{Source-Drain} = V_0 (\text{maximum voltage of pulse}) \qquad (4.2)$$

is plotted in Figure 4.9 (b). Both the DC and the transient mobility show an increasing trend with the voltage of the pulse. The DC mobility lie within the range of the transient mobility for the various pulse voltages applied.

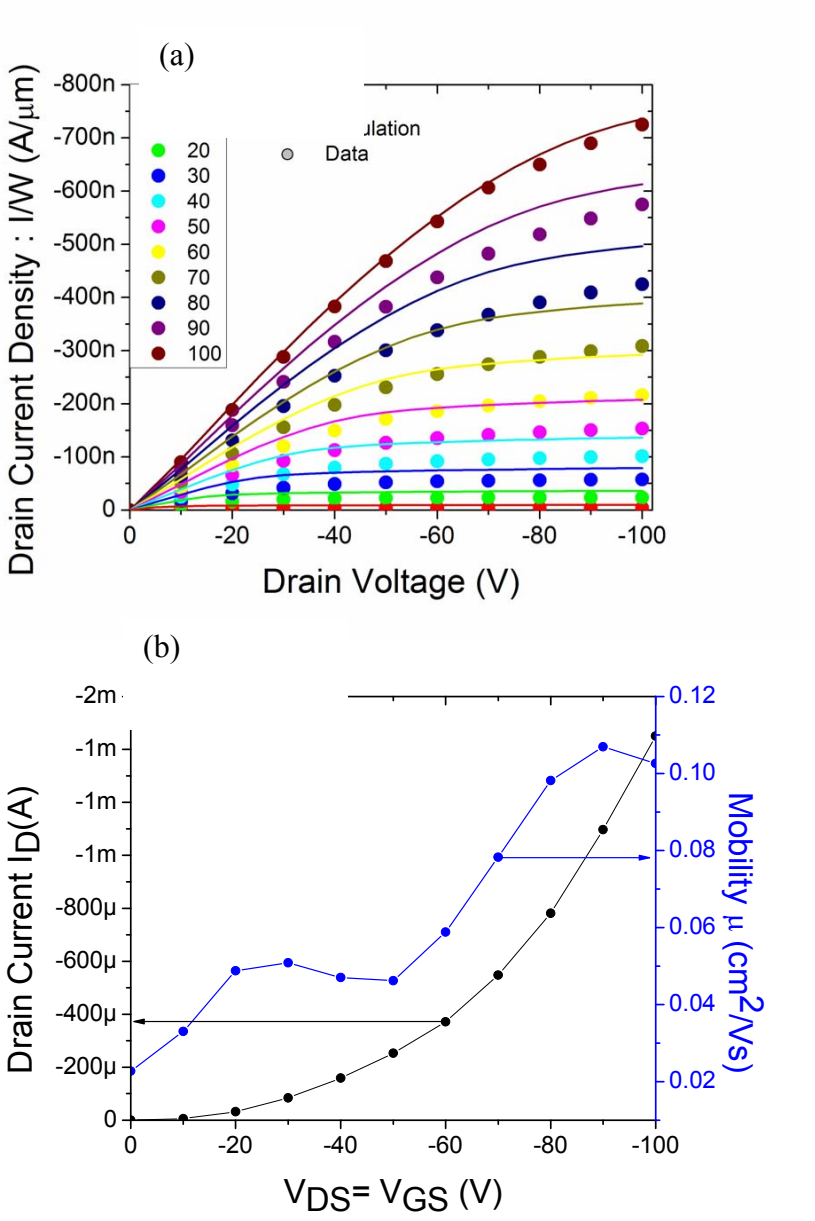

Figure 4.9. (a) Transistor characteristics of pBTTT OFET with silicon dioxide gate dielectric. The dots represent experimental data while the solid lines represent simulation in MEDICI® a drift-diffusion simulator. (b) Plot of DC saturation mobility and drain currents for pBTTT on silicon dioxide. (L = 7.5 μm)

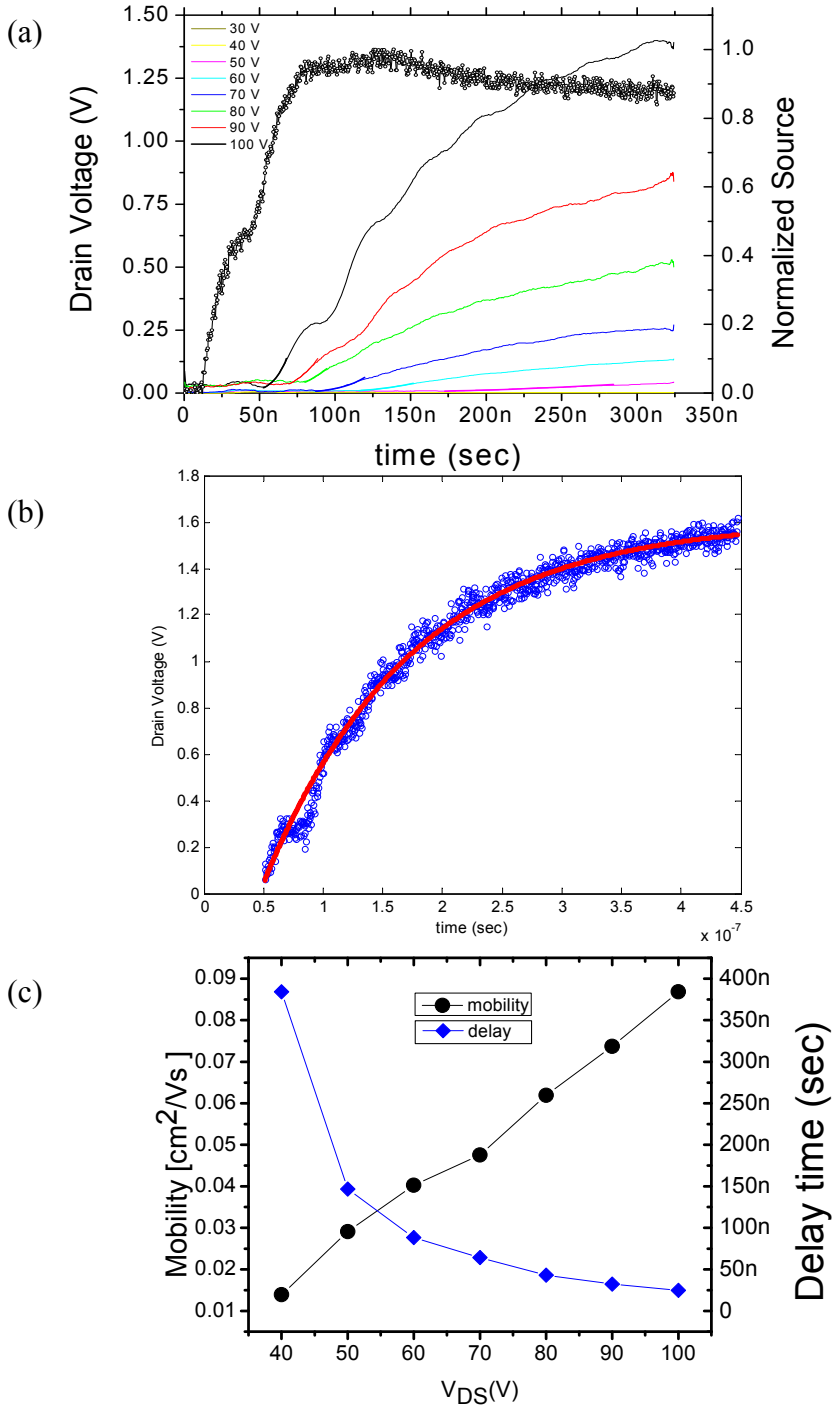

Figure 4.10 (a)Transient response of pentacene transistors on silicon dioxide dielectric. (b) Fitting of transient response data for pBTTT transistors on silicon dioxide insulator. The dots represent experimental data while the red line is the fit for V_0 = 100 V . (c) Plot of transient TOF mobility and delay times for pBTTT on silicon dioxide. (L = 7.5 µm, μ_{FET} = 0.1 cm^2/Vs at -100 V)

4.6 Field dependence

It can be seen from plots 4.7 (c) and 4.10 (c) that the drift mobility increases with the voltage of the pulse applied. An exact dependence of the mobility on the pulse voltage can not be predicted; however it can be explained along the following line of argument.

In the pulse voltage measurement, the gate and drain of an OFET are maintained at or very near to ground potential. Hence an applied source voltage not only creates a source to drain field but also a source gate bias which is equal to the source-drain bias. Therefore the variation of TOF mobility with pulse voltage can be due to the dependence of mobility on the source-gate bias or the source-drain bias or due to combination of both these biases.

An increase in field effect mobility of carriers with increasing gate voltage has been observed and explained in terms of multiple trap and release (MTR) with a distribution of traps located in the grain boundaries[14]. According to the MTR model, the initial increase corresponds to the filling of the traps in the grain boundaries thereby reducing the barrier for transport. Increased gate voltage results in increased density of carriers in the accumulation region. The variable range hopping model proposed by Vissenberg and Matters[15] have showed on the basis of the previous argument that increased gate voltage can lead to an increased mobility. The source-drain field provides the drive for carriers in the channel of a FET. An increase in field-effect mobility has been observed in optical time of flight methods[16]. At high fields, a $log\ \mu \sim E^{1/2}$ relationship was observed with a slope that approaches zero at high temperatures (Figure 4.11). The results were explained within the framework of the disorder transport

formalism proposed by Bässler[17] and modified by Kenkre[18]. However it should be noted that at high temperatures the mobilities decreased with increasing field at low fields.

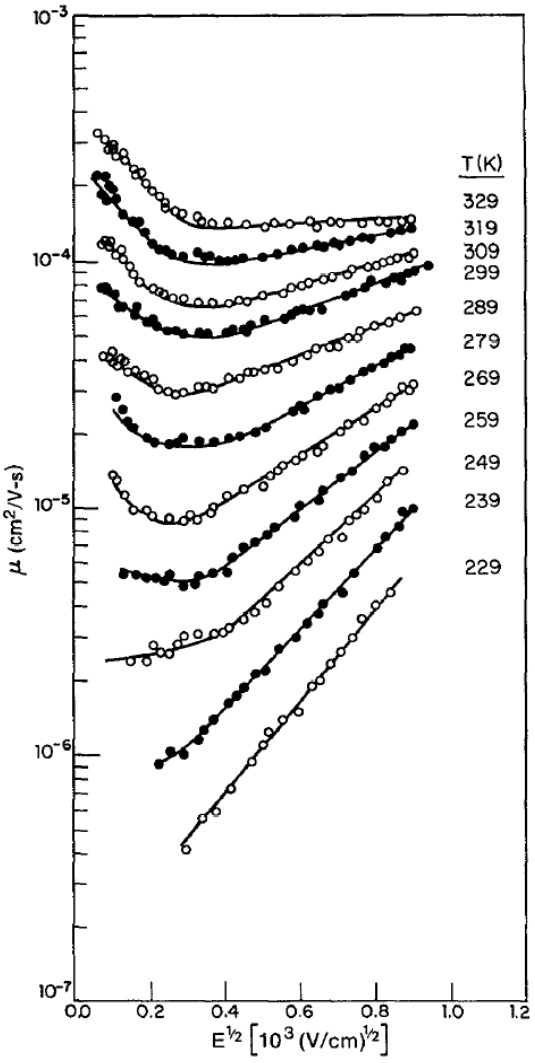

Figure 4.11 Plot of optical TOF mobilities as a function of the electric field for various temperatures. The mobility follows exponential square root dependence with the electric field. From 16 printed with permission from AIP.

Thus the increased in mobility with pulse voltage observed can be either a effect of source-gate voltage or the source-drain bias or a combination of both. Since the exact nature of the dependence would not only be extremely complicated but also dependent on

the density of states which is not known precisely, separation of these two phenomena in the information available would be nearly impossible. To further investigate the mobility behavior, independent control of gate and drain biases are necessary.

In the following section we have discussed an experiment which displays the variation of TOF mobility on the channel length of the transistor. By changing the channel length while keeping the pulse voltage constant the transverse electric field can be varied independent of the gate source voltage.

4.7 Channel length dependence

Transistors are fabrication with pBTTT as the semiconductor according to Scheme C. The bottom gate metal consists of chromium which is also the interconnect metal. A via is formed by etching through the PVP dielectric to contact the bottom gate. OTS treatment is performed on the substrate and the contacts are treated with 2,4-dichlorobenzenethiol. The channel lengths used in this scheme were 5, 10 and 20 μm.

The DC characteristics of the three transistors are plotted together in Figure 4.12. A field effect mobility of 0.13 cm^2/Vs, 0.16 cm^2/Vs and 0.22 cm^2/Vs was obtained in the saturation region for 5, 10 and 20 μm channel lengths respectively. The fact that the 5 μm channel length transistor has lower mobility can be ascribed to a non-ideal contact for injection into the electrodes.

The transient responses for the three channel lengths are shown in Figure 4.13 (a) for the same pulse voltage of 35V. The slowest being the 20 μm channel. The delay times are calculated by fitting the responses at various pulse voltages and the mobilities are plotted in Figure 4.13 (b). The smallest mobility is observed for the 5 μm channel. The TOF mobilities are also plotted with square root of the average electric field In the

channel in Figure 4.14. It is observed that for higher electric field existing in the 5 μm channel the mobilities tend to increase with applied voltage where as for larger channel lengths the TOF mobility reduces with increasing voltage. A smaller channel length implies a higher electric field for the same applied voltage. It can also be seen that the increase of mobility for the smaller channel length is linear indicating exponential square-root dependence on the applied voltage. So it can be concluded that mobilities decrease at lower electric field and increase proportional to the square-root of the electric field at higher fields. The mobilities of the smaller channel length transistor are lower compared to the higher channel length ones. This reduction in mobilities for can be due to a lower gate voltage for the same lateral electric field. Non-ideal injection can also reduce the value of mobility by affecting the time to inject through the contacts.

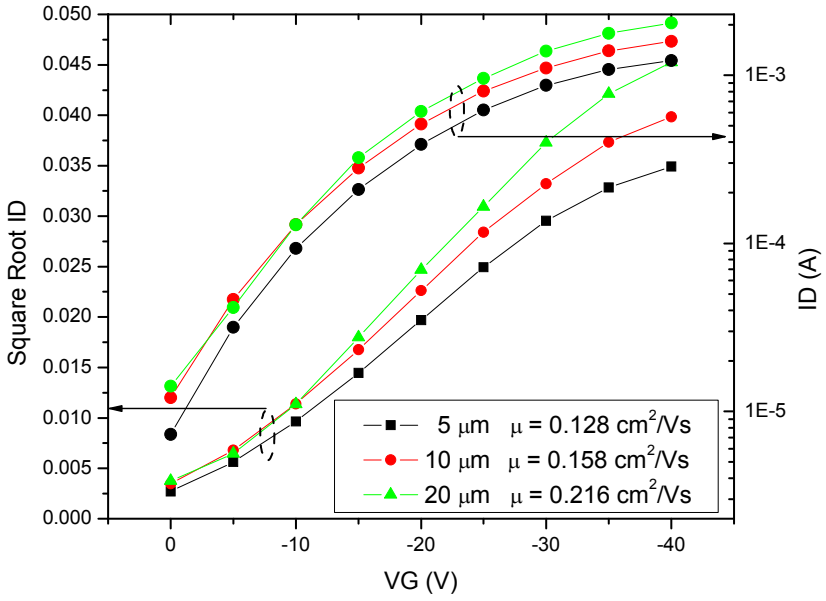

Figure 4.12 Plot of square root of drain current in linear scale and drain current in logarithmic scale against gate voltage. The field effect mobilities are also reported.

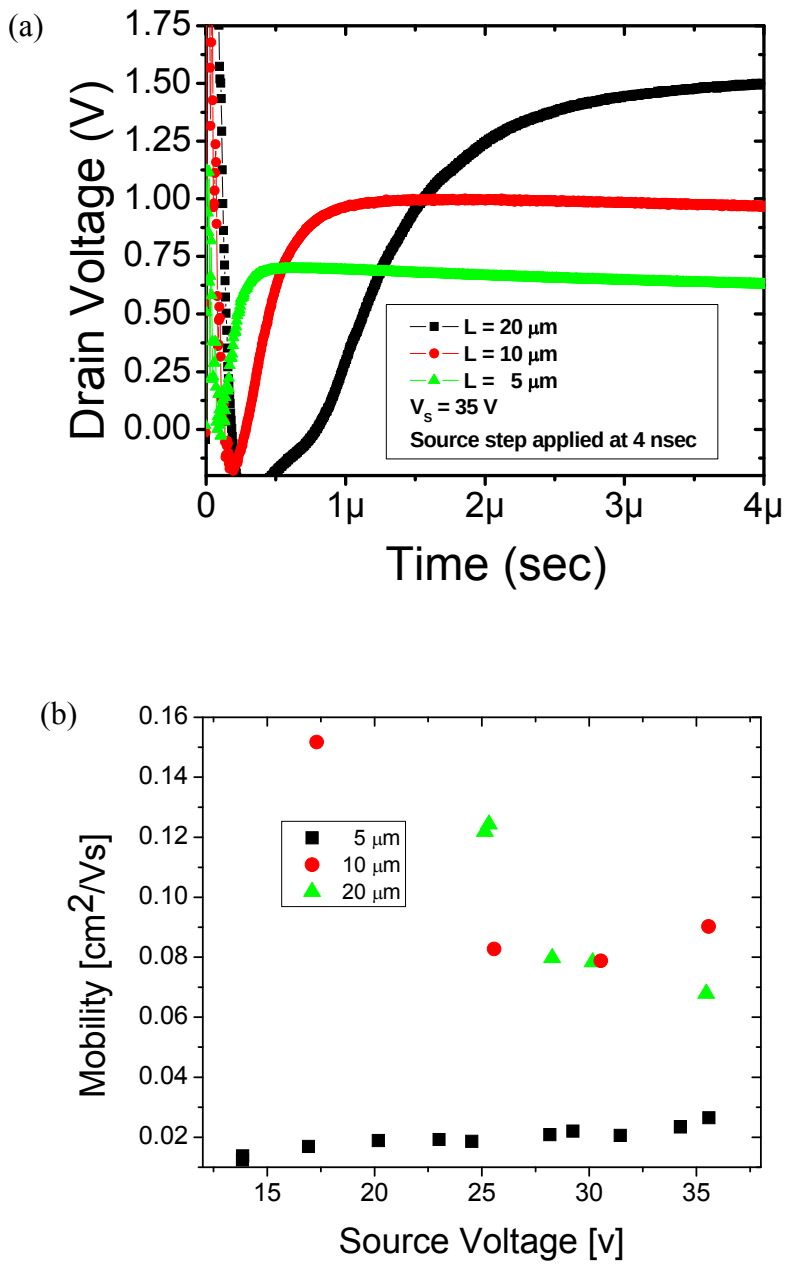

Figure 4.13 (a) Transient response of pBTTT on PVP for varying channel length transistors. The pulse voltage is constant at 35 V. (b) Plot of transient TOF mobility for pBTTT on PVP for three different channel lengths.

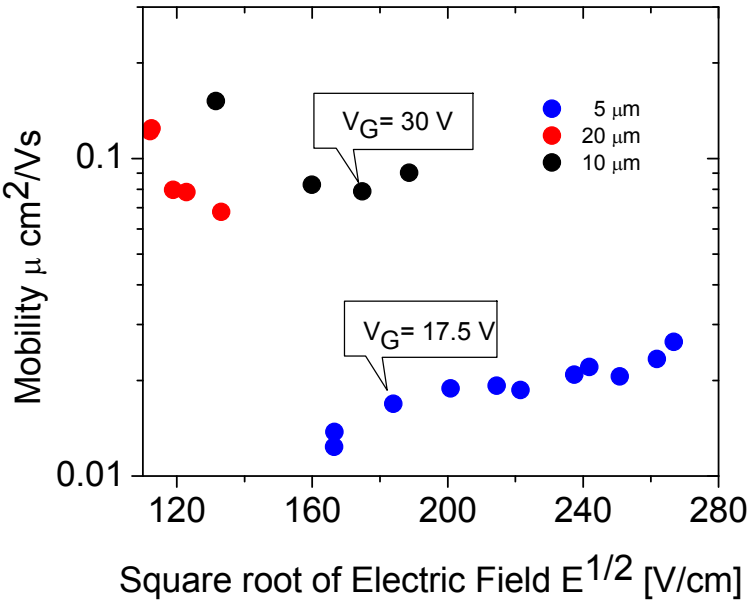

Figure 4.14. Plot of transient TOF in logarithmic scale as a function of the square root of electric field.

4.8 Conclusion

Time of flight measurement of drift mobility was performed in organic transistors with varying dielectrics fabricated by different methods of fabrication, the TOF mobility lies in the range of the DC mobility. Variation in drift mobility was also observed with the applied pulse voltage. This was explained to be due to a combination of following two phenomena, the increase in mobility with gate voltage and the increase in drift mobility at high lateral fields. Finally TOF measurements were done on transistors with varying channel length and it was observed that the mobility reduces at low electric field and increase proportional to the exponential square root of the source drain bias.

References

[1] L. Dunn, L. Wang, D. Basu, A. Dodabalapur, *App. Phys. Lett.*, **88**, 063507 (2006).

[2] Y.-Y. Lin *et al.*, *IEEE Trans. Electron Dev. Lett.* **18** (1997), p. 606.

[3] H. Klauk *et al.*, *J. Appl. Phys.* **92** (2002), p. 5259.

[4] I. McCulloch, M. Heeney, C. Bailey, K. Genevicius, I. MacDonald, M. Shkunov, D. Sparrowe, S. Tierney, R. Wagner, W. Zhang, M. L. Chabinyc, R. J. Kline, M. D. McGehee, and M. F. Toney, Nat. Mater. **5**, 328 _2006_.

[5] A. S. Dhoot, J. D. Yuen, M. Heeney, I. McCulloch, D. Moses, and A. J. Heeger, Proc. Natl. Acad. Sci. U.S.A. **103**, 11834 (2006).

[6] Dean M. DeLongchamp et.al. *AIChE 2006*, Session T6001.

[7] R. J. Kline, D. M. DeLongchamp, D. A. Fischer, E. K. Lin, M. Heeney, I. McCulloch, M. F. Toney, *App. Phys. Lett*, **90**, 062117 (2007).

[8] J. Tate, JA Rogers, CDW Jones, B Vyas, D. W. Murphy, W. Li, Z. Bao, R.E. Slusher, A. Dodabalapur, H. E. Katz, *Langmuir* **16**, 6054 (2000)

[9] Y-T. Jeong, B. Yoo, A. Dodabalapur, *MRS 2007*, Session O5.2

[10] H. Klauk, M. Halik, U. Zschieschang, F. Eder, G.Schmid, C. Dehm, *App. Phys. Lett.*, **82**, 4175, (2003).

[11] D.J. Gundlach, J. Li Li, T.N Jackson, *IEEE Elec. Dev. Lett.* **22**, 571, (2001)

[12] C. Dimitrakopoulos and D. J. Mascaro, *IBM J. Res & Dev.* **45**, 1. (2001).

[13] S. H. Kim, J. H. Lee, S. C. Lim, Y. S. Yang, T. Zyung, *Jap. J. App. Phys.* **43**, L60, (2003).

[14] M. Mottaghi, G. Horowitz, *Organic Electronics,* **7**, 528, (2006).

[15] M. Matters, M. C. J. M. Vissenberg, *Phys. Rev. B.*, **57**, 12964, (1998).

[16] P. M. Borsenberger, L. Pautmeier, H. Bässler. *J. Chem. Phys.* **94,** 5447 (1991).

[17] H. Bässler, *Phys. Stat. Sol. B*, **175**, 15, (1993).

[18] V. M. Kenkre, D. H. Dunlap, *Phil. Mag. B.*, **65**, 831, (1992).

5 TIME OF FLIGHT MEASUREMENT WITH ELECTRONIC IMPULSE.

5.1 Introduction.

In the previous chapters we described the use of an electronic pulse to obtain the drift velocity and mobility of charge carriers in the channel of an organic field effect transistor (OFET). The pulse voltage method involves the injection of carriers using a voltage pulse which also provides the electric field that drives the carriers towards the drain. The time between the injection and arrival at the drain is calculated from the time delay between the applied pulse and the resulting drain waveform. One disadvantage of the pulse method is that the source-gate and the source-drain biases couldn't be independently controlled. Therefore the variation of mobility with the lateral field and the gate voltage bias could not be independently determined.

In this chapter we will discuss an alternate approach, derived from the pulse voltage method, for exploring charge transport along the plane of the semiconductor/insulator interface in a field-effect transistor using the transit-time of an electronic pulse applied to the source[1]. The source to gate and the source to drain biases can be controlled independent of each other. This method is valid for low conductivity materials, like amorphous semiconductors, whose dielectric relaxation time is lower that the transit time of the carriers injected. It is also necessary for the validity of the impulse technique that the transport takes place through the channel rather than the bulk of the transistor.

5.2 Impulse voltage technique.

The impulse voltage technique is similar to an optical time-of-flight (TOF) method of characterizing mobility; the only difference being the process in which carriers are produced. The optical TOF method is more suited for an organic LED where the semiconductor is sandwiched between two non-injecting electrodes at least one of which is transparent. A short pulse of strongly absorbed light pulse is then exposed on a transparent electrode covering the semiconductor (Figure 5.1). The pulse gets strongly absorbed in the semiconductor and generates excitons that dissociate into positive and negative charge carrier pairs very close to the electrode. An electric field preexists in the semiconductor, being set-up by the voltages applied at the two electrodes. Depending on this preexisting electric field only one kind of carrier starts moving towards the other electrode which is nominally connected to ground through a resistor. The current through the resistor reflects the sum of conduction and displacement currents flowing in the material due to the movement of the charges.

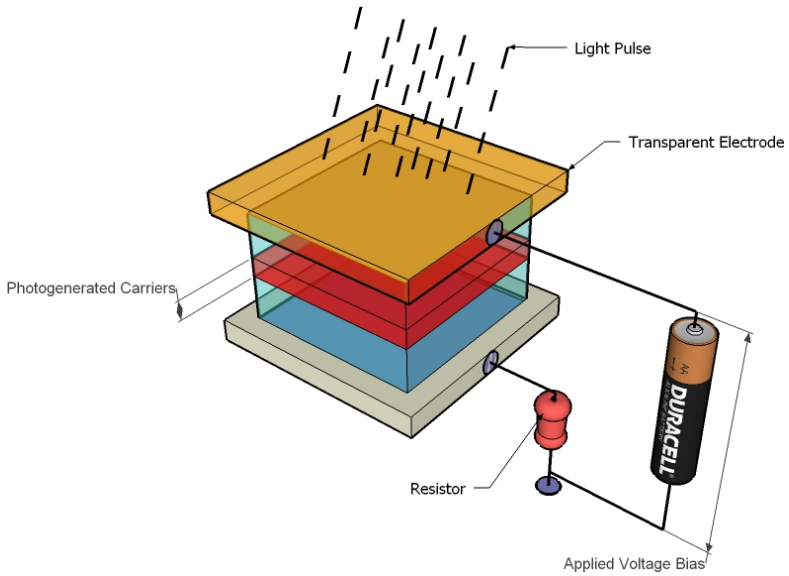

Figure 5.1 Schematic representation of the ptical time of flight experiment.

As opposed to the optical TOF measurement, the electronic method is suited to transistor geometries where the overlap between electrodes is small so as to minimize the displacement current originating from the application of an impulse. The electrodes in an OFET are biased at constant potential, with the source at higher potential than the drain. Therefore a constant current flows through the transistor in steady state. An electronic impulse is subsequently applied to the source contact the purpose of which is to inject carriers in the channel without disturbing the preexisting electric field. Following the application of the impulse the injected carriers undergo two simultaneous processes. Firstly, the carriers progress towards the drain due the action of the electric field and secondly the electric field tries to readjust itself after the disturbance created by the excess carriers, this process of readjustment of electric field is also known as dielectric relaxation. Dielectric relaxation is characterized by a time constant τ which is given by

$$\tau_D = \frac{\varepsilon\varepsilon_0}{\sigma} \quad \sigma = e \cdot \mu \cdot p_0 \tag{5.1}$$

where ε and ε_0 are the relative dielectric constant of the material and the permittivity of free space respectively, σ is the conductivity of the substance which is given by the product of e, the electronic charge, μ, the mobility of the majority carriers, and p, the concentration of majority carrier which, in the present case, is hole. If the dielectric time constant of the material is smaller than the transit time of the carriers the carriers will reach the drain before the relaxation of carriers cause the pulse to diminish to obscurity. The transit time of the pulse can then be calculated from the instant the injected carriers appear at the drain, by subtracting from it the instant at which the pulse was injected. The transit time of the excess carrier depends on their mobility, which can subsequently be extracted from it. In the following section we have analyzed the dynamics of excess charge carriers that the relation between its transit time and mobility.

5.3 Mathematical description.

The problem deals with obtaining the time dependent carrier distribution $\rho(x,t)$ flowing through the channel in response to an electric field E existing between the source and drain of a transistor. To reduce the complexity of the problem we have assumed a constant charge density in the channel given by p_0 , established by a constant gate voltage. This is the case when the transistor is operating in the linear region. The conduction in an OFET takes place in the channel therefore we have confined ourselves to a one dimensional system. Furthermore the impulse is assumed to inject at carrier packet at the source whose distribution is given by the delta function of magnitude $p_0+\Delta p$, and the injected packet of carriers is small enough to keep the field E undisturbed. Trapping of carriers is neglected in the analysis as the time constants of trapping are large compared to the time scale of the experiment.

5.4 Analysis and solution

Carrier flow in the system is governed by the Poisson's equation, the continuity equation and the expression for current. For the present system the equations, in the above order are:

$$\frac{\partial \vec{E}}{\partial x} = \frac{e}{\varepsilon\varepsilon_0} p \tag{5.2}$$

$$\frac{\partial J_C}{\partial x} = -e\frac{\partial p}{\partial t} \tag{5.3}$$

$$J_C = e \cdot \mu \cdot p \cdot E - e \cdot D_P \frac{\partial p}{\partial x} \tag{5.4}$$

where J_C is the conduction current and D_P is the diffusivity of the holes. The source electrode is assumed to have an ohmic contact with the semiconductor at $x = 0$.

The concentration of charge carriers at the electrode is sufficiently large for the electric field vanishes within the electrode. Similar conditions are assumed to hold at the drain electrode so as not to obstruct the current flow. The source electrode is maintained at ground potential except when the pulse voltage is applied, while the drain electrode is maintained at $-V_0$, where V_0 is a positive voltage. Hence before the application of the pulse the electric field is given by

$$E(x,t<0)=\frac{V_0}{L} \tag{5.5}$$

Since the voltages are maintained after the application of the pulse the following also hold true

$$\int_{x=0}^{x=L} E(x,t>0)\cdot\partial x = V_0 \tag{5.6}$$

The set of equations given by(5.2), (5.3) and (5.4) need simplification to assist the solution of dynamics of the system. We will neglect the diffusive component to the expression of current as it is of much lower value. Equation (5.4) stands modified as

$$J_C = e\cdot\mu\cdot p\cdot E \tag{5.7}$$

The following simplifying substitutions are also introduced to normalize the variable

$$\begin{aligned} z &= \frac{x}{L} \\ \xi &= \frac{E}{V_0/L} \\ \rho &= \frac{ep}{\varepsilon\cdot\varepsilon_0\frac{V_0}{L^2}} \\ j_C &= \frac{J_C}{\varepsilon\cdot\varepsilon_0\cdot\mu\cdot\frac{V_0^{\,2}}{L^3}} \\ \tau &= \frac{t}{T};T=\frac{L^2}{\mu\cdot V_0} \end{aligned} \tag{5.8}$$

these transformation convert the equation set into

$$j_C = \rho \cdot \xi \tag{5.9}$$

$$\frac{\partial j_C}{\partial z} = -\frac{\partial \rho}{\partial \tau} \tag{5.10}$$

$$\frac{\partial \xi}{\partial z} = \rho \tag{5.11}$$

$$\int_{z=0}^{z=1} \xi(z, \tau > 0) \cdot \partial z = 1 \tag{5.12}$$

Finally the boundary conditions expressed in the new set variables are

$$\xi(0, \tau \geq 0) = 0$$

$$\xi(z, \tau = 0) = 1$$

$$\rho(z, \tau = 0) = \rho_0 = \frac{e \cdot p_0}{\varepsilon\varepsilon_0 \frac{V_0}{L^2}} \tag{5.13}$$

Equations (5.10), (5.11) can be used to obtained the displacement component of the current, there fore the equation for the total current J is given by

$$j = j_C + \frac{\partial \xi}{\partial \tau} \tag{5.14}$$

The total current flowing through the system is constant hence by integrating equation (5.14) with respect to z and using equation (5.12) we get

$$j = \frac{1}{2}\xi^2(1, \tau) + \rho_0 \tag{5.15}$$

The given system of equation constitutes a hyperbolic system for the flow in a conducting crystal that has been solved by Many et. al.[2]. It was shown, as represented in Figure 5.2, that the distribution of carriers evolve with time while its position shifts according to

$$\frac{\partial z_0}{\partial \tau} = \xi \tag{5.16}$$

where z_0 is a reference point in the distribution. This, in the original system of variables, translates into

$$\frac{\partial x_0}{\partial t} = \mu E \tag{5.17}$$

which imply that the carrier distribution move according to the velocity dictated by the local electric field.

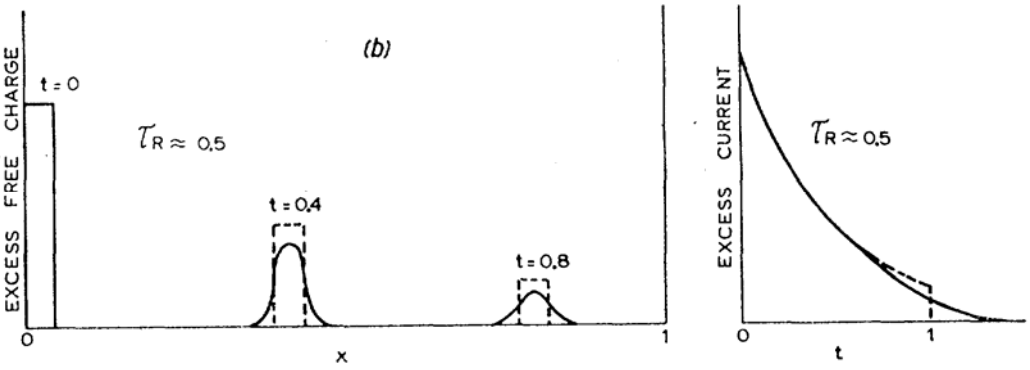

Figure 5.2 The propagation of a small pulse of injected majority carriers and the resulting current is displayed. The dashed curves correspond to the approximation which neglects dispersion whereas the solid lines illustrate the effect of charge dispersion. Reprinted from 2 with permission from AIP.

Using a mobile system of co-ordinates, with its origin at the reference point z_0 , the equation system is completely specified by

$$\frac{\partial \rho(z_0(\tau),\tau)}{\partial \tau} = -\rho(\rho - \rho_0) \tag{5.18}$$

$$\frac{\partial \xi(z_0(\tau),\tau)}{\partial \tau} = j(\tau) - \rho_0 \cdot \xi(z_0(\tau),\tau) \tag{5.19}$$

Equation (5.18) states that the rate of decay of charge carriers as they travel along the channel is due to Coulomb repulsion between the excess carriers ρ- ρ_0 and the intrinsic carriers ρ_0. Equation (5.19) states that while moving along a front of carriers the total current is composed of two components. The first being the displacement current while the other being the conduction current due to local charge density that, relative to the moving front, moves backwards with a velocity equal to that of the front. Equation

(5.18) can be easily integrated to represent the decay in carrier density as the distribution propagates. This can be written as

$$\rho(\tau) = \rho_0 \left[1 - \frac{\rho(0) - \rho_0}{\rho_0} \exp(-\rho_0 \cdot \tau) \right]^{-1} \tag{5.20}$$

where $\rho(0) - \rho_0 = \Delta\rho(0)$ is the concentration of excess carriers injected at the source electrode by the pulse. For the small signal case where $\Delta\rho << 1$, equation (5.20) can be simplified and written in terms of excess carrier density as

$$\Delta\rho(\tau) = \Delta\rho(0) \exp(-\rho_0 \cdot \tau) \tag{5.21}$$

This, when converted back into the original system of variables, becomes

$$\Delta p(t) = \Delta p(0) \cdot \exp(-\frac{t}{\tau_D}) \tag{5.22}$$

where τ_D is the dielectric relaxation constant of the semiconductor. There the carriers decay as they propagate with a time constant given by the relaxation constant, their movement being governed by the electric field. Since the electric field is left undisturbed by the movement of the carriers the transit time of the carries is given by

$$t_{TR} = \frac{L^2}{\mu V_0} \tag{5.23}$$

for $t_{TR} < \tau_D$ the carriers reach the drain before the pulse completely relaxes. The current consists of a constant DC current flowing through the transistor and an AC component, superimposed on top, due to the movement of the excess carriers. This transient component, as shown in Figure 5.3, decreases exponentially from the instant the impulse is applied till the carriers reach the drain. The rate of decrease is given by the dielectric relaxation time. The DC and the transient components current need to be diverted in order to measure the transit time. This is done using a bias-T as described in the next section.

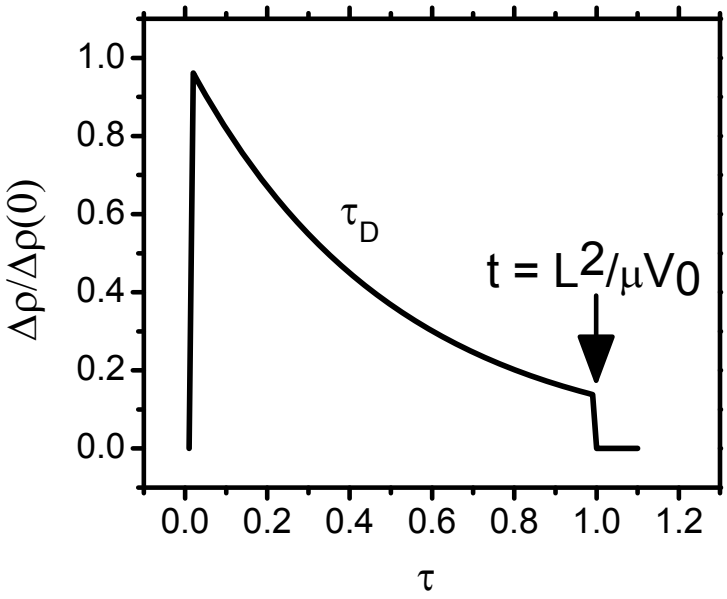

Figure 5.3. Plot of excess carrier current, given by Equation (5.22) . The current disappears when the carriers leave the drain.

5.5 Experimental set-up

The schematic of the experiment is shown in Figure 5.4. The source of the transistor is connected to an impulse generator which maintains the source potential at 0 V, except when the impulse is applied. The gate and drain potentials are set by a high voltage source. The drain is connected to a bias-T, which diverts the transient current (generated by the impulse) away from the DC current flowing into the voltage source. The bias-T is a simple RLC circuit that uses a capacitor to divert the transient current away from the constant DC current. The transient current is redirected into a 500 Ω

resistor which transforms the current into voltage. The impulse waveform and the transient voltage across the resistor are simultaneously displayed on an oscilloscope.

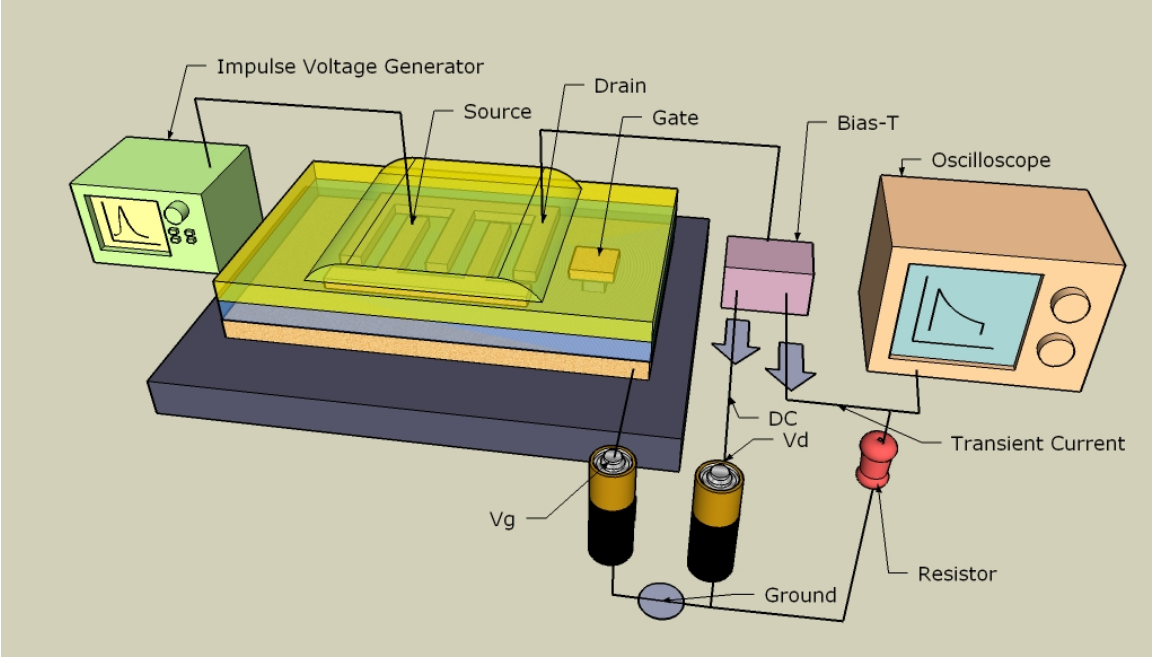

Figure 5.4. Experimental set-up of the impulse voltage experiment.

To study transport using the impulse method, the transistor is allowed to settle in a conducting state determined by the applied gate and drain biases. The drain bias is restricted to a small fraction of the gate voltage in order to ensure minimum non-uniformity in the accumulation layer formed (V_{GS} =-100 V V_{DS} =-10 V). The drain bias is kept much below the gate potential so that the linear region approximation hold true. MEDICI® simulation was also done to ensure that the assumption of a constant electric field inside the channel hold true. As shown in Figure 5.5 the equipotential lines are uniformly spread for V_{DS} =-10 V, implying that the electric field along the channel can be assumed constant. This is followed by the application of the impulse voltage at the source. The width (FWHM) of the pulse is 15 nsec and the peak voltage is 5V. The

impulse voltage is a fraction of the DC biases applied and it exists only for about 20 nanoseconds, this justifies the assumption that the impulse produces a relatively small perturbation, superimposed on top of the steady-state bias. The packet of charge carriers injected into the channel by the impulse travel through the semiconductor to the drain. Once the carrier flux arrives at the drain, the bias-T diverts the transient current into a 500 Ω resistor. Finally the output current is displayed on the oscilloscope along with the input so that the transit time can be calculated.

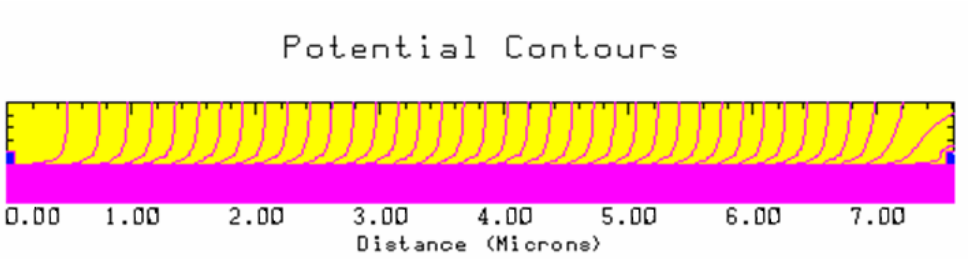

Figure 5.5 Plot of potential contours in a FET operating with Vds =-10 V and Vgs = -100 V. Uniformly distributed potential lines indicate a contant electric field. From 1, reprinted with permission from AIP.

5.6 Fabrication details

The thin film transistors used for the experiment had been fabricated according to Scheme C discussed in section 4.3.3. The OFETs had bottom contact geometries with patterned gate similar to those used by Crone et. al.[3]. The channel width (W) and length (L) were 2000 μm and 7.5 μm respectively. The dielectric consisted of a bilayer of silicon dioxide (1000 Å) and silicon nitride (2000 Å). A schematic diagram of the substrate is presented in Figure 5.6. To facilitate the efficient ordering of the polymer chains, a hydrophobic monolayer was deposited on the dielectric semiconductor interface, by treating it with 0.1 M solution of octyltrichlorosilane in toluene[4,5]. Poly(2,5-bis(3-tetradecylthiophen-2-yl)thieno[3,2-*b*]thiophenes) (pBTTT), was spin-coated from a

solution of 1,2-dichlorobenzene. As discussed earlier in section 4.5.3.2 it has one of the highest mobilities recorded for a polymer semiconductor. To further assist the ordering of chain, the sample was annealed at 120^{o} C, and then cooled down slowly to room temperature under nitrogen atmosphere.

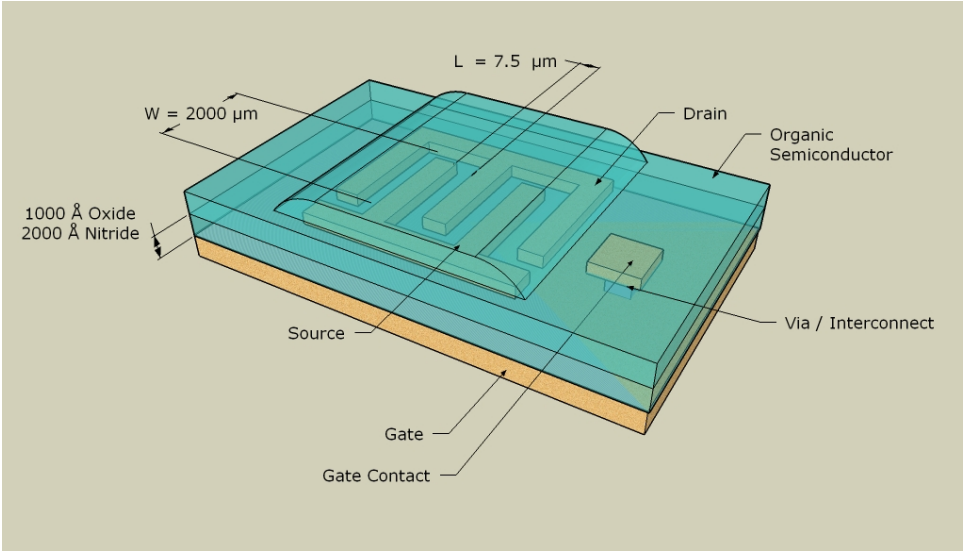

Figure 5.6. Structure of the bottom contact OFET used in the experiment.

5.7 Results.

The plot obtained from the oscilloscope for the transient impulse experiment is shown in Figure 5.7. To make the transition to zero of the current pulse clearer, the figure has been replotted in log-log scale in Figure 5.8. It can be seen that the transitions takes place around 120 nsec for V_{DS} = -10 V. It is tempting to conclude that the transit time for the carriers in the channel is 120 nsec; however a detailed investigation would divulge the fallacy in the previous statement. By remembering the rate of decay in the transient current is given by the dielectric relaxation time, we estimate the dielectric relaxation time to be about 100 nsec. The mobility can was independently calculated by the current-

voltage characteristics. Using equation(5.24), linear region mobilities of 0.12 – 0.18 cm^2/Vs were obtained at V_{GS} of -100 V.

$$\mu_{FET} = \frac{1}{C_{OX}\frac{W}{L}V_{DS}}\frac{\partial I_D}{\partial V_{GS}} \tag{5.24}$$

The mobility value is then used to calculate the carrier density of the pulse, which yield a value ~ 10^{13} cm^{-3}, which is extremely small for the accumulation region of the FET.

In actuality, the carriers travel both through the accumulation and the bulk of the semiconductor. However the concentration of charge carriers in the channel is high enough to cause a fast decay of the response. Therefore the response that appears on the oscilloscope is that of the carriers traveling through the bulk, where the carrier density is low.

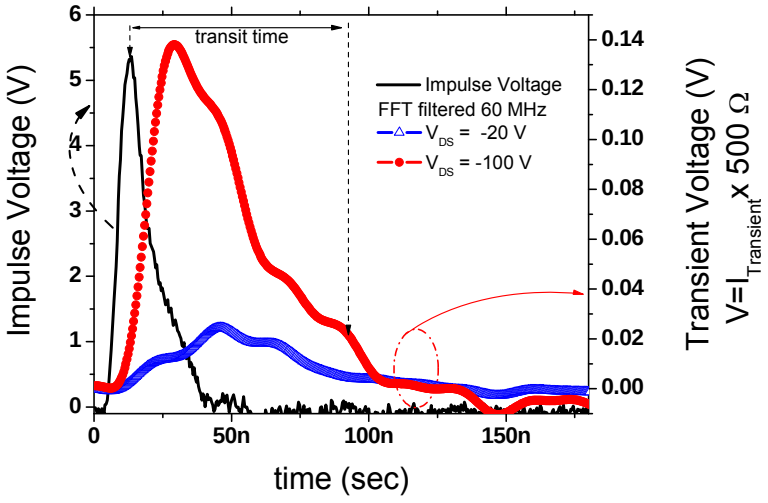

Figure 5.7. Plot of the transient current and the impulse voltage. From 1, reprinted with permission from AIP.

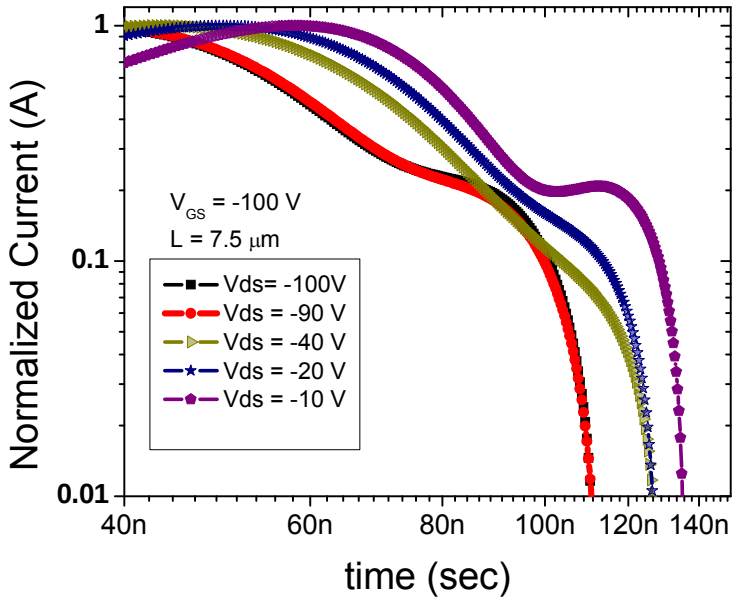

Figure 5.8. Plot of the transient current in log-log scale. From 1, reprinted with permission from AIP.

5.8 Conclusion

The electronic impulse is an alternate approach to measure the carrier drift mobility in a field effect transistor. It is derived from the pulse voltage method, but has an added advantage that the gate and the drain voltages can be independently controlled. However care must taken in extract the mobility value as this method is valid only for low conductivity materials, like amorphous semiconductors, whose dielectric relaxation time is lower that the transit time of the carriers injected. It is also necessary that the transport takes place through the channel rather than the bulk of the transistor.

In the present experiment the carriers traveled through the bulk of the semiconductor instead of the channel, hence this method cannot be used to measure the drift mobility of carriers in the transistor.

References

[1] D. Basu, L. Wang, L, Dunn, A. Dodabalapur, *App. Phys. Lett.*, **89**, 242104 (2006).

[2] A. Many, G. Rakavy, *Phys. Rev.* **126**, 1980, (1962).

[3] B. Crone, A. Dodabalapur, Y.-Y. Lin, R. W. Filas, Z. Bao, A. LaDuca, R. Sarpeshkar, H. E. Katz and W. Li *Nature* **403**, 521 (2000).

[4] A. Salleo, T. W. Chen, A. R. Voelkel and R. A. Street, *Phy. Rev. B* **70**, 115311 (2004).

[5] M. Shkunov, R. Simms, M. Heeney, S. Tierney and I. McCulloch *Adv. Mat.* **17**, 2608 (2005).

6 CONCLUSION

Organic semiconducting polymers are endowed with qualities such as easy processibility and variety of materials. Their potential for use in low cost electronics and photovoltaic applications has prompted technological and scientific interest in these materials. Although the electrical characteristics of organic semiconducting polymers has improved tremendously over recent years, yet the performance of organic circuit are hindered by low speeds of operation. This is due to the fact that majority of the carriers in an polymeric semiconductor are trapped in localized states resulting in low field-effect mobilities. Therefore it is important to understand the charge transport properties of organic polymers to improve their electrical performance.

Theoretical characterization of charge transport in organic semiconductors, is difficult due to the presence of non-linearities created by defects and traps. It is understood that movement of carriers depend on density of states, which is determined by density of localized or trap states in the forbidden gap. There have been multiple attempts to understand the density of states, most of which have involved either characterizing the field effect or the optical time-of-flight mobility.

In this dissertation we have introduced a new method that combines the advantages of both these methods. It uses the time-of-flight of a charge packet injected by a voltage pulse to calculate the drift velocity and mobility of carriers. This technique can help to improve our understanding of charge transport by providing a new method to characterize the mobility. This technique is a fast and simple way to determine the charge transport properties of the semiconductor. In addition it also presents itself as a source of information for understanding injection into the semiconductor and determining the trap distribution.

Theoretical modeling of the method was done using two approaches that lead to the same solution. Simulations were also performed to include non-idealities like finite rise time and charge trapping that are forbiddingly difficult to be solved analytically. Time of flight measurement of drift mobility was performed in organic transistors with varying semiconductors and dielectrics that were fabricated by different methods of fabrication.

It was observed that the electronic time-of-flight (eTOF) mobility lies in the range of the field-effect mobility. Variation in drift mobility was also observed with the applied pulse voltage. This was explained to be due to a combination of following two phenomena; the increase in mobility with gate voltage and the increase in drift mobility at high lateral fields. Finally TOF measurements were done on transistors with varying channel length and it was concluded that the mobility reduces at low electric field and increase proportional to the exponential square root of the source drain bias.

The pulse voltage method is a large signal method for characterizing the mobility. One of the drawbacks of this method is that the source-gate bias and the source-drain biases could not be independently controlled. So an alternate approach to measure the carrier drift mobility in a field effect transistor was discussed. It is a small-signal technique derived from the pulse voltage method, but has an added advantage that the gate and the drain voltages can be independently controlled. However this method could not be used to measure the drift mobility of organic semiconductors as it is valid only for low conductivity materials, like amorphous semiconductors, whose dielectric relaxation time is lower that the transit time of the carriers injected. It is also necessary that the transport takes place through the channel rather than the bulk of the transistor.

Appendix

The following MATLAB code is for simulating the pulse voltage method.

```
%
clear
figure(1);
set(1,'Position', [50 100 900 600]);

%parameters and constants
L = 1e-3;%10 μm
mup = 1e-1; %hole mobility cm^2/v/s
q = 1.602e-19; % C
eps0 = 8.854e-14;% F/cm
eps=3*eps0;
epsox = 3.9*eps0;
tox = 1e-5; %1000 Å
k = 1.381e-23;
T = 300; % kelvin
kT_q=k*T/q; % eV
Vappl=100; %V
Vd = 0; %potential at source
Vs = 1; %potential at drain
Tr = L^2/(mup*Vappl);
DT = 5e-5; %time interval sec
%device grid
x1 = 0;
dx = 1e-2;
x2 = 1;
x = [-dx x1:dx:x2 x2+dx]';
z = [0:1:10];
NP = round((x2-x1)/dx)+1;
NNP=NP+2;
display = 500;
loop = 30000;
P_3d = zeros(NP,length(z));
%setup sparse matrix for finite difference 1st derivative --> D1*x = x'
D1 = spalloc(NP+2,NP+2,2*NP+4);
D1(1,1) = 0; % point (1,1) is virtual
D1(NP+2,NP+2)=0; %point (NP+2,NP+2) is virtual
for i = 2:NP+1
    D1(i,i-1)=-1/(x(i+1)-x(i-1));
    D1(i,i+1)=1/(x(i+1)-x(i-1));
end

%setup sparse matrix for finite difference 2nd derivative --> D2*x = x''
D2 = spalloc(NP+2,NP+2,3*NP+6);
D2(1,1)=0; %don't change virtual grid point when calculating p+dp or n+dn
D2(NP+2,NP+2)=0; %don't change virtual grid point when calculating p+dp or n+dn
for i = 2:NP+1
    D2(i,i-1)=2*(x(i+1)-x(i))/((x(i)-x(i-1))*(x(i+1)-x(i))*(x(i+1)-x(i-1)));
    D2(i,i)=-2/((x(i+1)-x(i))*(x(i)-x(i-1)));
    D2(i,i+1)=2*(x(i)-x(i-1))/((x(i)-x(i-1))*(x(i+1)-x(i))*(x(i+1)-x(i-1)));
end

%set initial potential and charge distributions (no charges at beginnning)

V = zeros(NP+2,1);
J = zeros(NP+2,1);

% for i=1:NP+2
% V(i) = (Vs -(Vs-Vd)*x(i)/x2);
% end
%loop for main program
V(1) = Vs; V(2)=V(1);

V(NP+1) = Vd; V(NP+2)=V(NP+1);
mov = avifile('dd.avi')

for j = 1:loop
```

```
    %calculate new charge distributions
    dV =  DT/2*(D2*(V.*V)) ;
    V = V + dV;
    %set boundary
    V = (min([V';ones(1,length(V'))]))';
    V(1) = Vs; V(2)=V(1);
    V(NP+1) = Vd; V(NP+2)=V(NP+1);% for collecting contacts
    %solve poisson's equation

    %plot data
    if mod(j,display) == 0

        subplot(2,4,1:2);
        plot(x(2:NP+1)*L*1e4,V(2:NP+1)*Vappl);
        xlabel('distance along channel [µm]');
        ylabel('Volatge [V]');
        title('voltage');
%       M1(round(j/display))= getframe(1);
%       mov = addframe(mov,getframe(1));
        drawnow;

        p=epsox/(tox*q)*Vappl*V;
        for counter =1:length(z)
            P_3d(:,counter)=p(2:NP+1);
        end

        subplot(2,4,5:7);
        surf(z,x(2:NP+1)*L*1e4,P_3d);
        colormap hsv; alpha(.7);view(120,60);shading interp;colorbar;
%         axis([0; 10; 0; L*1e4; 1e10; epsox*Vappl*1.2/(tox*q)]);

%         axis([0; L*1e4; 1e10; epsox*Vappl*1.2/(tox*q)]);
        ylabel('distance along channel [µm]');
        zlabel('hole concentration [cm^-^3]')
        title('hole concentration along channel');
        drawnow;

        J=-mup*(Vappl^2/L)*epsox/tox*V.*(D1*V)*1e6/1e4;
        Jd(round(j/display))=J(NP);
        time(round(j/display))=j*DT*Tr*1e6;
        subplot(2,4,3:4)
        plot(time,Jd);
        axis([0; loop*DT*Tr*1e6; 0; mup*epsox*1.02*Vappl^2/(tox*L)*1e6/1e4]);
        ylabel('Drain Current Density (I/W) [µA/µm]');
        xlabel('time [µs]');
        title('current');
        drawnow;


        mov = addframe(mov,getframe(1));

    end
end
mov = close(mov);
```

The following code is for extracting the delay time for pulse voltage method

```
% read Vs
clear
clc
[sfilename, spathname] = uigetfile('*.txt', 'Select source
file','N:\Debarshi\Project_Data\10_22_06\');
fid_s = fopen([spathname '/' sfilename],'r');
if ( fid_s == -1 )
    'file cannot be read';
else
    'reading source file.......';
    [time, Source] = readChannel( fid_s );
end
% read Vd
[dfilename, dpathname] = uigetfile('*.txt', 'Select drain
file','N:\Debarshi\Project_Data\10_22_06\');
fid_d = fopen([dpathname '/' dfilename],'r');
if ( fid_d == -1 )
    'file cannot be read';
else
    'reading drain file.......';
    [time1, Drain] = readChannel( fid_d );
end
'drain and source files read successfully';

% remove unwanted variables
fclose(fid_s);
fclose(fid_d);
clear sfilename;
clear spathname;
clear dfilename;
clear dpathname;
% two time variables time and time1 if they are equal remove time1
if isequal(time,time1)
    clear time1;
else
    'the time variables are not equal';
end

% find the time when source voltage is applied ( actually mid point of the
% ramp up time. th_up is the index of that time.
threshold = max(Source)/2;
th_up = 1;
while (Source(th_up)< threshold)
    th_up = th_up + 1;
end
str1 = [ 'the time to at which the pulse is at half its maximum value is:',
num2str(time(th_up))];
% if the source waveform falls , th_down is the index of the midpoint of
% the ramp down part of the waveform

th_down = length(Source);

if Source(th_down) < threshold
    while (Source(th_down)< threshold) & (th_down > th_up)
        th_down = th_down - 1;
    end
end
% redefine the waveforms and time to include only the nescessary areas from
% ramp up to ramp down, use a few point margin.

Source = Source(th_up + 40 : th_down -20);
time = time(th_up + 40 : th_down -20);
Drain = Drain(th_up + 40 : th_down -20);
l = length(time);
% avoid calculating the maximum value from the overshoot in the Source
% waveform so you find the maximum value of source and drain waveforms 30
% points after it starts rising.
VS = mean(Source(40 : l-10));
str2 = ['maximum source voltage: ' , num2str(VS)];

VD = max(Drain(40 : l-10));
str3 = ['maximum drain voltage: ' , num2str(VD) ];
```

```
filtD = smooth(Drain,10,'sgolay',3);% filter with savitzky-golay to remove the
noise.
clear th_up th_down threshold;
%L = ; mu = 0.01; t0 =l^2/(mu*VS);
%t0 is set empirically ;need better algorithm to modify t0 =  time  at which the
drain waveform starts increasing
%t0_ind is the index of t0



t0_ind = find(Drain<VD/8, 1, 'last');

% once you find the starting point you need to find the part of the waveform
% that you want to use for the fit

% [vmin, t_ind] = min(Drain( max(t0_ind-5,1) : min(t0_ind+20,length(Drain)) ));
% t0_ind = min(t0_ind-20,1) + t_ind -21;
[vmax t1_ind] = max(Drain(t0_ind : min(t0_ind + 1000,length(Drain)) ));
t1_ind = t1_ind + t0_ind -1;
time_fit = time(t0_ind : t1_ind  );
Drain_fit = Drain(t0_ind : t1_ind );
vmax = vmax + eps ;

% before you do the the actual fit you use a trial fit to obtain parameters
% that you can use as starting poins for the actual fit. So define newtime
% and newdrain vectors for the trial fit.

%cftool(time_fit, Drain_fit);
%need to modify newtime and newdrain 300 points need not always be valid
newtime = time_fit(1:100);
newdrain = Drain_fit(1:100);
alpha = 0.83; beta = 0.17; beta_by_2_alpha = beta/(2*alpha);
y = -2*log( sqrt( beta_by_2_alpha^2 - (newdrain/vmax -1)/alpha ) -
beta_by_2_alpha);

fit1 = [ ones( size(newtime)), newtime ]\y;

startpoint = [ vmax alpha beta -fit1(1)/fit1(2) 1/fit1(2) 2/fit1(2)];

% clear newtime newdrain

clear t_ind filtD t0 vmin
opts = fitoptions('Method','Nonlinear','Robust','On','MaxFunEvals', 3000,'MaxIter',
1000, 'Lower',  eps*startpoint, 'Upper', 10*startpoint, 'StartPoint', startpoint );
ftype = fittype('I*(1 - a*exp( -(t-t0)/t2 ) -b*exp( -(t-t0)/(t3) )
)','independent','t','options',opts);
[fresult, gof, output] = fit(time_fit, Drain_fit, ftype, opts);
Drain_func =inline(' I*(1 - a*exp( -(t-t0)/t2 ) -b*exp( -(t-t0)/t3 ) )');
str4 = ['I = ' num2str(fresult.I)];
str5 = ['alpha = ' num2str(fresult.a)];
str6 = ['beta = ' num2str(fresult.b)];
str7 = ['delay = ' num2str(fresult.t0)];
fitted_drain = max( 0, Drain_func(fresult.I, fresult.a, fresult.b, time_fit,
fresult.t0, fresult.t2, fresult.t3));
plot(time_fit, Drain_fit, '.', time_fit, fitted_drain);
% [4 0.9 0.5 5e-6 1e-6 1e-6 ]
```

Bibliography

W. Shockley, Bell Syst. Techn. J. **28**, 435 (1949). U.S. Patent 2524035 — J. Bardeen et. al, U.S. Patent 2569347 — W. Shockley

U.S. Patent 3138743 , U.S. Patent 3138747 , U.S. Patent 3261081, U.S. Patent 3434015 – J. Kilby.

G.E. Moore, "Progress in Digital Integrated Electronics", *IEEE Int'l Electron Device Meeting Tech. Digest*, 11-13. (1975).

U.S. Patent 4124287— Xerox Corp.

http://nobelprize.org/nobel_prizes/chemistry/laureates/2000/presentation-speech.html.

Rogers, J.A.; Bao, Z.; Baldwin, K.; Dodabalapur, A.; Crone, B.; Raju, V.R.; Katz, H.E.; Kuck, V.J.; Amundson, K.; Ewing, J.; Drzaic, P. *Proc. Nat. Acad. Sci.* **98**, 4835-4840 (2001).

W. Clemens, W. Fix, J. Ficker, A. Knobloch, A. Ullmann, *J. Mater. Res.* **19**, 1963 (2004)

B. Crone, A. Dodabalapur, A. Gelperin, L. Torsi, H. E. Katz, A. J. Lovinger, and Z. Bao. *Appl. Phys. Lett.* **78,** 2229-2231. (2001)

B. R. Eggins, Chemical Sensors and Biosensors, J. Wiley & Sons. (2002).

S. R. Forrest, *MRS Bulletin*, **30**, 28 - 32 (2005).

http://www.orgworld.de/

N. Karl, K.-H. Kraft, J. Marktanner, M. Münch, F. Schatz, R. Stehle, and H.-M. Uhde, *J. Vac. Sci. & Tech.* **17**, 2318-2328 (1999).

J.L. Brédas, J.P. Calbert, D.A. da Silva Filho, J. Cornil, Organic semiconductors: a theoretical characterization of the basic parameters governing charge transport, *Proc. Nat. Acad. Science*. *USA* **99,** 5804-5809 (2002).

C. Dimitrakopoulos and D. J. Mascaro, *IBM J. Res & Dev.* **45**, 1. (2001).

A. Salleo, T. W. Chen, A. R. Völkel, Y. Wu, P. Liu, B. S. Ong, and R. A. Street, *Phys. Rev. B* **70**, 115311 (2004).

M. Pope and C.E. Swenberg, *Electronic Processes in Organic Crystals and Polymers*, Oxford University Press (1999).

H. Bässler, *Phys. Stat. Sol.* B **175**, 15 (1993).

E.M. Conwell, *Phys. Rev.* **103**, 51 (1956).

A. Miller and E. Abrahams, *Phys. Rev.* **120**, 745 (1960).

N.F. Mott and E.A. Davies, *Electronic processes in non-crystalline materials*, 2nd *Edition*, Oxford University Press, London (1979).

D. Monroe, *Phys. Rev. Lett*. **54**, 146 (1985).

M.C.J.M. Vissenberg and M. Matters, *Phys. Rev. B* **57**, 12964 (1998).

Y.-Y. Lin *et al.*, *IEEE Trans. Electron Dev. Lett.* **18** (1997), p. 606.

H. Klauk *et al.*, *J. Appl. Phys.* **92** (2002), p. 5259.

A. Facchetti, *Mater. Today,* **10**, 28 (2007)

A. Assadi *et al.*, *Appl. Phys. Lett.* **53** (1988), p. 195.

B.S. Ong *et al.*, *J. Am. Chem. Soc.* **126** (2004), p. 3378.

I. McCulloch, M. Heeney, C. Bailey, K. Genevicius, I. MacDonald, M. Shkunov, D. Sparrowe, S. Tierney, R. Wagner, W. Zhang, M. L. Chabinyc, R. J. Kline, M. D. McGehee, and M. F. Toney, Nat. Mater. **5**, 328 _2006_.

A. S. Dhoot, J. D. Yuen, M. Heeney, I. McCulloch, D. Moses, and A. J. Heeger, Proc. Natl. Acad. Sci. U.S.A. **103**, 11834 (2006).

H. Scher. E. W. Montroll, *Phys. Rev. B.* **12**, 2455 (1975)

G. A. Cox, P. C. Knight, *J. Phys. Chem. Sol.* **34**, 1655, (1973).

N. T. Corke, J. N. Sherwood, R. C. Jarnagin, *Crystal Growth* (1969).

A. Rose, *Phys. Rev.* **97**, 1538, (1955).

P. Mark, W. Helfrich, *J. App. Phys.*, **33**, 205, (1962).

J. S. Bonham, D. H. Jarvis, *Aust. J. Chem.*, **30**, 705 (1977).

E. A. Silinsh, *Organic Molecular Crystals: Their Electronic States* Springer-Verlag, (1980).

N. F. Mott, R. W. Gurney, *Electronic processes in ionic crystals,* Oxford (1946).

H. Ishii, K. Sugiyama, E. Ito and K. Seki, *Adv. Mater.* **11**, 605, (1999).

Z. Bao, *Adv. Mater.* **12**, 227 (2000)

N. W. Ashcroft, N. D. Mermin, Solid State Physics, Saunders, 1976

D. Emin, *Phys. Rev. Lett*., **28**, 604, (1972).

T. Holstein, *Annals of Physics,* **281** 706-724 (2000).

T. Holstein, *Annals of Physics,* **281** 725-773 (2000).

D. Emin *Phys. Rev. B.* **43**, 11720 (1991)

C. Wood, D. Emin *Phys. Rev. B*. **29**, 4582 (1985).

L. B. Schein, *Phys. Rev*. *B*. **15**, 1024, (1977).

J. D. Anderson, C. B. Duke, V. M. Kenkre, *Phys. Rev. Lett* **15**, 2202, (1983).

J. Yamashita, T. Kurosawa, *J. Phys. Chem. Sol.* **5**, 34 (1958).

W. E. Spear, Ann. Rept., Conf. Elect. Insul. Diel., Natl. Acad. Sci. Washington, DC., ISBN:0-309-02032-8 (1971).

P. G. Le Comber and W. E. Spear, *Phys. Rev.Lett.* **25**, 509, (1970).

G. Horowitz, P. Delannoy, *J. App. Phys.* **70**, 469, (1991).

M. A. Lampert, *Phys. Rev.* **103**, 1648, (1956)

M. Silver, K. Risko, H. Bässler, *Philos. Mag. B.* **40**, 247, (1979)

M. Matters, M. C. J. M. Vissenberg, *Phys. Rev. B.*, **57**, 12964, (1998).

E. A. Silinsh, V.Čápek, *Organic Molecular Crystals: Interaction, Localization, and Transport Phenomena* AIP-Press, New York, (1994).

E. A. Silinsh, G.A. Shlihta, A. J. Jurgis, *Chem. Phys.*, **138**, 347, (1989).

V. M. Kenkre, J. D. Andersen, D. H. Dunlap, C. B. Duke., *Phys. Rev. Lett.*, **62**, 1165, (1989).

V. M. Kenkre, D. H. Dunlap, *Phil. Mag. B.*, **65**, 831, (1992).

Y-L. Loo, T. Someya, K. Baldwin, Z. Bao, P. Ho, A. Dodabalapur, H.E. Katz, J.A. Rogers, *Proc. Natl. Acad. Sci.*, **99**, 10252 (2002).

H. Klauk, M. Halik, U. Zschieschang, F. Eder, G. Schmid, C. Dehm, *Appl. Phys. Lett.* **82** 4175, (2003).

C. D. Dimitrakopoulos, S. Purushothaman, J. Kymissis, A. Callegari, J. M. Shaw, *Science* **283** 822 (1999).

Horowitz, G., Fichou, D., Peng, X. and Garnier, F. *Synth. Met.* **45**, 163, (1991).

B. Crone, A. Dodabalapur, Y. Lin, R. W. Filas, Z. Bao, A. LaDuca, R. Sarpeshkar, H. E. Katz, W. Li, *Nature* **403**, 521, (2000).

Z. Bao, A. Dodabalapur, A. J. Lovinger, *Appl. Phys. Lett.* **69**, 4108, (1996).

G. Horowitz, R. Hajlaoui, D. Fichou, A. El Kassmi, *J. App. Phys.* **85**, 6, 1999.

R. A. Street, J. E. Northrup, A. Salleo, *Phy. Rev. B* **71** 16 (2005)

M. Matters, M. C. J. M. Vissenberg, *Phys. Rev. B.*, **57**, 12964, (1998).

L. Dunn, L. Wang, D. Basu, A. Dodabalapur, *App. Phys. Lett.*, **88**, 063507 (2006).

J. C. Scott, J. Vac. Sci. & Tech., 21, 521, (2003).

M. A. Baldo, S. R. Forrest, Phys. Rev. B. 64, 085201, (2001)

M. A. Alam, A. Dodabalapur, and M. Pinto, IEEE Trans. Elec.Dev. Spcl Issue, 44, 1332, (1997).

C. Wagner, J. chem.. Phys. 18, 1227, (1950).

J. R. Burns, RCA Review, 30, 15, (1969)

L. Wang, D. Fine, D. Basu, A. Dodabalapur, J. App. Phys. 101, 054515, (2007).

W. D. Gill, J. Appl. Phys. 43, 5033 (1972).

J. Frenkel, Phys. Rev. 54, 647 (1938).

H. Klauk, Organic Electronics: Materials, Manufacturing and Applications, Wiley-VCH, pp111 (2006)

S. M. Sze Physics of Semiconductor Devices 2ed, John Wiley and Sons, pp 252, (1981)

Y.-Y. Lin *et al.*, *IEEE Trans. Electron Dev. Lett.* **18** (1997), p. 606.

H. Klauk *et al.*, *J. Appl. Phys.* **92** (2002), p. 5259.

I. McCulloch, M. Heeney, C. Bailey, K. Genevicius, I. MacDonald, M. Shkunov, D. Sparrowe, S. Tierney, R. Wagner, W. Zhang, M. L. Chabinyc, R. J. Kline, M. D. McGehee, and M. F. Toney, Nat. Mater. **5**, 328 _2006_.

A. S. Dhoot, J. D. Yuen, M. Heeney, I. McCulloch, D. Moses, and A. J. Heeger, Proc. Natl. Acad. Sci. U.S.A. **103**, 11834 (2006).

D. M. DeLongchamp et.al. *AIChE 2006*, Session T6001.

R. J. Kline, D. M. DeLongchamp, D. A. Fischer, E. K. Lin, M. Heeney, I. McCulloch, M. F. Toney, *App. Phys. Lett*, **90**, 062117 (2007).

J. Tate, JA Rogers, CDW Jones, B Vyas, D. W. Murphy, W. Li, Z. Bao, R.E. Slusher, A. Dodabalapur, H. E. Katz, *Langmuir* **16**, 6054 (2000)

Y-T. Jeong, B. Yoo, A. Dodabalapur, *MRS 2007prodeedings*, Session O5.2

H. Klauk, M. Halik, U. Zschieschang, F. Eder, G.Schmid, C. Dehm, *App. Phys. Lett.*, **82**, 4175, (2003).

D. J. Gundlach, J. Li Li, T.N Jackson, *IEEE Elec. Dev. Lett.* **22**, 571, (2001)

S. H. Kim, J. H. Lee, S. C. Lim, Y. S. Yang, T. Zyung, *Jap. J. App. Phys.* **43**, L60, (2003).

M. Mottaghi, G. Horowitz, *Organic Electronics,* **7**, 528, (2006).

P. M. Borsenberger, L. Pautmeier, H. Bässler. *J. Chem. Phys.* **94,** 5447 (1991).

H. Bässler, *Phys. Stat. Sol. B*, **175**, 15, (1993).

D. Basu, L. Wang, L, Dunn, A. Dodabalapur, *App. Phys. Lett.*, **89**, 242104 (2006).

A. Many, G. Rakavy, *Phys. Rev.* **126**, 1980, (1962).

M. Shkunov, R. Simms, M. Heeney, S. Tierney and I. McCulloch *Adv. Mat.* **17**, 2608 (2005).

Vita

Debarshi Basu was born on the 28th of February, 1980 in Dūrgapur, West Bengal, India to Sri. Purnendu Bikash Bose and Smt. Chandi Bose. He attended DAV Model School till 1998. After graduating from the Indian Institute of Technology Madras with Bachelor of Technology in Electrical Engineering in 2002, he completed his Master of Science in Engineering at the University of Texas at Austin in 2004. He is currently working Texas Instruments, Dallas, TX as a spice modeling specialist.

Permanent address: 207 Bhubasan Housing Complex, Durgapur, West Bengal -713216

This dissertation was typed by Debarshi Basu.